

AD-A264 716



WL-TR-91-4150

Cryogenic Magnetic Bearing

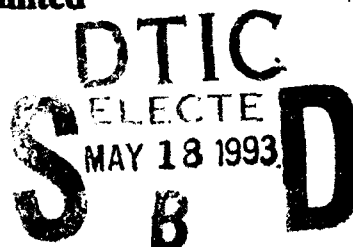
**J. Andrus, J. Kendig, J. Kroeger
Honeywell Inc.
Satellite Systems Operation
19019 N 59th Avenue
Glendale, Arizona 85308**



December 1992

Final Report for Period 1 November 1985 - 1 May 1991

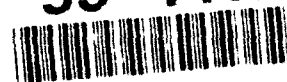
Approved for public release; distribution unlimited



**Materials Directorate
Wright Laboratory
Air Force Systems Command
Wright-Patterson Air Force Base, Ohio 45433-6533**

93 5 17 081

93-11021

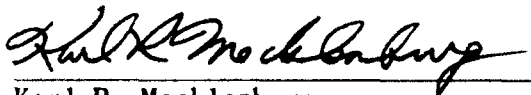


NOTICE

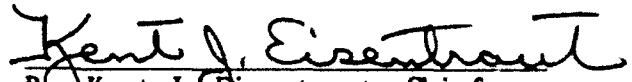
When Government drawings, specifications, or other data are used for any purpose other than in connection with a definitely Government-related procurement, the United States Government incurs no responsibility or any obligation whatsoever. The fact that the government may have formulated or in any way supplied the said drawings, specifications, or other data is not to be regarded by implication or otherwise in any manner construed as licensing the holder or any other person or corporation; or as conveying any rights or permission to manufacture, use, or sell any patented invention that may in any way be related thereto.

This report is releasable to the National Technical Information Service (NTIS). At NTIS, it will be available to the general public, including foreign nations.

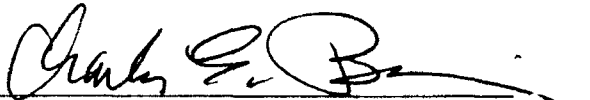
This technical report has been reviewed and is approved for publication.



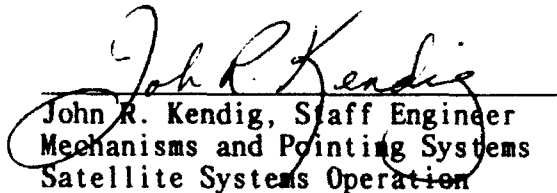
Karl R. Mecklenburg
Nonstructural Materials Branch
Nonmetallic Materials Division



Dr. Kent J. Eisentraut, Chief
Nonstructural Materials Branch
Nonmetallic Materials Division



Dr. Charles E. Browning, Director
Nonmetallic Materials Division
Materials Directorate



John R. Kendig, Staff Engineer
Mechanisms and Pointing Systems
Satellite Systems Operation

If your address has changed, if you wish to be removed from our mailing list, or if the addressee is no longer employed by your organization, please notify WL/MLBT WPAFB, OH 45433-6533 to help us maintain a current mailing list.

Copies of this report should not be returned unless return is required by security considerations, contractual obligations, or notice on a specific document.

UNCLASSIFIED

SECURITY CLASSIFICATION OF THIS PAGE

REPORT DOCUMENTATION PAGE

1a. REPORT SECURITY CLASSIFICATION Unclassified			1b. RESTRICTIVE MARKINGS None		
2a. SECURITY CLASSIFICATION AUTHORITY			3. DISTRIBUTION / AVAILABILITY OF REPORT Approved for Public Release: Distribution Unlimited		
2b. DECLASSIFICATION / DOWNGRADING SCHEDULE					
4. PERFORMING ORGANIZATION REPORT NUMBER(S) S71-1180-1.0-1			5. MONITORING ORGANIZATION REPORT NUMBER(S) WL-TR-91-4150		
6a. NAME OF PERFORMING ORGANIZATION Honeywell Satellite Systems Operation		6b. OFFICE SYMBOL (If applicable) SSO		7a. NAME OF MONITORING ORGANIZATION Materials Directorate (WL/MLBT) Wright Laboratories	
6c. ADDRESS (City, State, and ZIP Code) 19019 N. 59th Avenue Glendale, AZ 85308			7b. ADDRESS (City, State, and ZIP Code) Wright-Patterson AFB, OH 45433-6533		
8a. NAME OF FUNDING / SPONSORING ORGANIZATION Materials Directorate		8b. OFFICE SYMBOL (If applicable) WL/MLBT		9. PROCUREMENT INSTRUMENT IDENTIFICATION NUMBER F33615-86-C-5015	
8c. ADDRESS (City, State, and ZIP Code) Wright-Patterson AFB, OH 45433-6533			10. SOURCE OF FUNDING NUMBERS		
			PROGRAM ELEMENT NO. 62102F	PROJECT NO. 2421	TASK NO. 01
11. TITLE (Include Security Classification) CYROGENIC MAGNETIC BEARING					
12. PERSONAL AUTHOR(S) James Andrus, John Kendig, John Kroeger					
13a. TYPE OF REPORT Final		13b. TIME COVERED FROM 11-1-85 TO 5-1-91		14. DATE OF REPORT (Year, Month, Day)	
				15. PAGE COUNT 91	
16. SUPPLEMENTARY NOTATION					
17. COSATI CODES			18. SUBJECT TERMS (Continue on reverse if necessary and identify by block number)		
FIELD	GROUP	SUBGROUP			
			Suspension Isolation Magnetic		
			Magnetic Bearing Cryogenic Cryogenic Bearing		
19. ABSTRACT (Continue on reverse if necessary and identify by block number)					
<p>Magnetic suspension provides an alternative to rolling-element bearings for some precision gimbal applications. The Cryogenic Magnetic Bearing program includes studies of magnetic suspension for a gimbal bearing requiring long life (greater than 7 years); low runout (less than 5 μrad bore-sight error due to runout); and low, uniform drag torque. Additionally, the bearing is to operate in an oscillating mode, from room-ambient (300°K) to liquid nitrogen (77°K) temperatures at ambient pressure and in a hard vacuum ($<10^{-6}$ torr).</p> <p>Two magnetic suspension alternatives were studied: an all-active approach using electromagnets to control all five bearing degrees-of-freedom and a Passive-Radial Active-Axial (PRAA) approach using passive magnetics to stabilize four of the five bearing degrees-of-freedom and an electromagnet to control the fifth. The all-active approach provides a lower-weight, better-accuracy bearing system than the PRAA system, but requires more quiescent operating power and is electrically more complex. The PRAA was selected for hardware study to produce a simple, low-power magnetic system.</p> <p>The PRAA bearing components were tested at the component level and were integrated into a bearing test fixture for bearing system testing. The active axial electromagnet tests showed agreement with analytical predictions. The passive bearing elements, however, had only about 20% of the radial restoring stiffness predicted analytically. The cause of this discrepancy has not yet been found. Some postulated causes have been studied, and others should be pursued in future research. Although bearing system testing was not completed before the end of the contract, results, to date, are presented in this report. Continued development of the precision magnetic bearing technology, building upon the knowledge base from this contract and other programs at SSO, is recommended.</p>					
20. DISTRIBUTION / AVAILABILITY OF ABSTRACT <input checked="" type="checkbox"/> UNCLASSIFIED/UNLIMITED <input type="checkbox"/> SAME AS RPT <input type="checkbox"/> DTIC USERS			21. ABSTRACT SECURITY CLASSIFICATION Unclassified		
22a. NAME OF RESPONSIBLE INDIVIDUAL K. Mecklenburg			22b. TELEPHONE (Include Area Code) (513) 255-2465		22c. OFFICE SYMBOL WL/MLBT

TABLE OF CONTENTS

	Page
LIST OF FIGURES.....	iv
LIST OF TABLES.....	v
LIST OF ACRONYMS.....	vi
1. INTRODUCTION.....	1
2. BACKGROUND.....	4
3. CRYOBEARING GIMBAL DESCRIPTION.....	6
3.1 Cryobearing 4-DOF Test Fixture.....	9
3.1.1 4-DOF System Description.....	9
3.1.1.1 Measuring Runout.....	17
3.1.2 Mechanical Description.....	20
3.1.3 Electromagnetic Component Description.....	23
3.1.3.1 Passive Radial Bearing - Design.....	25
3.1.3.2 Active Magnetic Actuator - Design.....	27
3.1.3.3 Angle Position Sensor.....	27
3.1.3.4 Torque Motor.....	29
3.1.4 Electrical Description.....	32
3.1.4.1 Bearing System Electronics.....	36
3.1.4.2 Bearing Test Electronics.....	40
4. TEST RESULTS.....	45
4.1 Magnetic Bearing Component Test Results.....	45
4.1.1 Passive Radial Bearing - Resultant Performance.....	45
4.1.2 Active Magnetic Actuator - Resultant Performance.....	47
4.2 Integrated Test Results.....	47
4.2.1 Geometric Deficiencies.....	50
4.2.2 Interface Shortcomings.....	50
4.2.3 Assembly Compliance.....	51
4.2.4 Impact on System Performance.....	62
5. CONCLUSIONS.....	64
6. RECOMMENDATIONS.....	66
APPENDIX - COSMOS/M ANALYSIS INPUT AND CASE A & K RESULTS.....	67

LIST OF FIGURES

Figure		Page
3-1	Cryobearing Magnetically Suspended Gimbal.....	7
3-2	Cryobearing System Interface Block Diagram.....	8
3-3	Passive Radial Magnetic Bearing Assembly.....	10
3-4	Active Axial Magnetic Bearing Assembly.....	11
3-5a	Magnetic Bearing Armature.....	12
3-5b	Magnetic Bearing Armature Tooth Detail.....	13
3-6	Passive Magnetic Bearing Parts.....	14
3-7	Active Axial Electromagnet.....	15
3-8	4-DOF Test Fixture.....	16
3-9	4-DOF Test Fixture Sketch.....	18
3-10	Flex Pivot Gimbal Assembly.....	22
3-11	Armature with Stops and Lower DIT Target.....	24
3-12	Actuator Configuration.....	26
3-13	Resolver Assembly.....	28
3-14	Torque Motor.....	33
3-15	4-DOF Electrical System Block Diagram.....	35
3-16	Active Axial Electronics Block Diagram.....	37
3-17	Active Axial Control Block Diagram.....	38
3-18	Active Axial Control Electronics Block Diagram.....	39
3-19	Actuator Linearization Block Diagram.....	41
3-20	Current-loop Magnetic Actuator Model.....	42
3-21	Gimbal Control Electronics Block Diagram.....	44
4-1	Magnetic Bearing Armature Interface.....	52
4-2	Two-point Armature Deflection Test Setup.....	54

LIST OF FIGURES (cont)

Figure		Page
4-3	Single-point Armature Deflection Test Setup.....	55
4-4	FEA Model and Results.....	58
4-5	FEA Model Displacement Results Plot.....	59
4-6	FEA Model Stiffness Plot.....	60
4-7	Two-dimensional Ideal Passive Actuator Magnetic Flux Paths...	63
4-8	Magnetic Flux Path Due Armature Tilt.....	63

LIST OF TABLES

Table		Page
1-1	Cryobearing Analyses.....	2
3-1	Active Axial Actuator Parameters.....	28
3-2	Resolver (1 Speed and 8 Speed) with Rotary Transformer (P/N 5430-10717).....	30
3-3	Torque Motor Trade-off Parameters.....	31
3-4	Brushless DC Torque Motor (P/N 5430-10716).....	34
4-1	Stiffness Evaluations.....	48
4-2	Active Magnetic Actuator Performance Summary.....	49
4-3	Cryobearing Magnetic Bearing Armature Stiffness Test Results.....	56

DTIC QUALITY INSPECTED 8

Accession For	
NTIS GRA&I	<input checked="" type="checkbox"/>
DTIC TAB	<input type="checkbox"/>
Unannounced	<input type="checkbox"/>
Justification	
By _____	
Distribution/	
Availability Codes	
Dist	Avail and/or Special
A-1	

LIST OF ACRONYMS

A/D	Analog to Digital
AFML	Air Force Materials Laboratory
BDC	Brushless Direct Current
CCA	Circuit Card Assembly
CDRL	Contract Data Requirements List
DAC	Digital to Analog Converter
DAE	Data Acquisition Electronics
DAS	Data Acquisition System
DIT	Differential Impedance Transducer
DOF	Degree Of Freedom
DRC	Digital to Resolver Converter
EDM	Electrical Discharge Machine
FMS	Force Measurement System
GCE	Gimbal Control Electronics
GMA	General Machining Assemblies
ICD	Interface Control Document
ID	Inside Diameter
I/O	Input/Output
IR&D	Independent Research and Development
KDST	K-Band Data S-Band Tracking
LVDT	Linear Variable-Differential Transformer
LVT	Linear Velocity Transducer
OD	Outside Diameter
PC	Personal Computer
PIO	Parallel Input/Output
PRAA	Passive Radial/Active Axial
RDC	Resolver to Digital Converter
RME	Runout Measurement Electronics
SRC	Systems and Research Center
SSO	Satellite Systems Operation

1. INTRODUCTION

This final report summarizes work performed at Honeywell Inc., Satellite Systems Operation (SSO), under contract F33615-86-C-5015 for the Aeronautical Systems Division/PMRRB of Air Force Systems Command at Wright-Patterson Air Force Base. Completion of this report satisfies Contract Data Requirements List (CDRL) 9 of this contract.

This report summarizes applied research relative to development of a magnetic gimbal bearing system. The system is to operate in an oscillating mode in both space vacuum and laboratory pressures and at cryogenic ($\sim 77^\circ\text{K}$) and laboratory ambient temperatures.

Section 2 introduces the background problem objectives and design considerations used during the design and development stages for the Cryogenic Magnetic Bearing (Cryobearing).

Section 3 briefly describes a preliminary gimbal design developed as part of this program. Details of this gimbal design are included in the Cryogenic Magnetic Bearing Biannual Report covering the period between 1 April 1988 to 30 September 1988. A limited Degree Of Freedom (DOF) magnetic bearing test fixture was designed and built to test the performance of the magnetic bearing that is baselined in the preliminary gimbal design. The test fixture and the magnetic bearing designs are presented in Section 3.1.

Bearing component tests were completed to evaluate performance relative to design predictions. System performance tests were initiated, but contract funds were expended prior to obtaining complete system performance test results. Although complete system data are not available, Section 4 presents bearing component data and integration test results that provide insight into the advantages and obstacles associated with the cryobearing magnetic gimbal bearing approach.

A list of analyses generated as part of this program is included in Table 1-1. These are separated into system, mechanical, electromagnetic, and electrical analyses. These analyses are referenced throughout this report, and reside in the program engineering files.

TABLE 1-1
CRYOBEARING ANALYSES

Analysis Number	Date	Description
0118.2.4-1	3-19-87	Component Specifications I
0118.2.4-2	3-11-87	Preliminary Cryobearing Forces and Position Bandwidth
0118.2.4-3	6-10-87	Preliminary Actuator Trade Studies
0118.2.4-4	6-15-87	Error Budget Analysis
0118.2.4-5	4-1-88	Preliminary Test Considerations
0118.2.4-6	12-11-87	Torque Motor Disturbance Assessment
0118.2.4-7	12-15-87	Destabilizing Torque/Unbalance Stiffness
0118.2.4-8	12-19-87	Use of Complimentary Filter to Eliminate Limit Cycle in KDST Position Loop
0118.2.4-9	1-27-88	Hysteresis Model Parameter Error
0118.2.4-10	1-29-88	Mag Actuator with Current Loop
0118.2.4-11	2-3-88	Actuator Model for Current Loop Operation
0118.2.4-12	2-11-88	Position Loop Nonlinear Analysis
0118.2.4-13	4-27-88	Cryobearing Gimbal Axis Control System Design
0118.2.4-14	4-20-88	Active Axial Control System Study
0118.3.4-1	5-26-87	Cryobearing; Mechanical, Thermal
0118.3.4-2	7-30-87	Cryobearing Conceptual Design
0118.3.4-3		** No Analysis **
0118.3.4-4	11-12-87	Cryoshroud for Cryo-Thermal-Vac Test of Cryobearing Subassemblies
0118.3.4-5	9-3-87	Cryobearing Telescope and Stub Shaft Thermal Analysis
0118.3.4-6		
0118.3.4-7		

TABLE 1-1 (cont)
CRYOBEARING ANALYSES

Analysis	Date	Description
0118.4.4-1	9-11-87	Connector Requirements (Cryobearing)
0118.4.4-2	11-9-87	Preliminary Electronics Conceptual Design
0118.4.4-3	6-16-88	Startup-Interlock Electronics Description
0118.4.4-4	6-18-88	Vacuum Electronics CCA Design
0118.4.4-5	8-15-88	Force Linearization Electronics
0118.4.4-6	11-30-91	Cryobearing Four DOF Electronics
0118.4.4-7	11-30-91	Cryobearing Electrical ICD
0118.5.4-1	6-15-87	Preliminary Magnetics Components Sizing
0118.5.4-2	11-3-87	Magnetic Suspension Configuration Tradeoffs
0118.5.4-3	12-1-87	Radial Unbalance Stiffness of Conventional BDC Motor
0118.5.4-4	7-28-88	Passive Bearing Fabrication Investigation
0118.5.4-5	10-14-88	Active Actuator Coil Bobbin Material Selection
0118.5.4-6	10-14-88	Suitability of 3M Co. 2216 B/A Epoxy for use to -150 deg C to Ambient
0118.5.4-7	1-23-91	Passive Radial Magnetic Bearing Evaluations
0118.5.4-7A	8-2-89	Torque Motor Radial Force Characterization
0118.5.4-8	7-16-91	Active Axial Magnetic Force Actuator Characterization Tests

2. BACKGROUND

The objective of the Cryogenic Bearing (Cryobearing) program was to develop a gimbal bearing to improve operating life (greater than 7 years) and pointing accuracy (less than 5 μ rad boresight error due to bearing runout) for bearings required to operate in an oscillating mode in both the vacuum of space and the air atmosphere of earth. The bearing should meet performance objectives at both cryogenic temperatures ($\leq 77^\circ\text{K}$) and at laboratory temperatures (300°K).

One technology that shows promise toward meeting specified objectives is that of magnetic suspension. A magnetic bearing system should magnetically levitate yet restrain its payload in all DOF except about the gimbal bearing rotational axis. This final "unrestrained" DOF is normally controlled with a brushless, DC torque motor.

Two magnetic bearing configurations were considered under the cryobearing contract: 1) an entirely active magnetic bearing system using an array of electromagnets to control motion in all DOF, and 2) a Passive Radial/Active Axial (PRAA) magnetic bearing system using permanent magnets to passively restrain radial motion and an electromagnet to control axial motion.

Major advantages of the "all-active" configuration include superior pointing performance, lower-weight magnetic components, and independent control of each DOF. Advantages of the PRAA approach include lower electrical complexity, lower quiescent operating power, and that no gravity offload fixtures are required to operate in Earth's gravity.

Initial magnetic suspension tradeoffs, reported in Analysis 0118.5.4-2 in November 1987, baselined the all-active suspension system primarily to achieve a minimum-weight, superior-performing payload suspension system. The passive radial bearings were excluded because the high radial stiffness (force/displacement) required to meet specifications resulted in a substantial weight penalty (approximately 13:1) over the all-active approach.

Although the all-active system provides the lowest-weight magnetic components and better accuracy than the PRAA systems, it incurs considerable electrical and interface complexity. The all-active approach also dissipates heat in a cryogenic environment. Electrical interface complexity and power needed to control all DOF penalizes the all-active system for use in practical cryogenic applications. Therefore, the PRAA-type bearing was selected for development based on the following:

- The cryogenic environment is sensitive to dissipated power.
- A new magnetic bearing idea showed promise in evening the radial-to-axial stiffness (force per displacement) ratio to nearly 1:1. This problem was identified with previous PRAA magnetic bearing designs (i.e., the Air Force Materials Laboratory (AFML) magnetically suspended reaction wheel) where the radial-to-axial stiffness ratio is about 1:7. With a 1:1 ratio, the gimbal bearing is self-supporting in any orientation in a lg environment. The self-supporting feature reduces test complexity.

- As a technology development program, the PRAA option appeared to hold greater potential for the required application and for future programs related to rotating interfaces with low to moderate cross-axis torque requirements.

To allow serious consideration of the PRAA system, the stiffness requirement for each of the two radial magnetic bearings was reduced from 62×10^6 N/m to 5×10^6 N/m. Lowering the required stiffness reduced the weight of the passive radial bearing elements. The radial bearing design predicted an axial unbalance stiffness approximately equal to the radial stiffness. Given the new stiffness, a 50-kg payload/rotor mass would be suspended with about a 0.05-mm radial offset (sag) in a 1g environment. The magnetic gaps were sized to accommodate this displacement during ground testing.

3. CRYOBEARING GIMBAL DESCRIPTION

A full description of the cryogenic magnetic gimbal is found in the biannual report for the period 1 April 1988 to 30 September 1988. This section provides a brief description of the major cryobearing gimbal components and operational functions.

The cryobearing magnetic gimbal consists of two passive radial magnetic bearing assemblies and an active axial magnetic bearing assembly. When combined as shown in Figure 3-1, translation along and rotation about the x and z axes is stabilized with the radial bearing assemblies. An active magnetic bearing controls translation along the y axis. A noncontacting, brushless, DC torque motor controls rotation about the y axis.

The cryobearing system is functionally distributed into five major subassemblies (see Figure 3-2):

- Axial control module
- Torque control module
- Gimbal yoke
- Simulated payload (dummy mass)
- System electronics

The axial control module and the torque control module are located on either side of the simulated payload. Each control module houses a passive radial bearing element. The axial module also contains the active axial electromagnetic actuator assembly, axial Differential Impedance Transducer (DIT) probes, and a Linear Velocity Transducer (LVT). The DIT probes provide axial (y axis) position feedback information and the LVT provides axial velocity feedback information; both are used to control motion along the gimbal y axis. The DIT probes and the LVT are noncontacting sensors so that contact between sensor stator and rotor elements is not required to obtain position or rate information.

In addition to a passive radial element, the torque module houses the gimbal torque motor and a resolver used for motor commutation and y axis rotational position feedback information. The two modules define the gimbal axis and are the interface between the payload (simulated telescope in Figure 3-1) and the yoke. The yoke has a provision for attachment to another gimbal axis or to the spacecraft.

System electronics include axial module electronics, torque module electronics, and command/telemetry control electronics, as shown in Figure 3-2. Axial module electronics provide DIT and LVT sensor conditioning, axial bearing control law implementation, and axial actuator drive electronics. Torque module electronics provide resolver processing, implementation of the gimbal position control compensation, and torque motor driver electronics. Command/telemetry control electronics process commands from and telemetry to the system host computer.

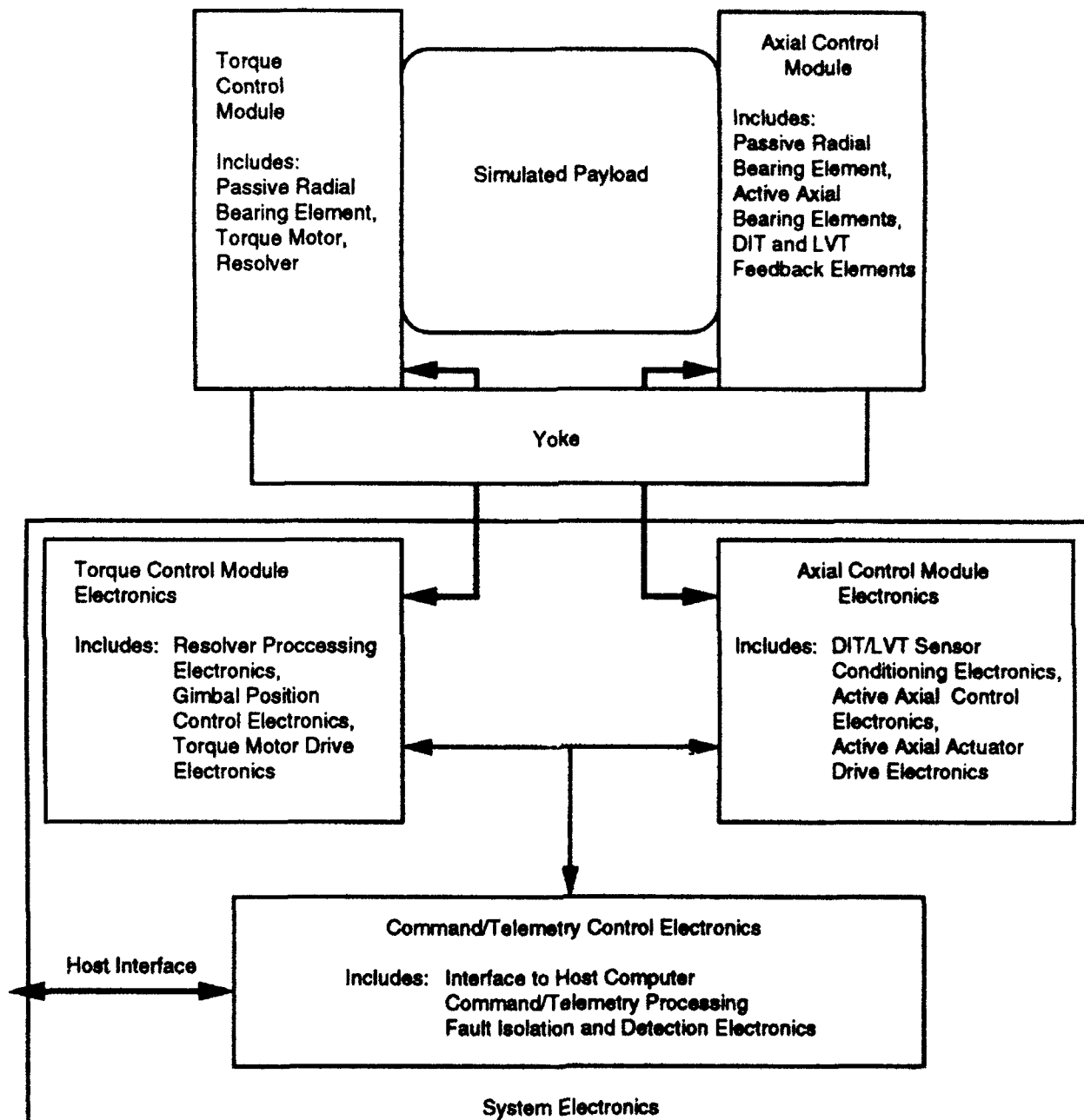


Figure 3-2. Cryobearing System Interface Block Diagram

Figure 3-3 shows the design of the passive radial magnetic bearing. The active axial assembly design is depicted in Figure 3-4. Figure 3-5 illustrates the armature, which is common to both passive radial and active axial magnetics. Figure 3-6 is a photograph of the passive radial bearing elements built under this program. Also shown is the magnetic bearing armature. Figure 3-7 shows one of the active axial actuators built and tested as part of the Cryobearing program.

In its unpowered state, the cryobearing payload rests against a set of mechanical hardstops held by the axial attractive force of the passive radial bearing assembly. A controlled startup profile generates currents through the active axial magnetic actuators to levitate the payload, lifting it from the axial (y axis) hardstops. The restoring forces along the radial axes (x and z) from the passive bearing assemblies center the payload and restrain subsequent motion along and about the x and z axes. The active axial control system seeks to position the magnetic armature within the magnetic gap so that minimum power is dissipated through the active actuator coils, while keeping the armature suspended.

Once the payload is levitated, the torque motor system is enabled to control rotational motion about the y axis. The biannual report for the period between 1 October 1987 and 1 April 1988 contains a detailed bearing control system design description for the cryogenic magnetic bearing.

3.1 Cryobearing 4-DOF Test Fixture

As an effect of limited program funding, the cryogenic magnetic gimbal depicted in Figure 3-1 was not built.

Though the reasons for having a fully functional gimbal axis seem overwhelming, the key bearing performance parameters are measured at reduced cost with a simplified approach. Such an approach has the disadvantage of limiting the development scope to the cryogenic magnetic bearing assembly rather than testing the gimbal application. The advantage, however, is that it separates the effects of subsystems present in the gimbal assembly and focuses on the bearing element, which is the focal point of the program. To focus efforts on the bearing, the program was restructured to concentrate on the building and test of the PRAA magnetic bearing and a 4-DOF test fixture.

3.1.1 4-DOF System Description

A single passive radial magnetic bearing assembly, integrated with the active axial magnetic bearing assembly, can be functionally tested using the 4-DOF test fixture shown in Figure 3-8. The 4-DOF test fixture provides a test bed to obtain bearing runout and drag torque data at room ambient and LN₂ (77°K) temperatures.

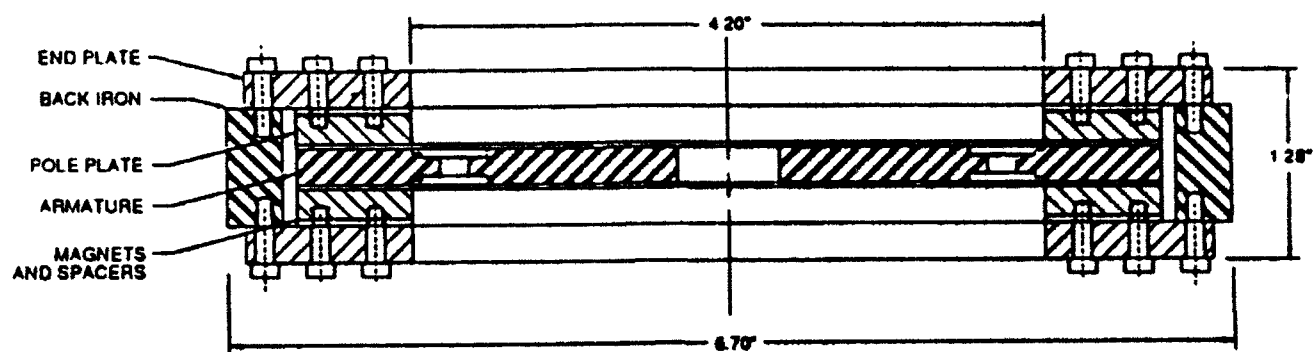


Figure 3-3. Passive Radial Magnetic Bearing Assembly

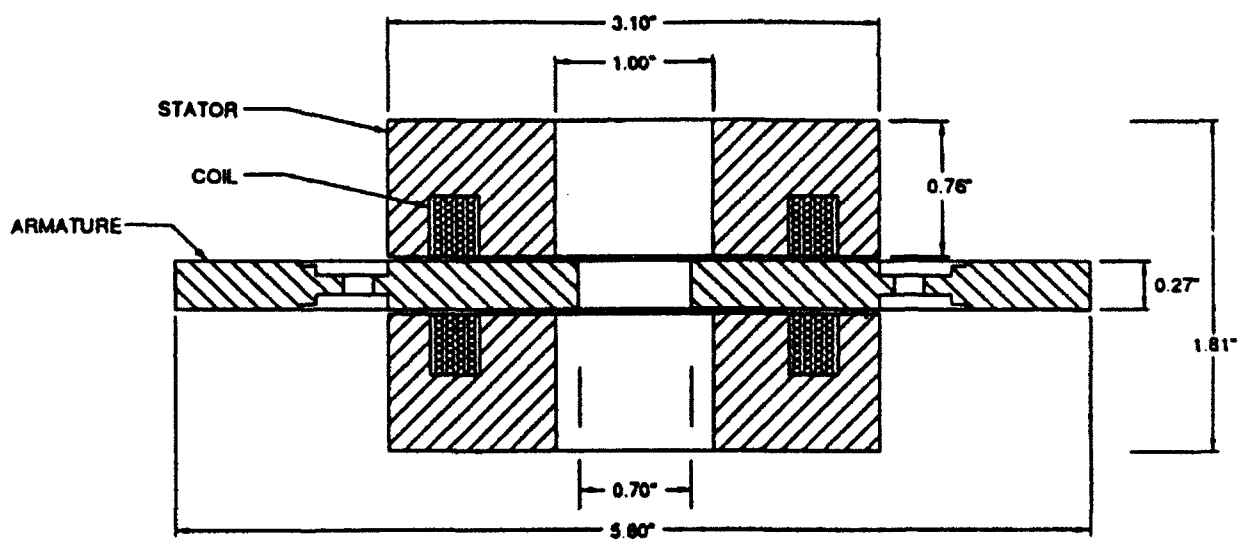
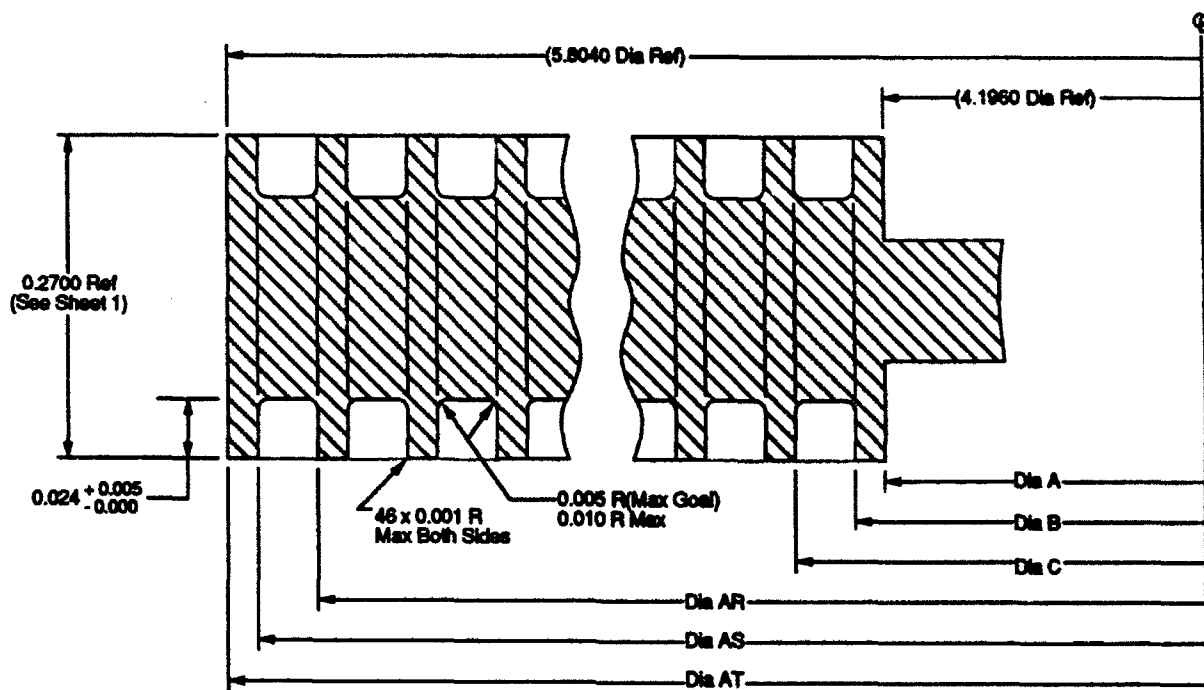


Figure 3-4. Active Axial Magnetic Bearing Assembly



Note:

1. All diameters are basic and shall be

± 0.005 C90 A

(Goal ± 0.0001)

Exploded View of Ring
Surface Areas

Dia No.	Dia Dimension	Dia No.	Dia Dimension
A	4.1980	X	5.0120
B	4.2200	Y	5.0600
C	4.2680	Z	5.0840
D	4.2920	AA	5.1320
E	4.3400	AB	5.1560
F	4.3640	AC	5.2040
G	4.4120	AD	5.2280
H	4.4360	AE	5.2760
I	4.4840	AF	5.3000
J	4.5080	AG	5.3480
K	4.5560	AH	5.3720
L	4.5800	AI	5.4200
M	4.6280	AJ	5.4440
N	4.6520	AK	5.4920
O	4.7000	AL	5.5160
P	4.7240	AM	5.5640
Q	4.7720	AN	5.5880
R	4.7960	AO	5.6360
S	4.8440	AP	5.6600
T	4.8680	AQ	5.7080
U	4.9160	AR	5.7320
V	4.9400	AS	5.7800
W	4.9880	AT	5.8040

Figure 3-5b. Magnetic Bearing Armature Tooth Detail

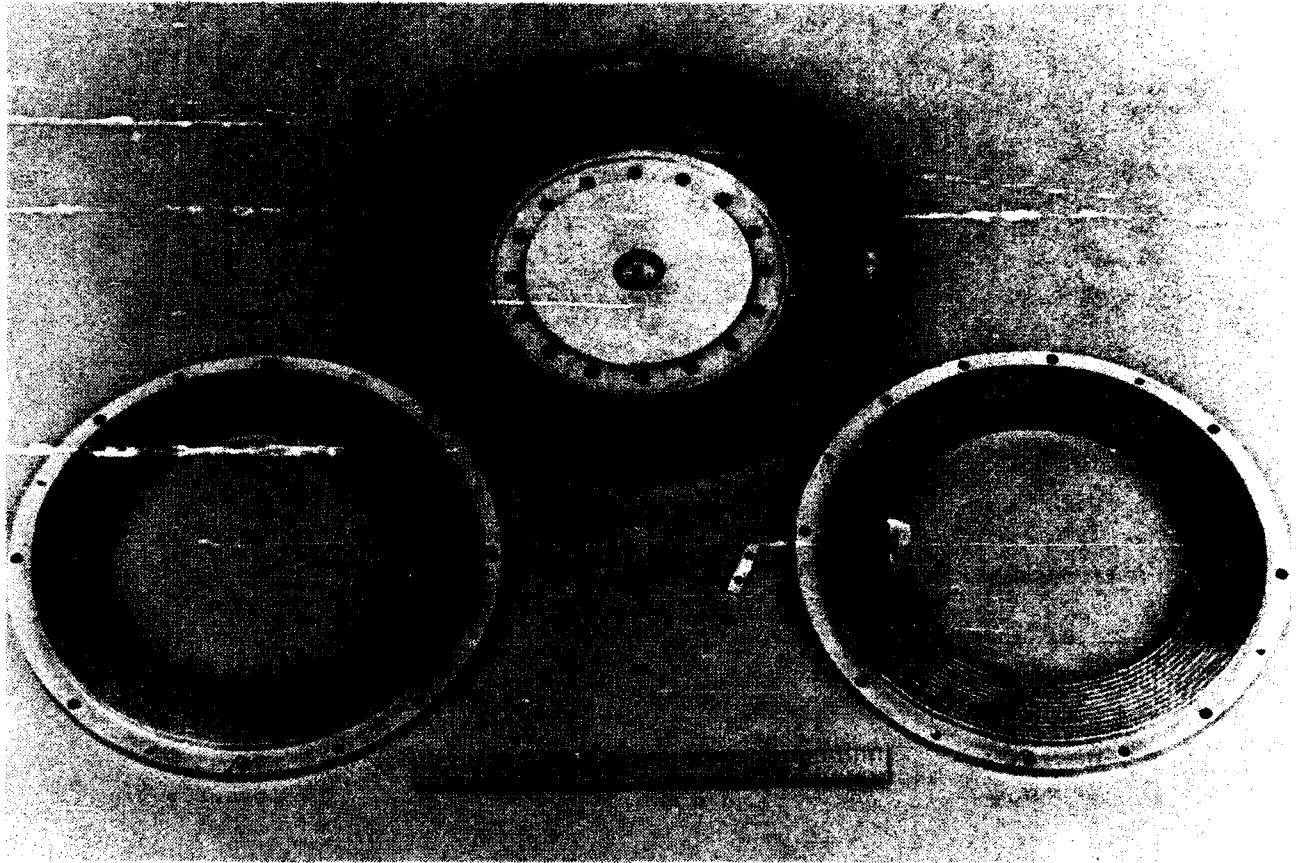


Figure 3-6. Passive Magnetic Bearing Parts

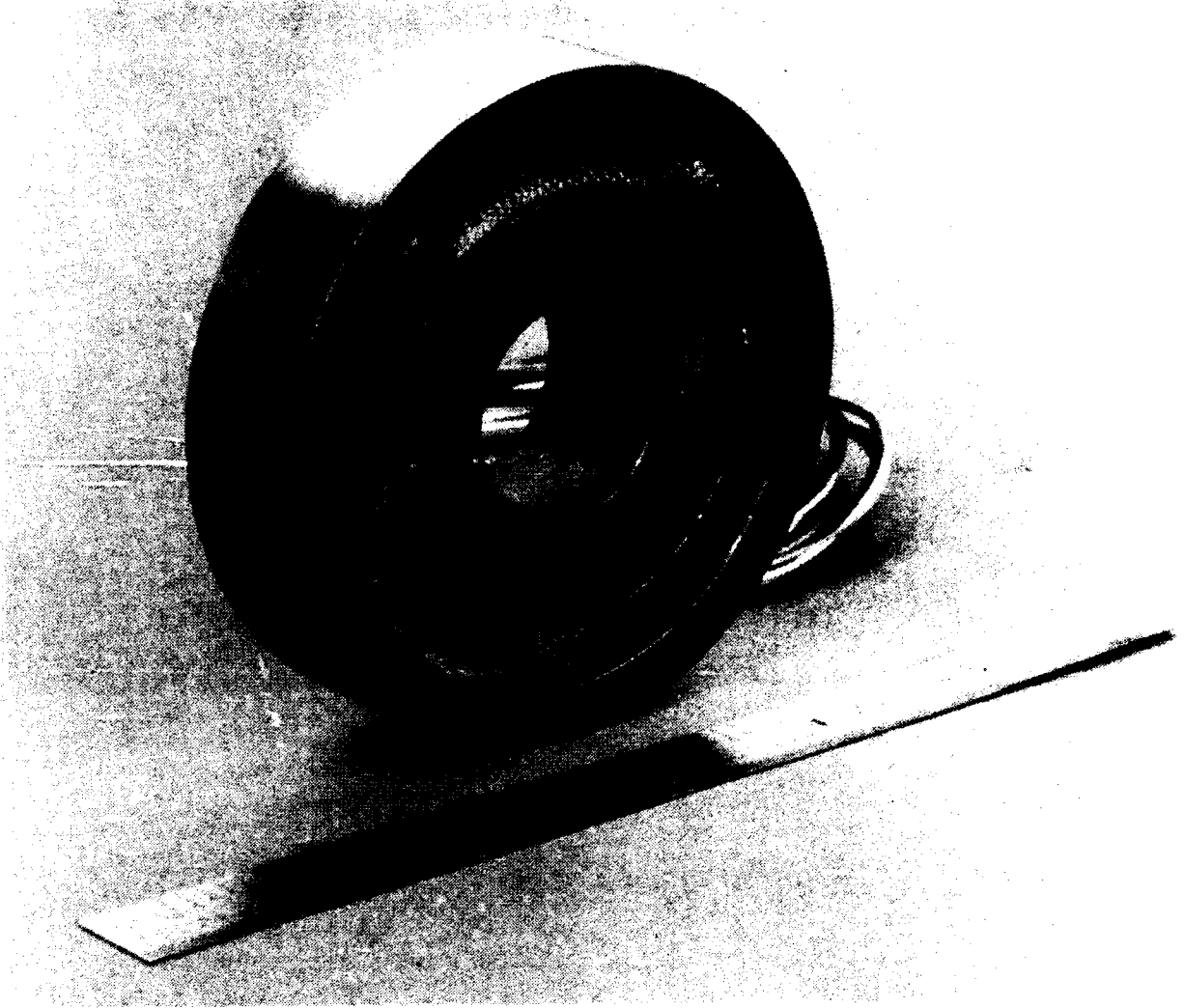


Figure 3-7. Active Axial Electromagnet

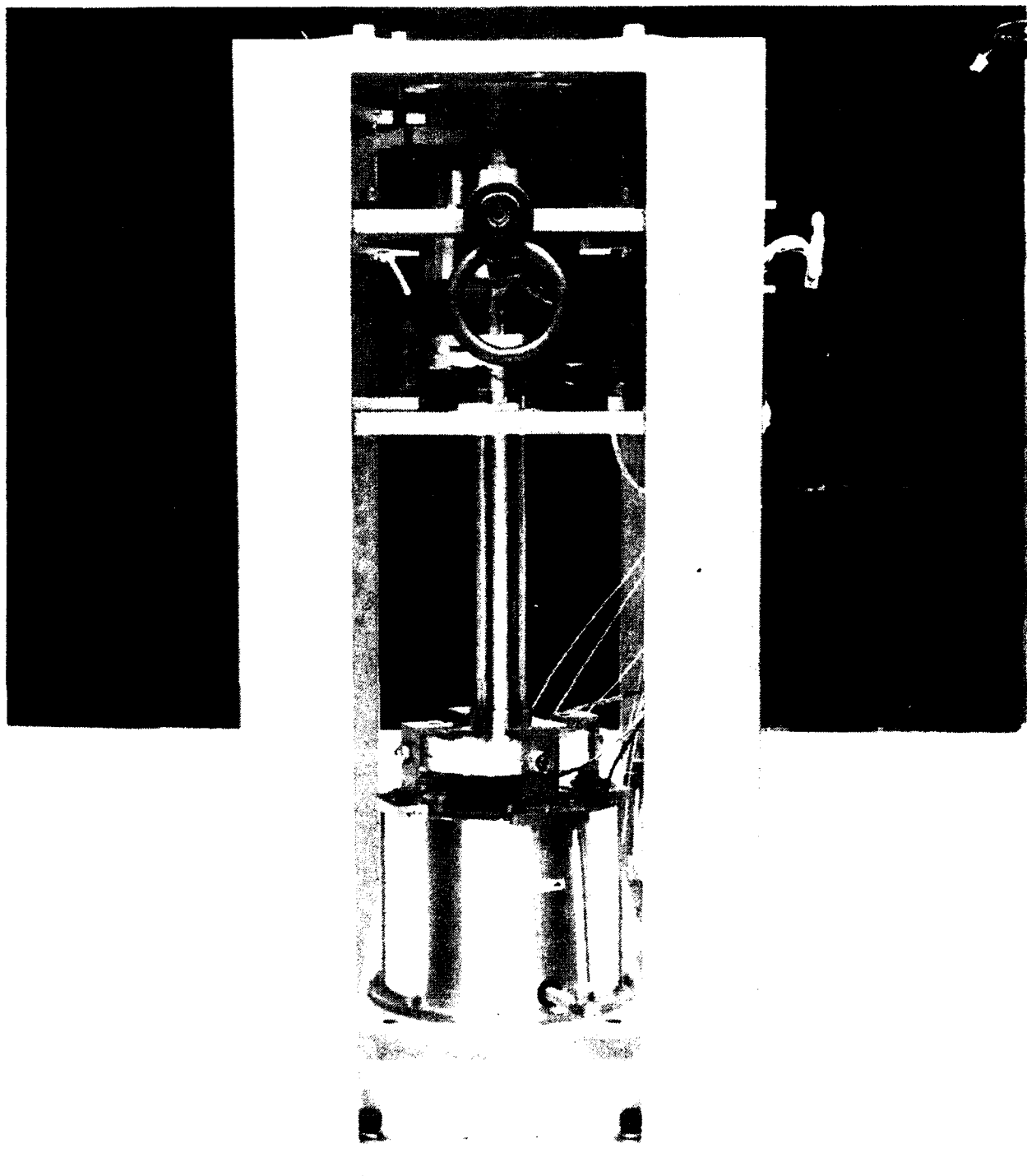


Figure 3-8. 4-DOF Test Fixture

The 4-DOF fixture allows 4 degrees of unrestricted motion at the armature-stator bearing interface, and restrains motion in the remaining 2 DOF. The magnetic bearing stator reference frame is defined in Figure 3-9. The y axis lies along the bearing rotational axis and the x-z plane lies parallel to and centered between the stator pole face surfaces. The fixture should restrain rotational motion of the magnetic bearing armature relative to the stator sections about the x and z axes. Translation of the armature relative to the stator, parallel to the x and z axes, is unrestricted by the test fixture, but is restrained via restoring forces of the passive magnetic bearing assembly. The active magnetic bearing controls motion along the y axis. The final DOF (rotation about the y axis) is controlled through a brushless, DC torque motor.

Two DIT targets are mounted to the main fixture shaft. Four DIT probes at each target measure target displacement parallel to the x-z plane. Four DIT probes at the bottom target measure target motion along the y axis. The DITs provide displacement information to characterize bearing runout performance and to provide position feedback to the axial magnetic bearing control system. The runout measurement concept is described briefly later in this section.

A Force Measurement System (FMS), mounted at the base of the test fixture, measures dynamic forces and torques exerted at its mounting plate relative to the fixture base plate. Given a rigid base, when the armature is suspended in the magnetic gap, the forces and torques measured by the FMS represent the forces and torques across the magnetic bearing interface. This setup allows direct measurement of drag torque and internal disturbance forces and torques transmitted through the magnetic bearing interface.

When filled with liquid nitrogen, the tub surrounding the magnetic bearing assembly cools the bearing assembly to approximately 77°K.

3.1.1.1 Measuring Runout

An ideal bearing will rotate about the y axis without perturbations in any remaining DOF. Runout, defined for the cryobearing, is translation of the armature with respect to the stator reference frame as a function of rotational motion about the y axis. In the gimbal configuration of Figure 3-1, x-z translation of one bearing module armature relative to the other, results in a telescope boresight rotational pointing error. The bearing test fixture is used to measure radial (armature motion in the x-z plane as a function of rotation about the y axis) and axial (armature motion along the y axis as a function of rotation about the y axis) runout.

The design goal for radial runout is 1 μm (0.00004 in). This translates to 5 μrad of boresight rotation given a 0.4 m bearing span. Axial runout is less important from a line-of-sight argument, but from a control and induced vibration perspective, the axial variation also should be small. The axial runout goal for cryobearing is 25 μm (0.001 in) about its nominal operating point.

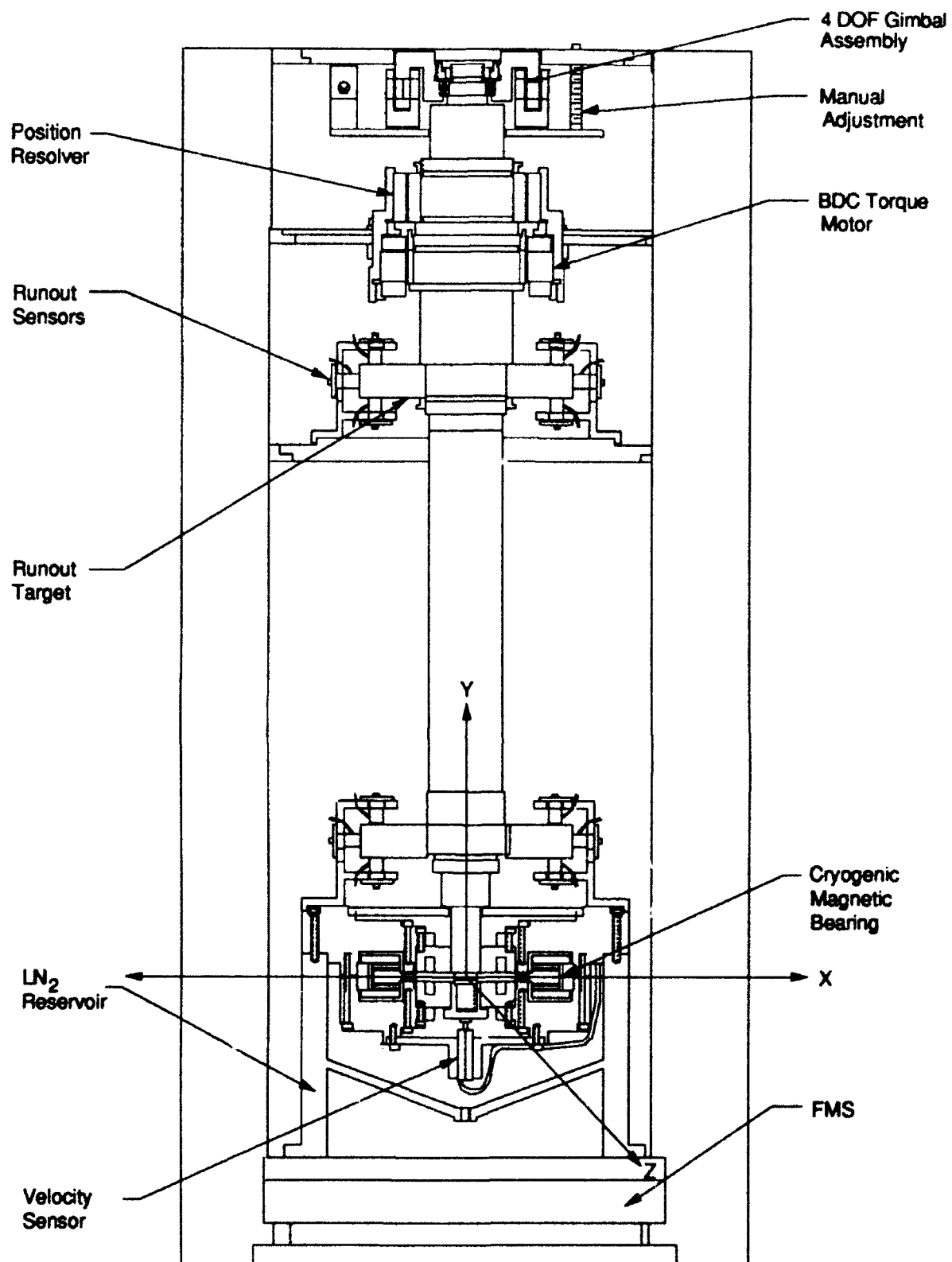


Figure 3-9. 4-DOF Test Fixture Sketch

DIT proximity sensors measure radial translation of the rotor shaft relative to the test fixture frame at two precision targets separated by a known distance along the shaft. With the bearing suspended and the armature rotating, radial runout measurement consists of three major components:

1. Radial runout of the passive magnetic bearing assembly
2. Eccentricity and surface irregularities of the DIT targets about the y axis in the plane of the DIT target
3. Radial runout of the ball bearing located at the shaft end opposite the magnetic bearing assembly

Components 2 and 3 are measured and subtracted from the total runout measurement to obtain the net magnetic bearing runout performance. This yields good results since the dominant components of 2 and 3 are repeatable from revolution to revolution. An angular resolver having a resolution of 0.0055° provides a rotational datum for each measurement.

With the bearing system suspended, a datum block (V-Block) is placed against the lower DIT target surface so that the DIT target displaces approximately $25\text{ }\mu\text{m}$ (0.001 in) from its centered position at $\Theta = 0.0 \pm 0.01^\circ$. The shaft is rotated at $\Theta = 1.0 \pm 0.1^\circ$ increments about the y axis. Proximeter and resolver measurements are recorded by a data acquisition system at each incremental position. Data are averaged over five revolutions, with peak and mean variations recorded for each data point. The process is repeated three additional times with the datum block locations approximately 120° apart. The same measurement process is repeated with the datum block against the upper target surface, pushed against the surface to measure $-25\text{ }\mu\text{m}$ of displacement at the lower DIT interface.

The datum block, against a target surface, provides direct measurement of Component 2. The proximeters at the other target measure variations due to Components 2 and 3. Having a direct measurement of Component 2 for each target and knowing the influence of 3 over a fixed geometry allows separation and identification of Components 2 and 3 as a function of bearing rotation. With Components 2 and 3 identified, the bearing is rotated without the datum block and Components 2 and 3 subtracted to obtain the passive magnetic bearing radial runout as a function of bearing rotation.

The axial runout component is measured similarly, except the axial runout of the ball bearing is not required for this measurement. Calibration about a datum at the lower axial surface is sufficient to obtain the passive magnetic bearing axial runout as a function of bearing rotation.

3.1.2 Mechanical Description

The driving mechanical requirements on the 4-DOF test fixture are as follows:

1. Temperature: Operational from 77 to 300°K
2. Pressure: Operational between room ambient and a hard vacuum
3. Suspended Mass: Variable over the range from 25 to 50 kg
4. DOF:
 - a. Unlimited rotation about bearing axis (DOF 1)
 - b. Translation along bearing axis (DOF 2)
 - c. Rotations normal to bearing axis (DOF 3 and DOF 4)

The hardware resulting from these fixture requirements is shown in Figure 3-8.

A cutaway of the 4-DOF test fixture with the cryogenic magnetic bearing installed for testing is shown in Figure 3-9.

The cryogenic magnetic bearing test fixture is a reinforced box frame with base dimensions of 18.0 inches on each side. The complete assembly ready for test is roughly 41.0 inches tall.

Fabrication of the entire test fixture is from 300 series stainless steel. Selection of 300 series stainless steel not only assures compatibility with the pressure environments but also minimizes thermal differential growths over the test temperature range of 77 to 300°K.

The fixture is the primary support structure, with adapters to attach functional elements. The number of interfaces is minimal to optimize rigidity. The primary structure has 0.5-inch-thick structural angles at each corner. These are welded to a 1.0-inch-thick baseplate, two 0.75-inch-thick intermediate plates and a 1.0-inch-thick top plate.

The construction yields one integrated structure to achieve maximum rigidity while retaining assembly simplicity. The configuration yields a compact, stand-alone unit with all forces and reactions contained within the unit itself. This makes all test measurements independent of fixture location or mounting.

The stator element for the cryogenic magnetic bearing is encased in a two-piece "clam shell" housing. This housing is recessed into a support that functions as a reservoir for liquid nitrogen for low temperature testing, and as a rigid interface to the FMS. Air vents into the bearing housing eliminate any trapped air and moisture for

low-temperature operation. An external fill and drain port allows replenishment of liquid nitrogen without interruption of test operations. Condensate buildup and loss of liquid nitrogen during low temperature testing are minimized with a removable fiberglass cover.

The liquid nitrogen reservoir affixes to a 1.25-inch-thick G-10 fiberglass plate. Independent of the nitrogen reservoir, the fiberglass plate is secured to the top of the FMS. This arrangement minimizes thermal losses during cryogenic testing and serves to thermally isolate the FMS, preventing the FMS from exposure to damaging temperatures.

The base of the FMS bolts to the baseplate of the bearing test fixture. This allows the FMS to directly measure reaction forces and torques produced by the cryogenic magnetic bearing in all 6 DOF.

The magnetic bearing armature is suspended in the magnetic gaps of the stator by means of a shaft mounted to a 4-DOF gimbal. This 4-DOF gimbal assembly attaches to the top plate of the cryogenic test fixture. One DOF is provided by a set of preloaded ball bearings identical to those used in Honeywell's antenna pointing systems. These bearings allow unlimited rotation about the magnetic bearing axis.

A system of flex pivots allows limited angular travel about both axes normal to the magnetic bearing rotational axis, which provides 2 additional DOF. By this means, small angular misalignments attributable to the test setup are removed, allowing the magnetic bearing to center itself so true runout of the cryogenic bearing can be measured.

An additional set of flex pivots are offset from the magnetic bearing axis. This is the fourth DOF of the test setup. The motion afforded by this arrangement allows the bearing rotor elements to translate axially along the magnetic bearing axis, enabling the cryogenic magnetic bearing to be operated over its range of magnetic gaps. For measurements at fixed magnetic gap locations, a manual mechanical adjuster disables this axial DOF, locking the magnetic bearing at a specific gap. The mechanical adjuster does not affect the other 3 DOF.

Figure 3-10 is a photo of the top portion of the test fixture. The 3 DOF flex pivot gimbal assembly and the mechanical adjuster are seen at the top of the figure. Ball bearings are housed within the flex gimbal assembly and are not visible in the view shown. The shaft to which the cryogenic magnetic bearing armature attaches is seen suspended from the 4-DOF gimbal in the figure.

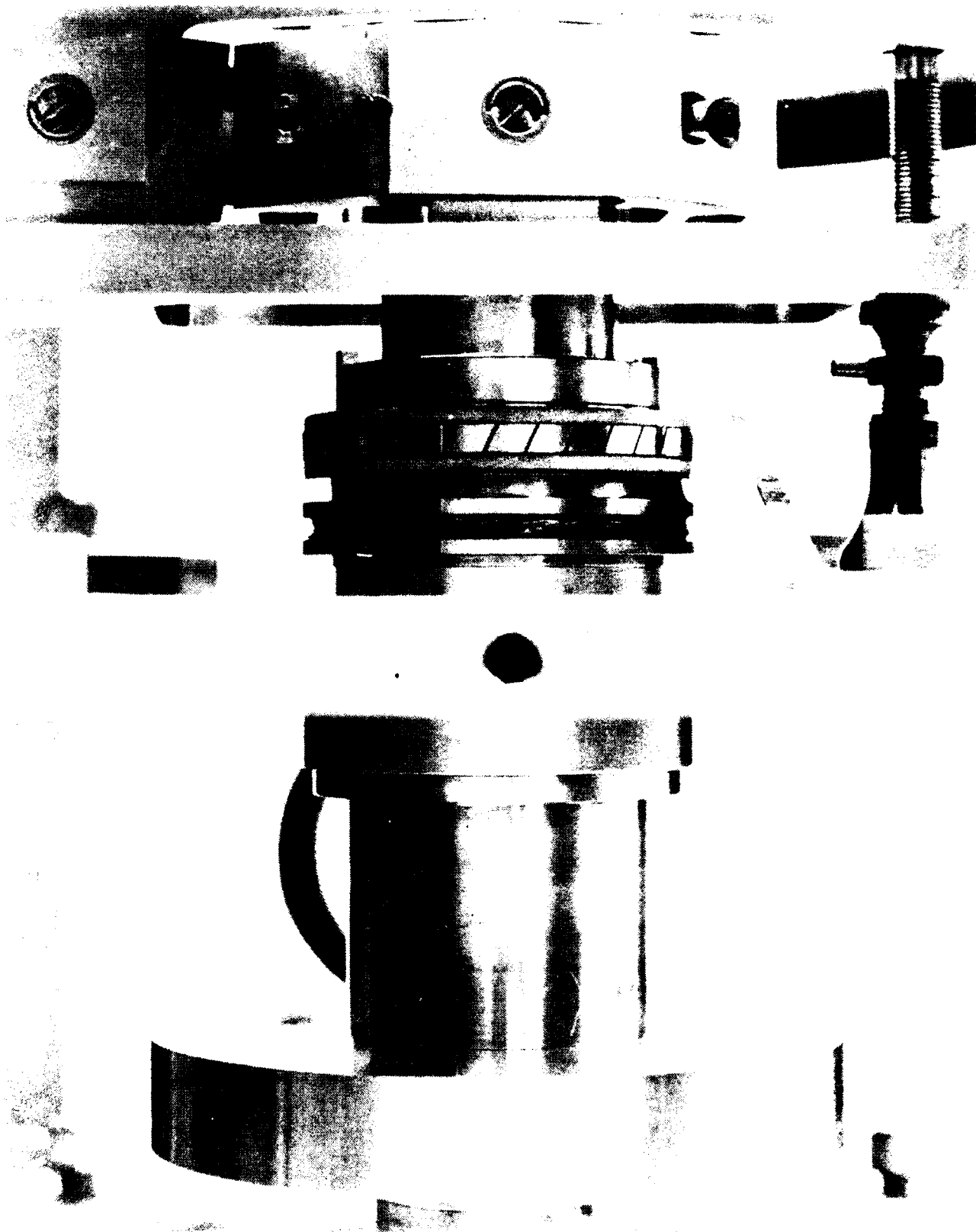


Figure 3-10. Flex Pivot Gimbal Assembly

Touchdown of the magnetic bearing surfaces is prevented by a set of stops mounted to both sides of the bearing housing. These operate in the stop ring recesses of the armature and are sized to establish the nominal operating gaps of ± 0.005 inch along the y axis. The stops also prevent the armature from moving more than a fraction of a magnetic tooth radially. This ensures that the magnetic bearing can passively return to its nominally centered and aligned orientation, regardless of events.

Rotation of the shaft and magnetic bearing armature about the magnetic bearing axis is provided by a brushless, DC, direct-drive torque motor mounted on the 4-DOF-gimbal end of the shaft. This is the motor that was to be used in the cryogenic magnetic gimbal. The motor has small ripple and cogging torques, which when combined with its location far removed from the magnetic bearing under test, minimizes its affect on the magnetic bearing operation. Incorporation of the motor into the test fixture enables testing to be performed in any environment and bearing rotational control to be removed as a factor in the runout measurements.

A transformer-coupled, two-speed resolver provides angular location for correlation with the runout data. This device also is used to electronically commutate the torque motor.

Runout is measured by a series of DIT probes placed around the shaft assembly at two widely separated axial locations. The targets for the DIT probes are two aluminum disks thermally fitted and then mechanically attached to the shaft. The targets can be located by referring to Figures 3-8 and 3-9. Figure 3-8 shows the targets covered with masking tape to protect them from damage during integration operations.

Figure 3-10 shows the torque motor and resolver armatures attached to the shaft below the gimbal assembly. The upper runout target is seen at the bottom of the photo.

Figure 3-11 is a photo of the bottom of the shaft assembly. In this photo the magnetic bearing stator and fixed portions of the test fixture are not shown. The cryogenic magnetic bearing armature can be seen attached to the end of the shaft. Above the magnetic bearing armature is the lower runout target.

The portion of the shaft between the targets is used to mount modular weights. One of these is shown at the top of Figure 3-11. Modular weights allow the mass of the suspended body to be varied as required.

3.1.3 Electromagnetic Component Description

As previously mentioned, the baseline gimbal system includes two radial bearings that provide passive positioning for 4 DOF (two radial offset directions and the two rotations of the bearing axis). Also included is an active, cup-style axial actuator stabilizing the fifth DOF along the bearing axis. The passive radial and active axial designs are described in the ensuing sections.

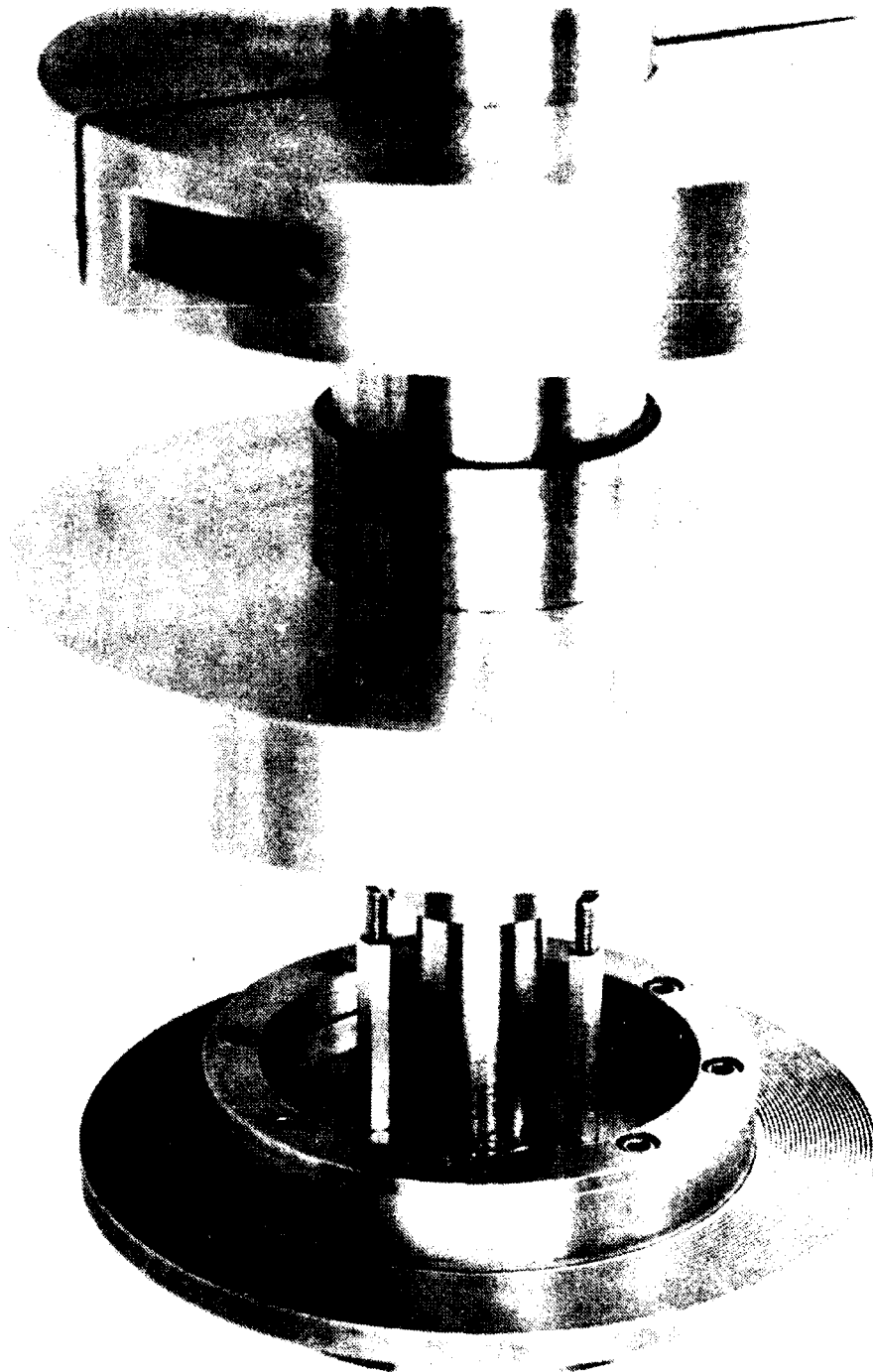


Figure 3-11. Armature with Stops and Lower DIT Target

3.1.3.1 Passive Radial Bearing - Design

The passive radial bearing includes a unique configuration designed to achieve approximately equal stiffness (radial restoring stiffness to axial unbalance stiffness).

Radial bearing requirement goals were established as follows:

Radial Stiffness (K_r)	5×10^6 N/m (28.6×10^3 lb/in)
Axial Unbalance Stiffness (K_u)	-5×10^6 N/m (28.6×10^3 lb/in)
Radial Range	± 0.13 mm minimum (± 0.005 in)
Axial Range	± 0.13 mm minimum (± 0.005 in)

Design characteristics for each radial actuator are as follows:

Initial Stiffnesses	
Radial (K_r)	5.0×10^6 N/m (28.3×10^3 lb/in)
Axial Unbalance (K_u)	-4.6×10^6 N/m (-26.4×10^3 lb/in)

Mechanical Features	
Teeth Per Surface	23
Tooth Width	0.30 mm (0.012 in)
Valley Width and Depth	0.61 mm (0.024 in)
Gap	0.20 mm (0.008 in)
Operating Range	
- Axial	0.13 mm (0.005 in)
- Radial	0.20 mm (0.008 in)

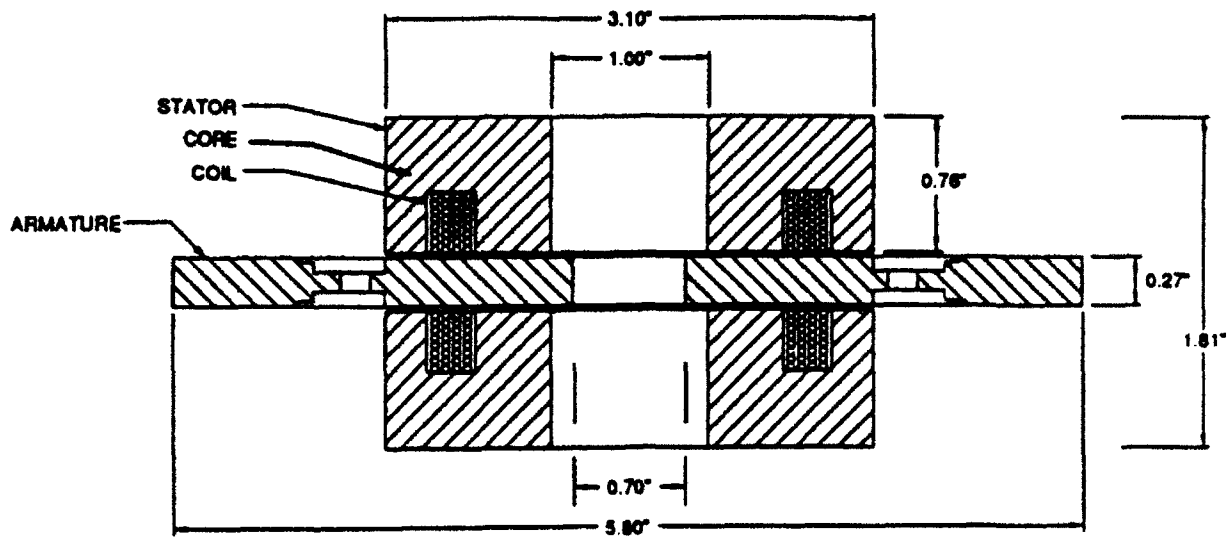
Weight *	
Stator	2.2 kg (4.8 lb)
Armature	0.4 kg (0.9 lb)
Total	2.6 kg (5.7 lb)

* Weights shown are magnetics design values, but are expected to increase due to mechanical requirements and assembly integration constraints.

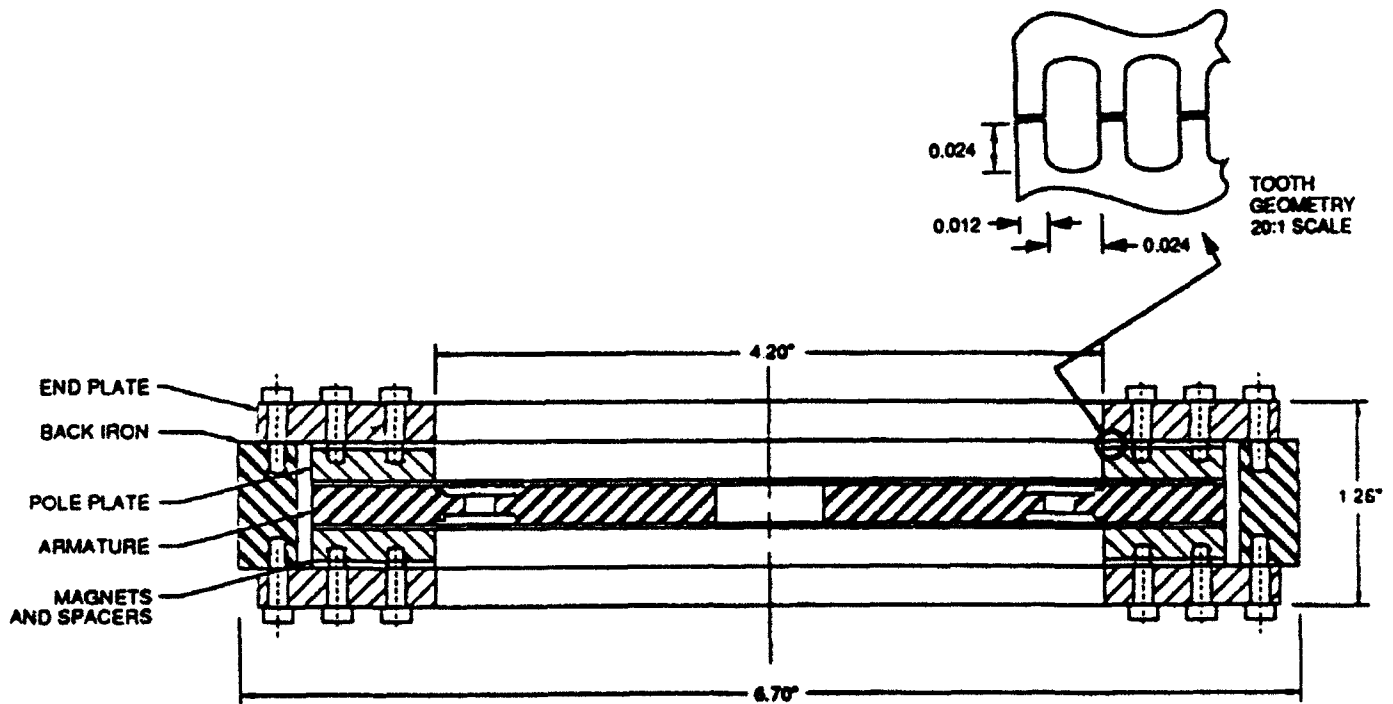
Two passive bearings were designed to produce the following forces:

- Radial Force at 0.05 mm (0.002 in) Radial Offset: 480 N (108 lb); to suspend payload and rotor in lg, axis horizontal
- Axial Force at 0.05 mm (0.002 in) Axial Offset: 485 N (109 lb); to suspend payload and rotor in lg, axis vertical.
- Axial Force at 0.13 mm (0.005 in) Axial Offset (at axial stops): 1560 N (350 lb); force must be overcome by the axial actuator when payload and rotor are lifted from the stops.

The basic mechanical configuration is shown in Figure 3-12.



Active Axial Actuator



Passive Radial Actuator

Figure 3-12. Actuator Configuration

3.1.3.2 Active Magnetic Actuator - Design

The active actuator is a cup-style, electromagnet-type actuator designed to the following requirement set:

Axial operating range	± 0.13 mm (± 0.005 in)
Peak force (linear region)	± 600 N (± 135 lb)
Peak force (saturation region)	± 2450 N (± 550 lb)

The above peak force level requirement was determined as follows:

Lift-off from the stops against attractive force of passive bearing	1560 N	(350 lb)
Lift-off and suspend payload and rotor weights	490 N	(110 lb)
Margin (-20%)	<u>400 N</u>	<u>(90 lb)</u>
TOTAL FORCE REQUIRED	2450 N	(550 lb)

Having selected the peak force level needed for lift-off with the actuator core in saturation, the maximum force available in the linear operating region is approximately 1250 N (280 lb), easily meeting the 600 N requirement.

The flux feedback method of controlling force provides an actuator system that minimizes actuator-induced errors; however, for this application, it is possible to achieve adequate performance using current and position feedback. To operate the actuator using flux feedback requires a nominal magnetic gap at 1 mm (0.040 in), 0.7 mm for Hall effect device, 0.13 for the motion range and 0.17 for clearance. Without the flux sensor, the nominal magnetic gap reduces to about 0.25 mm (0.010 in). A design was selected to operate at the 1 mm nominal gap and also to be well suited to operate at a 0.25 mm gap at lower power levels.

The actuator design parameters over the two proposed gap ranges are presented in Table 3-1. Actuator design is shown in Figure 3-12, with weights for this configuration as follows:

Stator (each of 2)	0.73 kg	(1.6 lb)
Armature	0.27 kg	(0.6 lb)
Total actuator	1.73 kg	(3.8 lb)

3.1.3.3 Angle Position Sensor

The angle position sensor is a brushless, multispeed resolver. The resolver assembly consists of a rotary transformer and a multispeed resolver mounted in a common set of rotor and stator sleeve housings (Figure 3-13). The rotary transformer transfers the resolver excitation signal from the stator element to the rotor.

TABLE 3-1
ACTIVE AXIAL ACTUATOR PARAMETERS

GAP (mm) [in]	AT FORCE = 1250 N (280 lb)			AT FORCE = 2450 N (550 lb)		
	Power (watts)	Current (amps)	Voltage (volts)	Power (Watts)	Current (amps)	Voltage (volts)
0.13 [0.005]	8	1.0	8	20	1.6	13
0.25 [0.010]	26	1.8	15	65	2.9	23
0.38 [0.015]	55	2.6	21	138	4.1	33
0.89 [0.035]	269	5.8	46	675	9.2	73
1.02 [0.040]	346	6.6	53	865	10.4	83
1.14 [0.045]	432	7.3	59	1080	11.6	93

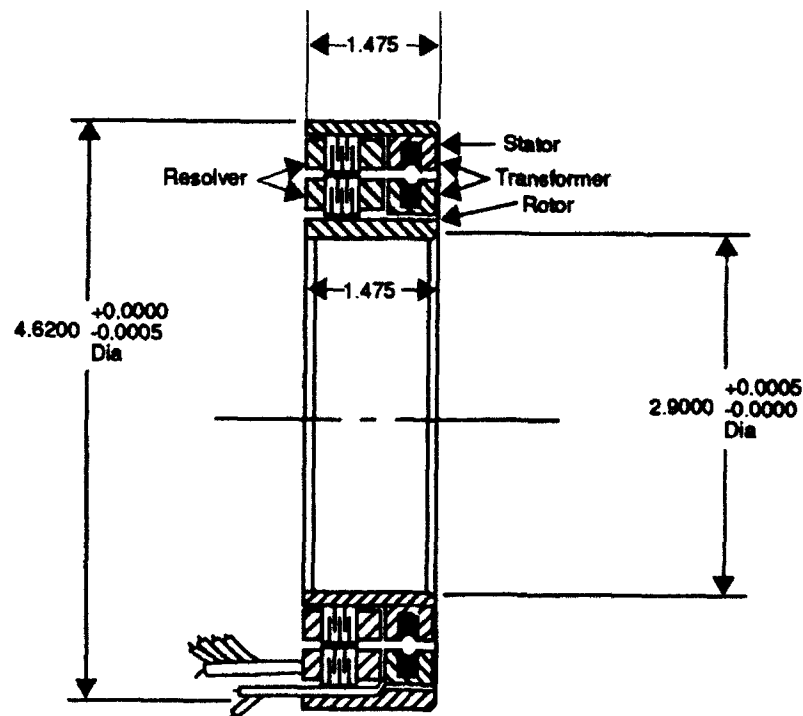


Figure 3-13. Resolver Assembly

The resolver is multispeed, consisting of both a single-speed channel and an eight-speed channel, with the windings for both channels wound on a common set of lamination stacks. The resolver rotor contains an excitation winding for each channel, with the two windings connected in parallel and fed from the transformer rotor. The resolver stator contains four discrete output windings. The two single-speed output windings provide signals at the same frequency as the excitation (2500 Hz), with amplitudes proportional to the sine and cosine of the mechanical angle between the rotor and stator elements from a reference zero angle position. The single-speed resolver function is to provide coarse position information.

The other two stator windings provide output signals with amplitudes proportional to the sine and cosine of eight times the mechanical angle. The eight-speed resolver is capable of much lower angular error than the single-speed (see Table 3-2); however, the single-speed is still needed to resolve ambiguity due to the eight-speed resolver repetition every 45 degrees. The eight-speed resolver function is to provide fine position information and commutation signals for the 16 pole (eight-speed) torque motor.

The resolver was purchased with internal, capital equipment funds. The established specification values and the vendor's acceptance test performance for the resolver are provided in Table 3-2.

3.1.3.4 Torque Motor

A motor to provide rotational torque about the bearing axis was required. The motor selected was a conventional (iron-core stator) brushless, DC motor with 4 ft-lb minimum torque capability.

An ironless-armature torque motor is often used with magnetic suspension systems because it produces no drag torque, cogging torque, or side forces. The armature (stationary element) in this type of motor consists of only the windings and a nonmagnetic support structure. With no core material on the armature, there is essentially no magnetic interaction between elements to cause anomaly torques and forces. Evaluation of available and other potential designs concluded that there were no suitable existing designs and a custom design would be required. Acceptable torque and power levels were established and an ironless-armature design was determined and compared against a conventional (iron-core stator) torque motor. These tradeoffs, summarized in Table 3-3, concluded that the size and weight penalties incurred by the ironless-armature motor overshadowed the low anomaly torque/force benefits. Primary considerations, excluding the ironless-armature motor, were as follows:

- Rotor weight is about three times that of the selected conventional motor. This would be acceptable for the demonstration, but would exclude it from a flight system.

TABLE 3-2
RESOLVER (1 SPEED AND 8 SPEED) WITH ROTARY TRANSFORMER
(P/N 5430-10717)

Parameter	Spec Value	Test Value
Angular Sensor Type	Brushless, Multispeed Resolver with Rotary Transformer	
Operating Temperature Range	-150°C to +70°C	Same
OD (in)	4.620	Same
ID (in)	2.900	Same
O A Length (in)	1.475	Same
Excitation (V rms / Hz)	7 / 2500	Same
Input Impedance (ohms)	100 + j150*	20 + j35
Input Current (amps-rms)	0.04 maximum*	0.174
Input Power (watts)	0.25 maximum*	0.603
1 Speed Resolver Channel		
Output Voltage (V rms)	3.5 ± 5%	3.43
Phase Shift (Deg)	5 ± 3*	2.2
Electrical Error (arc min)	± 10 maximum	-9.6, +7.2
8 Speed Resolver Channel		
Output Voltage (V rms)	3.5 ± 5%	3.40
Phase Shift (Deg)	15 ± 3*	4.6
Electrical Error (arc sec)	± 40 maximum	-36, +27
Weight (oz)	32 maximum*	44

* Preliminary goal values

TABLE 3-3
TORQUE MOTOR TRADE-OFF PARAMETERS

Motor	Conventional (Iron Core Stator)	Ironless-Armature
Type	Brushless DC, 2 Phase	Brushless DC, 2 Phase
Commutation	Continuous, Resolver Radial Gap	Continuous, Resolver Axial Gap
Orientation		
Power at 2 Ft-Lb Torque at 4 Ft-Lb Torque	50 Watts 200 Watts	50 Watts 200 Watts
Cogging Torque	2 oz-in	0
Drag Torque	1 oz-in	~ 0
Radial Force Stiffness	~ 500 lb/inch	0
Ripple Torque	<1%	<3%
Weight (total) (rotor)	3.1 pounds ~ 1.2 pounds	4.7 pounds ~ 4 pounds
Outer Diameter	5.3 inches	~ 8.5 inches
Inner Diameter	3.3 inches	~ 2 inches
Axial Length	1.6 inches	~ 1.5 inches
Cost	~ \$6K	~ \$22K

- Large outer diameter exceeded the planned gimbal envelope. Estimated radial force unbalance stiffness of the conventional motor, while being a concern at 0.5K lb/in, was still less than 2% of the predicted radial restoring stiffness of the passive radial magnetic suspension bearing.

The accepted plan was to perform a test to characterize the conventional motor radial unbalance stiffness and, in system testing, determine its effect on performance. As a backup, a lower-torque capacity, ironless-armature motor, purchased for an earlier Independent Research and Development (IR&D) program, was in-house and could be adapted to the present gimbal should the conventional motor performance create serious problems.

The conventional motor described in Figure 3-14 was purchased on internal capital equipment funds. After delivery of the motor, a test to characterize the radial force produced by the motor as functions of rotor radial offset and motor excitation level were performed. Static measurements were obtained with no motor excitation, yielding a radial stiffness of approximately 900 lb/in for motor radial offsets up to 18 mils.

Plots were obtained incrementing radial offset from 0 to 20 mils and motor excitation currents from 0 to 8.5 A, with various combinations of angular alignment, offset direction, and excitation winding and polarity. Motor radial stiffness with no excitation averaged 874 lb/in at the large offset and is reasonably linear over the offset range. The radial stiffness acts as a negative spring since offsets produce forces that act to increase the offset. Motor excitation, in every test, reduced the radial force and stiffness by an average of 11.3 lb/in-A (varying from 4 to 21 lb/in-A). This equates to an average 12.1% drop in stiffness for the 9.4 A rated current.

In conclusion, the radial unbalance stiffness of this motor is 874 to 900 lb/in without excitation. Excitation reduces this value by up to 22%. This correlates well with the 1550 lb/in value of analysis 5243-16.7-MAG-52 for a larger motor with a larger air gap, but is larger than the 500 lb/in value assumed for this motor in Analysis 0118.2.4-6. Test report 0118.5.4-7A contains full details of the radial force test.

A summary of the vendor acceptance test data and the SSO radial force test is provided in Table 3-4.

3.1.4 Electrical Description

The 4-DOF cryobearing test fixture electronics consists of bearing system electronics and bearing test electronics, as shown in Figure 3-15. Bearing electronics functions include: position and rate feedback conditioning, implementation of control law compensation, magnetic actuator force-gap nonlinearity compensation, and magnetic

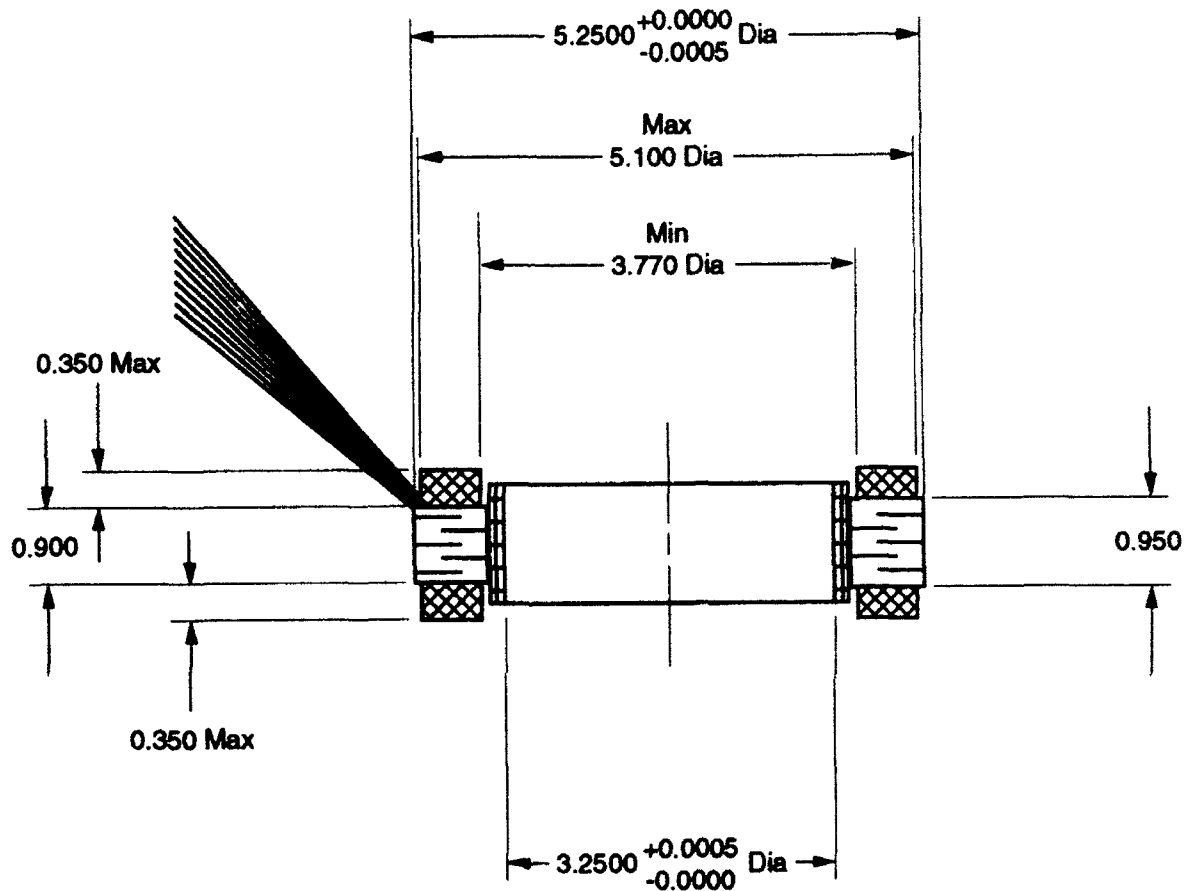


Figure 3-14. Torque Motor

TABLE 3-4
BRUSHLESS DC TORQUE MOTOR
(P/N 5430-10716)

Parameter	Spec Value	Test Value
Type	Conventional, Brushless D C , 2 phase, 16 pole	
Commutation	Continuous, resolver	
Operating temp range	-150°C to +70°	
OD (in)	5.250	Same
ID (in)	3.250	Same
O A Length (in)	1.61 maximum	Same
Poles/Phases	16/2	Same
Permanent Magnets	SmCo	Same
Rated Torque (ft-lb)	4.0	Same
Torque Constant (ft-lb/amp)	0.49 ± 10%	0.472
D.C. Resistance (ohms)	3.0 ± 10%	3.0
Inductance (mH)	TBD	5.15
At rated torque Power loss Peak voltage Peak current	200 watts (nom) < 30 volts < 9.2 amps	Same Same Same
Output Torque Ripple (%) (spectrum)	0.5 maximum	0.38 maximum
Cogging Torque (oz-in, 0-pk)	1.8 maximum	2.0
Drag Torque (oz-in, 0-pk)	0.8 maximum	0.6
Weight (pounds)	3.3 maximum	3.03
Radial Unbalance Stiffness (pounds/inch)	< 500 (goal)	874 to 900 * (no excitation) Reduced by 4% to 20% by full excitation

* Reference test report 0118.5.4-7

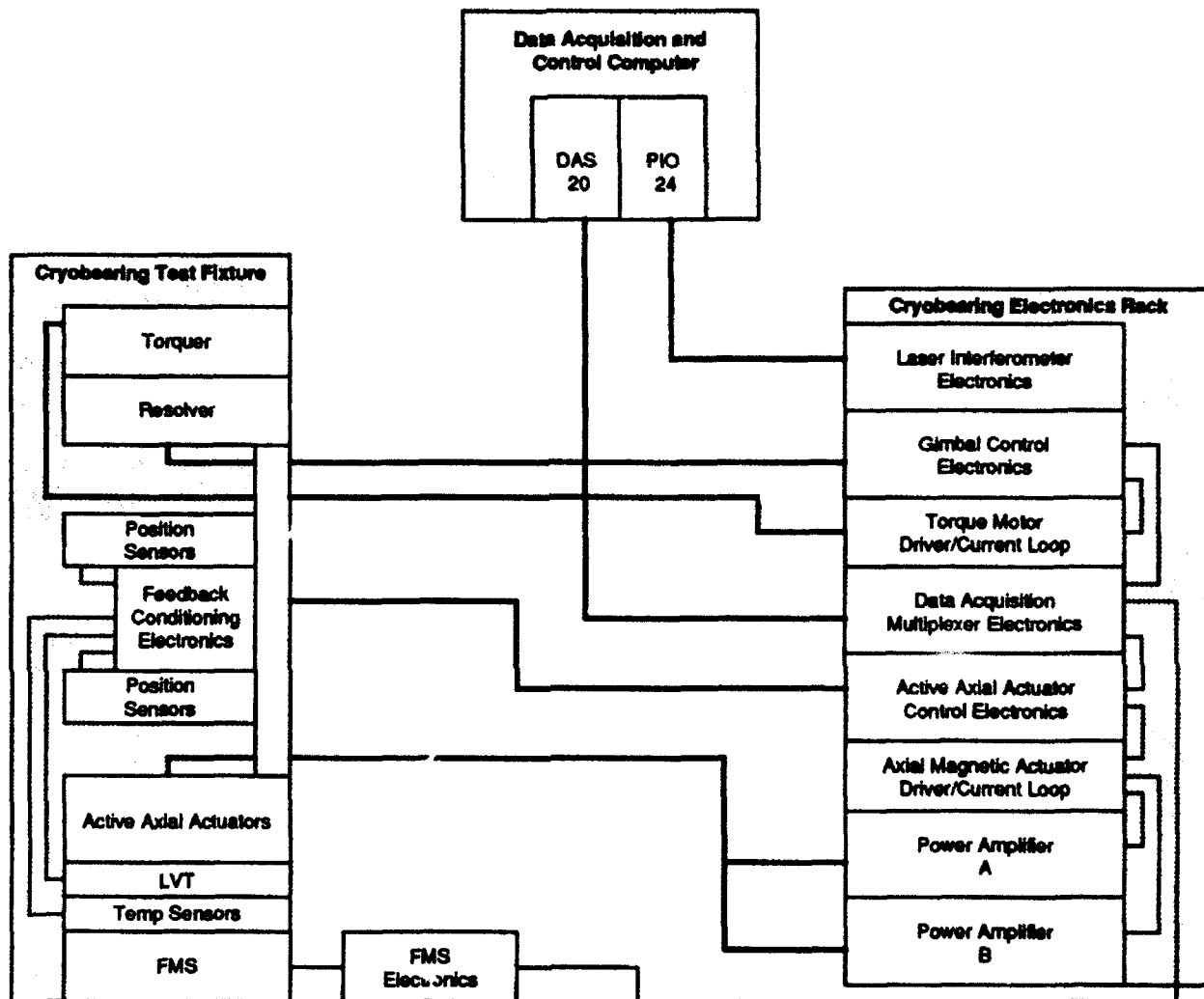


Figure 3-15. 4-DOF Electrical System Block Diagram

actuator current drive and control. Bearing test electronics include special test items such as torque control and runout measurement electronics and the data acquisition and control system. Also included are special laboratory equipment such as the laser interferometer and the force measurement system. Analysis 0118.4.4-6 describes the 4-DOF electronics and Analysis 0118.4.4-7 is the cryobearing electrical interface control document.

3.1.4.1 Bearing System Electronics

The bearing electronics provide all functions required to control the active axial axis of the PRAA magnetic bearing assembly. Each of these functions is required for the gimbal configuration, although implementation and packaging of these electronics would be different than for the 4-DOF implementation. Figure 3-16 illustrates these functions in the block diagram form.

Feedback Conditioning Electronics

The baselined active axial magnetic actuator control system uses position and rate feedback sensors to control magnetic bearing armature motion within the magnetic gap along the y axis. Two inductive DITs measure axial displacement. An LVT provides a measure of the armature positional rate of change along the y axis. The active axial control system block diagram is shown in Figure 3-17. Figure 3-18 is a block diagram of the feedback conditioning electronics and control compensation electronics. Axial position signals are processed through DIT hybrids whose output is an electrical signal proportional to axial displacement scaled at 50 V/m. Their linear range is ± 0.2 mm about a null gap of 0.5 mm. The conditioned velocity sensor output provides a linear ± 10 VDC analog signal scaled at 50 V/m/s.

Control Compensation Electronics

The control compensation electronics generate force commands to control the magnetic bearing armature motion along the axial axis. The force command is based on gap displacement and gap rate-of-change feedback signals received from the feedback conditioning electronics. A startup command filter and a minimum-power positive feedback path are also implemented. These are shown in the block diagram of Figure 3-18. The startup path filters the initial turn-on transient to control overshoot and to prevent the armature from accelerating into the opposite side hardstop. The positive feedback path acts to adjust the position of the armature within the magnetic gap where minimum power is dissipated. In a zero-gravity environment, this position is at the magnetic null between the two passive actuator pole pieces. In an Earth-gravity environment, the armature is displaced such that the attractive force of the passive magnetics counteracts the force vector due to gravity on the payload mass.

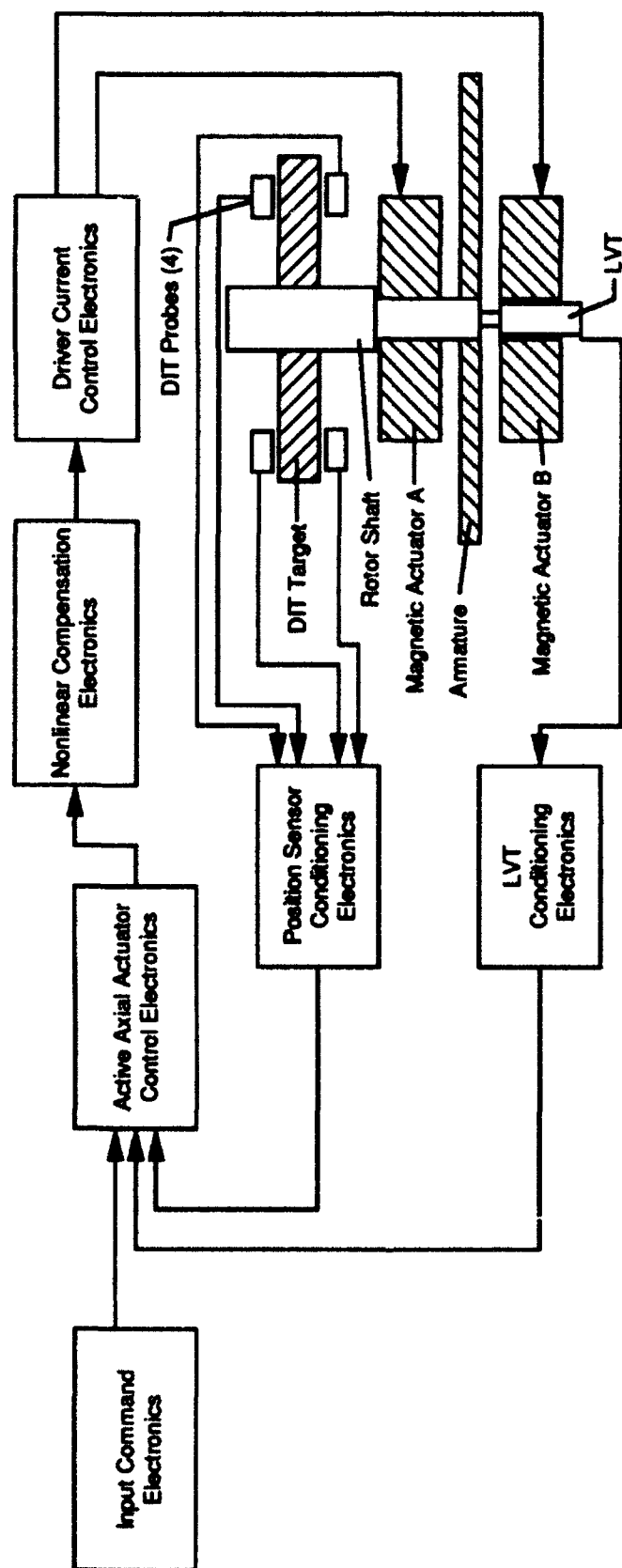


Figure 3-16. Active Axial Electronics Block Diagram

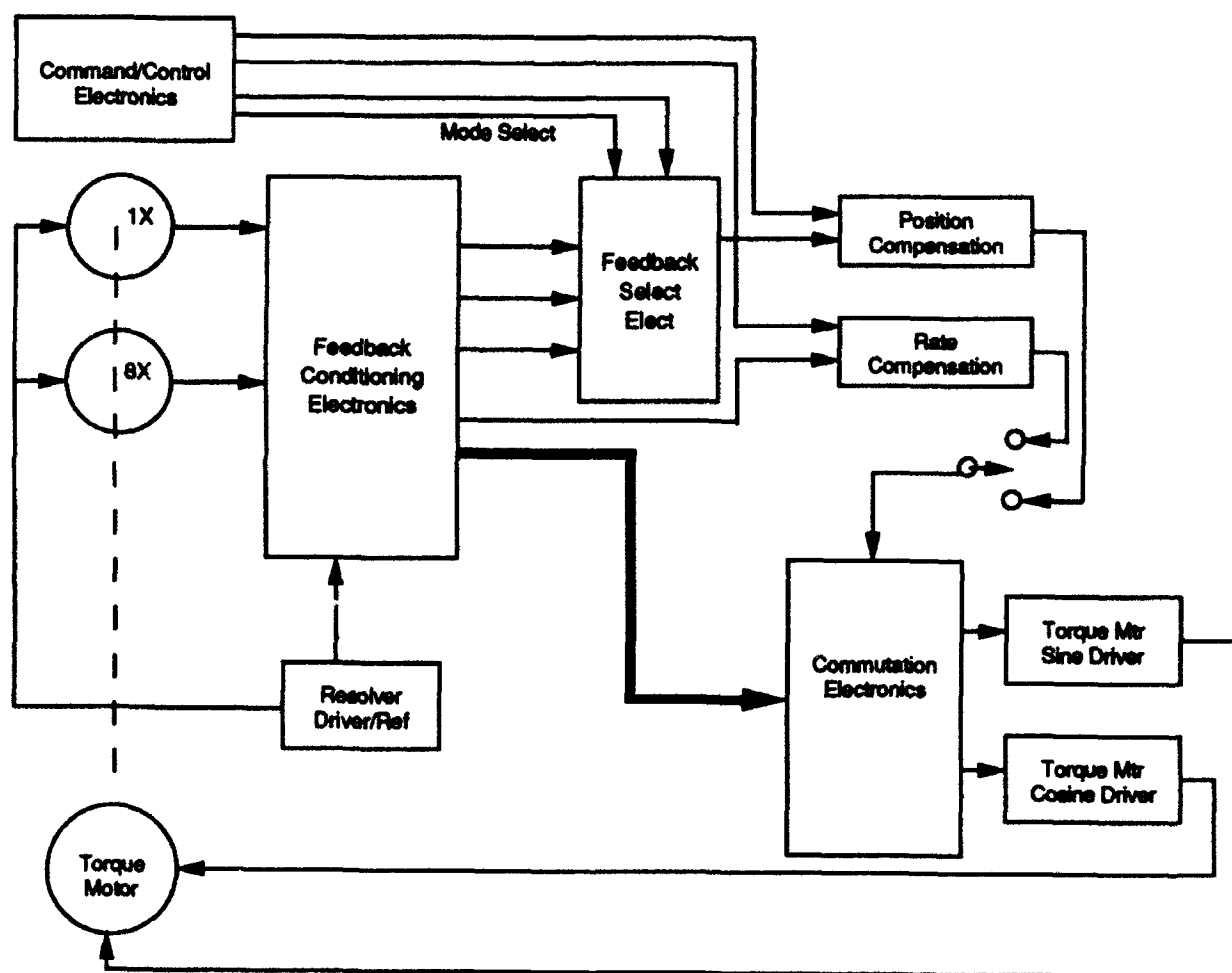


Figure 3-18. Active Axial Control Electronics Block Diagram

Force Linearization Electronics

The force command from the control compensation electronics passes to the force linearization electronics illustrated in the block diagram of Figure 3-19. These electronics compensate for first-order, force-gap, and saturation nonlinearities. The force-gap compensation accounts for the fact that axial actuator force is proportional to the square of the current through the actuator coil and inversely proportional to the square of the gap between the actuator pole face and the armature (magnetic gap). A current command generated by the force linearization circuit is the input to magnetic actuator current loop drivers. Depending on the initial conditions of the system, startup forces approaching 1000 N are required to lift the armature from its hard stop. Normal operation after stabilization requires only a few Newtons force. An automatic gain scheduler, designed within the force linearization electronics, adjusts for this wide dynamic range; otherwise, quantization of the current commands cause unacceptable limit-cycle amplitudes. Analysis 0118.4.4-5 provides a detailed description of the force linearization electronics and their implementation.

Magnetic Actuator Drive Electronics

Driver electronic functions, shown in Figure 3-20, control current through the magnetic actuator at the level dictated by the current command received from the force linearization circuit. Two high-bandwidth linear amplifiers are used in the 4-DOF test fixture to reduce program expenditures. These are general laboratory amplifiers that would be replaced by efficient pulse-width modulated drivers for a flight application. Drivers are scaled for 0.45 A/V and are limited to 4.1 A full scale. The compensation network components are selected for a nominal 1000-Hz current control bandwidth.

3.1.4.2 Bearing Test Electronics

Test electronics for the cryobearing system consists of Gimbal Control Electronics (GCE), Runout Measurement Electronics (RME), Data Acquisition Electronics (DAE), an FMS, and a laser interferometer system.

Gimbal Control Electronics

The GCE controls rotational motion about the principal bearing rotation axis. The GCE is software or hardware selectable to operate in position or rate control modes. Position control uses feedback from either the one-speed or the eight-speed resolver, depending on the desired resolution and range of motion. Each resolver winding has its own Resolver to Digital Converter (RDC) that generates a 16-bit digital word proportional to the mechanical angle. The rate mode uses feedback derived from the eight-speed resolver. This derived rate feedback signal is generated within the RDC. In either control mode, current commands generated from respective compensation

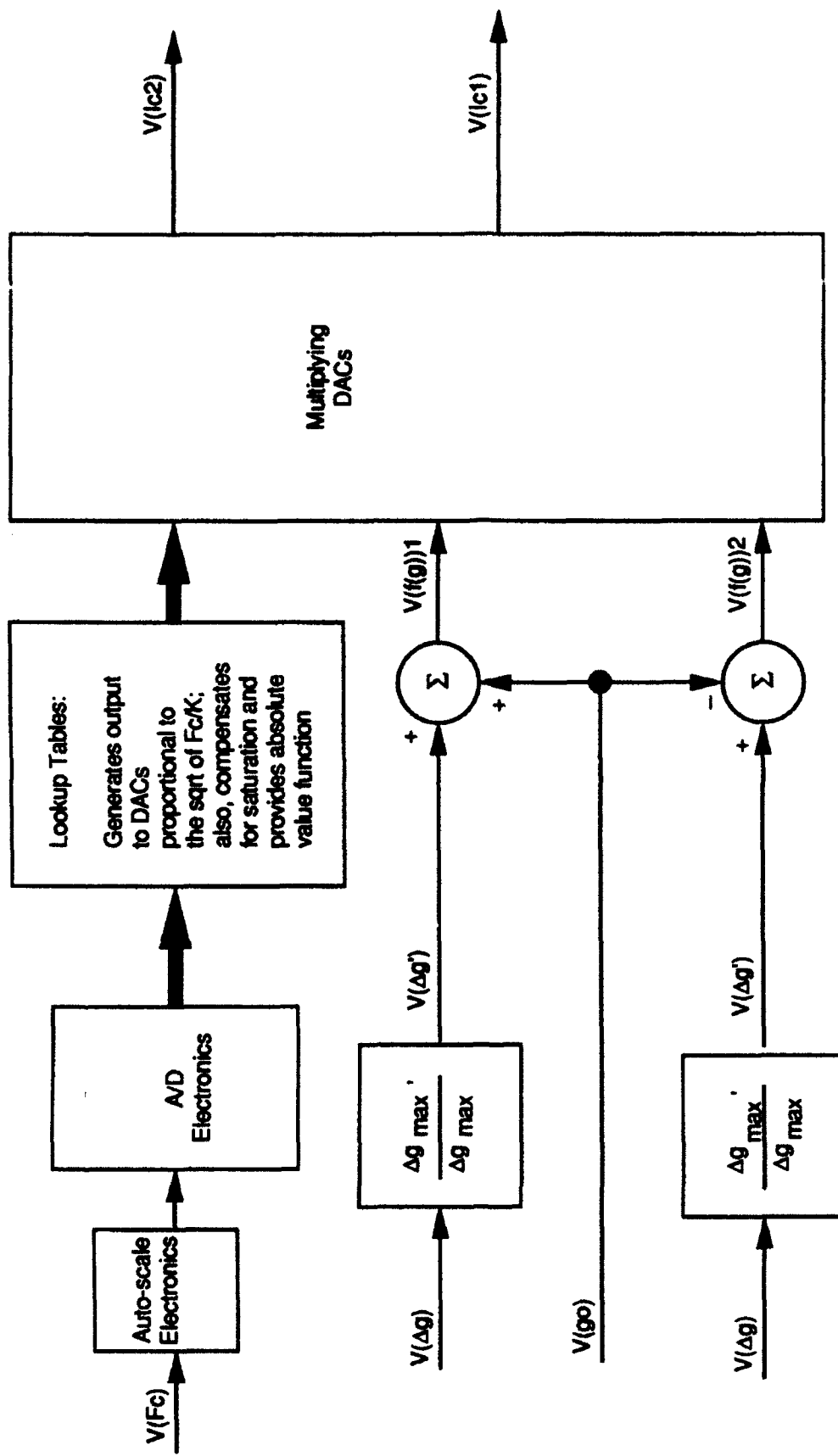


Figure 3-19. Actuator Linearization Block Diagram

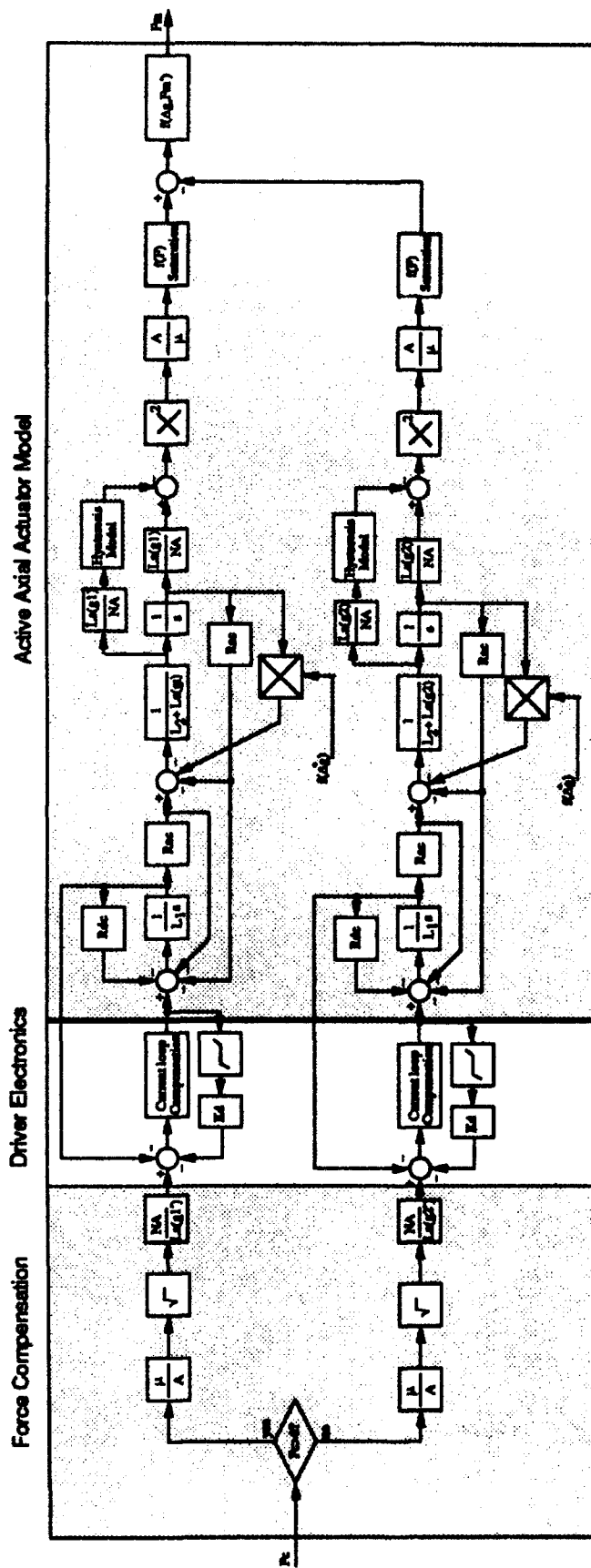


Figure 3-20. Current-loop Magnetic Actuator Model

networks feed current control loops, which drive the commanded current through a 16-pole, brushless, DC torque motor. A multiplying Digital to Resolver Converter (DRC) combines the torque command and the eight-speed RDC output to generate commutated current commands. Figure 3-21 shows the GCE electronic block diagram, and Analysis 0118.4.4-6 provides a detailed GCE design description.

Runout Measurement Electronics

The runout measurement technique is described in Section 3.1.1.1. DIT probes measure deflections at the runout target interfaces. The measured displacements are captured and stored for runout processing by a PC-based Data Acquisition System (DAS). Once captured, this "raw" data are conditioned to provide radial and axial runout components of the unit under test.

Data Acquisition and Control Electronics

The DAE consists of analog and digital Input/Output (I/O) channels that interface with a control computer. Analog signals monitored by the DAE include: all DIT channels, conditioned LVT output, GCE position and rate feedback, FMS signals and bearing temperature, the digital interface controls bearing and gimbal electronics operating modes, driver enable/disable commands, and the laser interferometer control. The control computer is programmed to read data channels based on the required measurement. Once in the computer, data are stored and processed.

Laboratory Test Equipment

Two dedicated, general-purpose laboratory items were integrated into the 4-DOF test fixture. The FMS converts dynamic forces and torques at the magnetic bearing interface into electrical signals. These are passed directly to the DAE. The test fixture is configured such that forces and torques measured by the FMS represent those passing through the magnetic interface, providing a direct measurement of drag torque and reaction forces and torques.

A laser interferometer is used for DIT calibration and special measurements. The interferometer used (HP 5501 System) provides incremental displacement information with a resolution of approximately 10 nm.

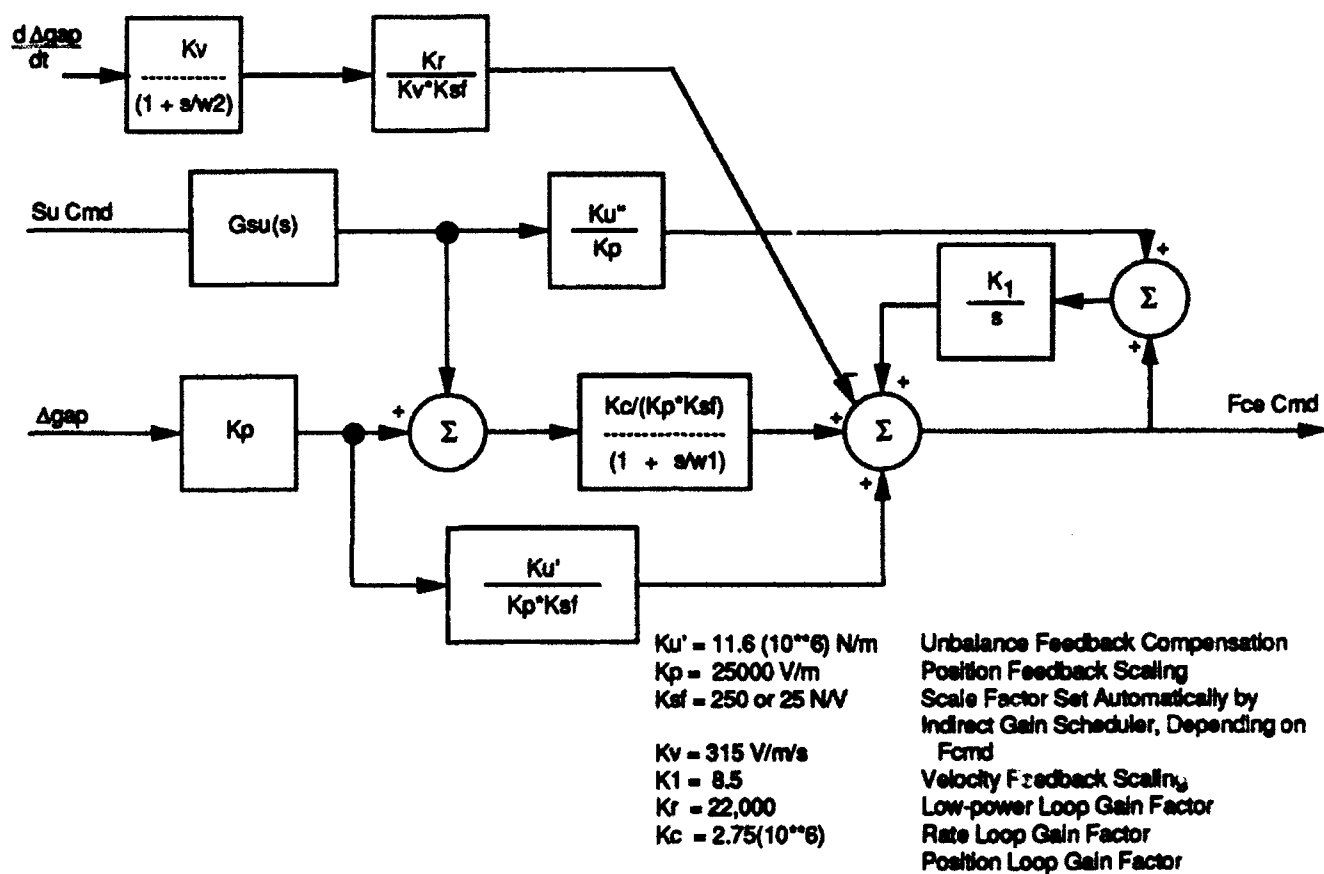


Figure 3-21. Gimbal Control Electronics Block Diagram

4. TEST RESULTS

This section presents bearing component test results and subsystem test results.

4.1 Magnetic Bearing Component Test Results

Characterization test results for both passive radial and active axial magnetic bearing components are summarized in the following two sections. Analyses 0118.5.4-7 and 0118.5.4-8 detail the results for the passive radial magnetics and active axial magnetics tests, respectively.

4.1.1 Passive Radial Bearing - Resultant Performance

Performance test results on the passive radial bearings were very disappointing. The radial restoring stiffness was significantly lower than predicted (13 to 17% of prediction), while the axial unbalance stiffness was in the predicted range (65 to 110% of prediction). When assembled into the demonstration gimbal, the bearing exhibited a significant torsional unbalance stiffness that produced alignment problems, partially because of the small mounting diameter at which the armature plate was attached.

Passive bearing assembly S/N 1 was tested in August 1989. Initial tests yielded radial restoring that was only about 13% of design prediction, while the axial unbalance stiffness was 65% of the prediction.

An explanation for the poorer-than-predicted performance of the S/N 1 passive bearing was desired, but parts had already been fabricated for a second bearing. Also, the test gimbal had been descoped to require only one bearing and the cryobearing study funding could not support any further investigative efforts. Several possible causes of the inadequate performance were proposed and considered. Honeywell Inc., Systems and Research Center (SRC) reviewed the design and agreed with the design predictions, but proposed still another potential cause for the lost radial stiffness. An SSO-funded IR&D project was initiated in an attempt to determine the cause of the deficient performance of the passive magnetic bearing.

In this IR&D effort, two of the more likely causes were investigated further, with outputs being the second annealed, assembled, and tested passive bearing and a final report.

The IR&D activity was scoped as follows:

1. Design Analytical Evaluations - Evaluate the more likely design deficiencies of the bearing.

Review Design Calculation Routines - Review the original design calculation routines to assure that no errors exist that could explain the radial stiffness deficiency.

Evaluate Flux Redistribution Hypothesis - Analytically evaluate the SRC hypothesis that as the bearing rotor displaces radially and there is no displacement in the region perpendicular to the displacement the magnetic flux may redistribute around the bearing circumference to the undisplaced region, thus reducing the radial restoring force produced by the displacement. In-house developed calculation routines and the Ansoft magnetics finite element program would be used as appropriate.

2. Reanneal, Assemble, and Test the Second Bearing Set - Evaluate the hypothesis that the omission of the final anneal (to protect the geometry) after the final Electrical Discharge Machine (EDM) machining operation caused the magnetic properties at the edges and corners of the fine teeth to be lost, resulting in the deficient radial stiffness.

Evaluate Local Anneal Capabilities - Locate local vendor with appropriate capabilities to perform the required reanneal and identify fixtures needed to protect the critical geometry of the parts.

Design/Fab Anneal Fixtures - Design and fabricate the fixtures identified above.

Reanneal Bearing Core Parts - Vendor will perform the reanneal with engineering supervision.

Assemble and Test Bearing - Assemble and test the second passive magnetic bearing using same procedures and fixtures established and used on the first bearing.

Calculation routines were verified and evaluation of the flux redistribution hypothesis concluded that for 0.006 inch radial displacement, the gap reluctance difference between quadrants was only 10%, resulting in less than 10% reduction in radial force for the displaced quadrants, and that this was far less than the 80 to 85% loss sought.

In the reanneal, test and part evaluation activities include the following:

- Grain structure of bearing parts core material was evaluated at Spang Speciality Metals.
- Magnetic B/H loops on parts were obtained and evaluated both at Spang Metals and at SS0.
- Bearing parts were evaluated and tested.

Evaluations of the parts identified deficiencies that could contribute to the inadequate performance. Reanneal significantly improved some of the magnetic properties (B_{max} and B_r); however, others (H_c) remained poor. Performance testing of the reannealed hardware yielded marked stiffness increases: radial 32% and axial 58%; however, the radial stiffness is still only 17% of prediction, leaving the cause unresolved. Magnetic damage to the fine teeth (due to either EDM machining or an over-temperature initial anneal), which could not be restored by the reanneal, is still a possible cause.

A summary of the stiffness test results for S/N 1 and 2 bearings is given in Table 4-1 and full documentation of the test results is contained in Test Report 0118.5.4-7.

4.1.2 Active Magnetic Actuator - Resultant Performance

Two actuator stators were fabricated, assembled, and tested. The actuator stators, when combined with the armature plate, make up the force actuator station to be installed in the cryobearing model.

Correlation between the measured performance and the design predictions was good. The average measured force constant values over the primary operating range were 13% stronger than predicted and the variation between actuators was 4.2%. The worst-case deviation from the ideal force/current squared control law due to saturation effects was less than 1%.

A comparison between the predicted parameters and tested values is shown in Table 4-2 and full documentation of the test results is contained in Test Report 0118.5.4-8.

4.2 Integrated Test Results

During system integration, difficulties were encountered in getting the cryogenic magnetic bearing to function properly. The principal symptom of this was an inability to maintain proper magnetic bearing gaps. Although the magnetic bearing armature could be positioned statically in the magnetic gaps, any attempt to translate or rotate the shaft resulted in a touchdown of the armature onto its stops. The armature exhibited a tendency toward an unstable equilibrium. When the unit was perturbed it sought an equilibrium that manifested itself as a "cocking" of the armature across the magnetic gaps.

Inspection of the assembly found the armature was not tight on the shaft. Because of the significant magnetic attractive forces, sufficient friction torque was generated at touchdown to loosen the shaft nut that retained the armature. Consequently, the armature became more loose with continued operation until further operation was not possible.

The discovery of this behavior led to an investigation that identified shortcomings in the design of both the 4-DOF cryogenic test fixture and the magnetic bearing itself. Weaknesses were found in the areas of geometrics, interfaces, and rigidity. Description of these weakness and their impact on system performance is described in the following sections.

TABLE 4-1
STIFFNESS EVALUATIONS

	Predicted Performance	Bearing Assy #1 (Oct '89)	Bearing Assy #2 (Dec '90)	#2 % Inc from #1
<u>Radial Restoring</u>				
<u>Total Stiffness</u>				
Avg at ~0 mils disp	32.4 KLb/In	4.1 KLb/In	5.4 KLb/In	32%
Avg at 5 mils disp	21.8 KLb/In	3.8 KLb/In	4.4 KLb/In	16%
Avg at 10 mils disp	16.8 KLb/In	3.1 KLb/In	3.3 KLb/In	6%
Zero Stiff at disp	28.3 mils	14.5 mils	14.5 mils	
<u>Incremental Stiff</u>				
Avg at 0 mils disp	---	4.1 KLb/In	5.5 KLb/In	34%
Avg at 5 mils disp	---	3.3 KLb/In	4.0 KLb/In	21%
<u>Axial Unbalance</u>				
<u>Total Stiffness</u>				
Avg at ~0 mils disp	28.0 KLb/In	~18 KLb/In	~29 KLb/In	~58%
Avg at 1 mils disp	28.2 KLb/In	19 KLb/In	31 KLb/In	63%
Avg at 2 mils disp	29.1 KLb/In	21 KLb/In	~36 KLb/In	~71%
Avg at 5 mils disp	37.1 KLb/In	25 KLb/In	N/A	N/A

Note: The high Axial Unbalance Stiffness in S/N 2 tests may have been partially due to armature tilt or flexing which also limited axial displacement range to less than 0.002 inch.

TABLE 4-2
ACTIVE MAGNETIC ACTUATOR PERFORMANCE SUMMARY

PARAMETER	UNITS	PREDICTED VALUES	TESTED VALUES
FORCE RANGE	LB	282 MIN	> 282
GAP RANGE (PRIMARY)	INCH	0.040 ± 0.005	SAME
GAP RANGE (ALTERNATE)		0.010 ± 0.005	"
FORCE CONSTANT K	LB-IN ² /A ²		
at 0.035" GAP		0.01028	0.0116
at 0.040" GAP		0.01045	0.0118
at 0.045" GAP		0.01060	0.0120
at 0.010" GAP (ALT)		0.0086	0.0115
FORCE ERRORS			
SATURATION @282 Lb	%	< 5%	< 1%
GAP SQUARE LAW	%	< 2%	< 2%
HYSTERESIS *	LB	----	± 6 @ 0.040"
CURRENT	AMPERE		
at 282 Lb & 0.040" GAP		6.57	6.18
at 282 Lb & 0.045" GAP		7.34	6.90
at 282 Lb & 0.010" GAP		1.81	1.56
D.C. RESISTANCE	OHMS		
POWER COIL		8.01	8.19
SIGNAL COIL		----	0.54
POWER	WATTS		
at 282 Lb & 0.040" GAP		346	313
at 282 Lb & 0.045" GAP		432	390
at 282 Lb & 0.010" GAP		26.3	20.1
STATOR WEIGHT	LB	1.59	1.39

* Value is dependent on test conditions.

4.2.1 Geometric Deficiencies

Geometric deficiencies included the following:

- Lack of flatness
- Lack of parallelism
- Lack of perpendicularity

Measurements of the magnetic bearing and 4-DOF test fixture parts yielded flatness and parallelism indications varying from less than 0.0005 to 0.002 inch. Typical measurements were 0.001 inch per part per surface. Overall, the geometrics, as represented by these measurements of flatness and parallelism, were excellent; however, the cryobearing metal-to-metal magnetic gaps are nominally 0.008 inch. The operational range is 0.005 inch. The resulting nominal design clearance is 0.003 inch. This means that although the tolerance control was very good for the cryobearing parts, the tolerance buildups substantially reduced the available working clearances within the assembly.

Modifications and reworking of the parts were performed to enhance control of the geometry of the parts and assemblies. This included grinding of the armature to improve flatness and parallelism, removal of the shims from the stops to increase the operational gaps before touchdown, and selectively locating the armature on the shaft to ensure the armature was tight on the shaft. This relieved some of the parallelism and perpendicularity issues.

Overall, all parts were made to print. Further, there were no problems with control of any dimensions on any of the parts; however, a lesson learned was that for assemblies with small physical gaps, any tolerance buildup is significant and can cause problems with unit integration and operation. Therefore, for such assemblies, greater use should be made of assembly-level machining to control tolerance buildups in critical areas.

4.2.2 Interface Shortcomings

The cryogenic magnetic bearing and the test fixture were intentionally designed with a minimum number of interfaces; however, two of these demonstrated the need for improvements. One was the armature-to-shaft interface. The other was the flex pivot interfaces with the 3-axis test fixture flexure gimbal.

The magnetic bearing armature interface to the shaft is the most important of these. The previous section touched on some of the geometric aspects addressed in this area. Another aspect is the design of the interface. The important point about this interface is the limited mounting surface available for attaching the magnetic bearing armature to the shaft.

Referring to Figure 4-1, the magnetic bearing armature has a central mounting bore of 0.703 inch. This bore has a mating diameter on the shaft. The armature is axially located on the shaft by a 0.938-inch diameter step on the shaft. The shaft nut is sized similarly and is used to clamp the armature to the shaft. For the armature to attach to the shaft, the shaft nut and a portion of the shaft must pass through the active axial stator assembly. The axial stator has a through bore of 1.000 inch. Accounting for tolerances, clearances, and allowable DOF, this results in the 0.938 inch dimension on the shaft and nut.

The shaft-to-armature mounting surface has a radial dimension of 0.1175 inch. The ratio of this to the armature radial dimension is 22:1.

The small size of the interface is a direct result of minimizing the size of the magnetics to make them weight and power efficient. The disadvantage is that this small mounting surface must react all imposed magnetic forces. The active axial actuator can generate more than 550 pounds of force on the armature. The passive radial magnetic bearing generates 350 pounds of axial force on the armature assembly at a gap of 0.005 inch.

The small diametral interface, in conjunction with the large magnetic forces and the tolerance buildups of the components, combined to allow the armature to touchdown and loosen the armature nut. The previous paragraphs discussed the actions taken to correct the geometry of the parts. In addition, other actions were also taken as discussed below.

The armature angular orientation on the shaft was selected based on the position where the shaft nut could be tightened sufficiently to securely clamp the armature to the shaft. Further, epoxy and Loctite were used during reassembly to lock the assembly together and to prevent any subsequent loosening. This was also done to help stiffen the small armature mounting interface. This approach had previously been avoided because of concerns about the temperature range involved, a desire to ensure easy disassembly and refurbishment, and a belief that adequate retention capability existed with the interface.

The other interface, which was not ideal, was the 3-DOF flex pivot gimbal assembly. Despite the loads applied to the flex pivots and a set of set screws to lock the flexures in place, the pivots were discovered to display a tendency to "walk" axially out of their bores. This resulted in the gimbal binding when pieces came into contact and rubbed. This was corrected by reinstalling the flexures and applying adhesives for better retention. A close-up photo of the gimbal assembly is shown in Figure 3-10.

4.2.3 Assembly Compliance

During the course of intensive integration testing, the magnetic bearing assembly came under intense scrutiny as a potential source of unwanted compliance and deformations.

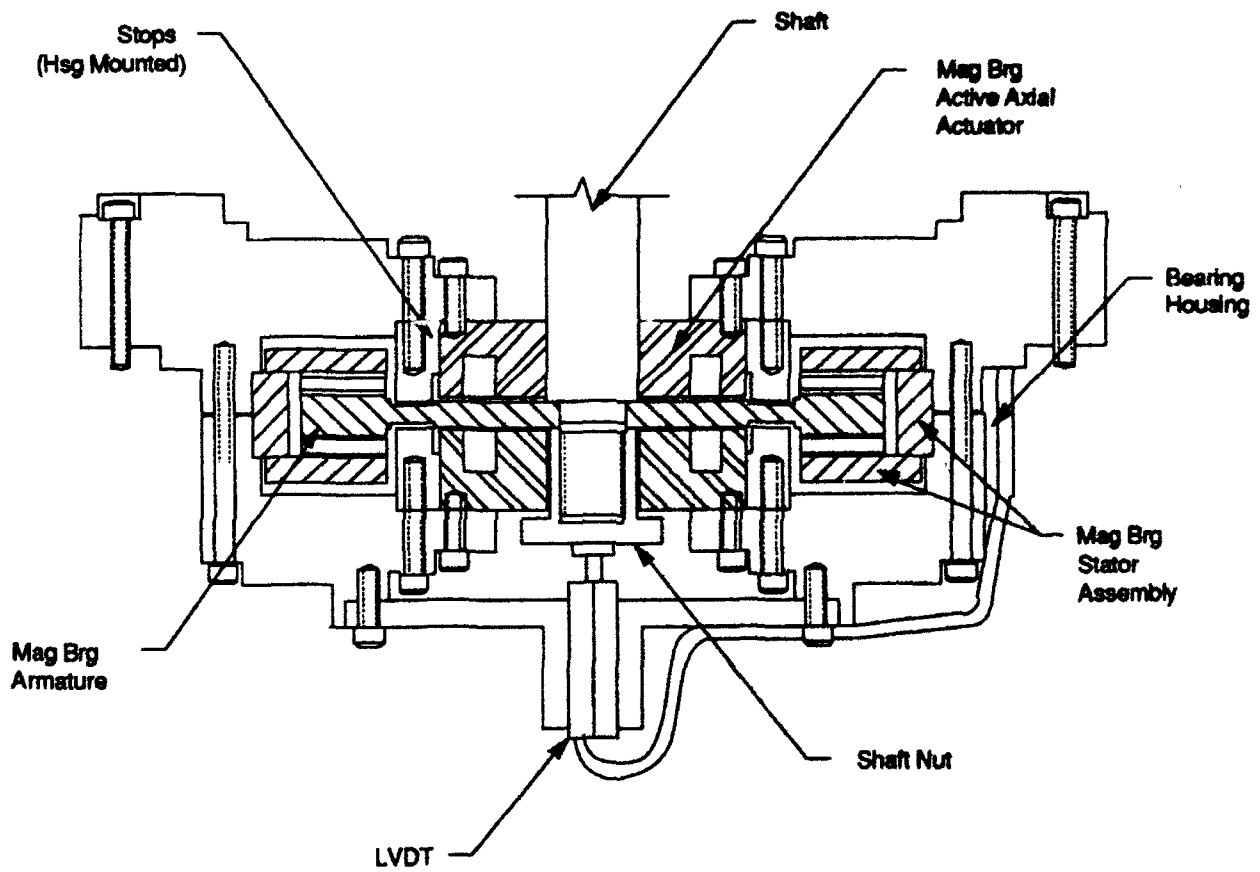


Figure 4-1. Magnetic Bearing Armature Interface

Numerous tests and analyses were run. Based on these, it was determined that the magnetic bearing stator assembly, the bearing housings, and the support structures possessed no undesirable compliance characteristics. The armature, however, was found to be a major contributor of system compliance.

Two factors determine the magnitude of compliance of the magnetic bearing armature. First, the mounting interface directly affects system compliance. If the mounting interface is not rigid, a system compliance will result. Second, if the armature itself exhibits any flexibility, a compliance will be manifested at the system level.

A series of load-deflection tests were performed on the magnetic bearing armature to assess any contributions to system compliance. With the armature mounted on the shaft in the 4-DOF test fixture, loads were applied to the armature with the manual adjuster. Reaction forces were measured with the FMS. A laser interferometer measured axial deflections. All data were recorded through the data acquisition system and processed after test completion. Data were recorded during incremental load application up to a maximum load of approximately 800 N (185 lb). To ensure test accuracy, data were also recorded while the load was incrementally removed. Test data were considered valid if the system deflection returned to zero with all of the load removed.

Two test setups were used as shown diagrammatically in Figures 4-2 and 4-3. Figure 4-2 illustrates a two-point load reaction, yielding a direct measurement of the armature stiffness. Figure 4-3 is a representation of the single-point load tests and generates data on the effective system stiffness, which is a function of the stiffnesses of both the armature and its interface to the fixture shaft.

Results from the two-point reaction testing yielded an armature stiffness value in excess of 3×10^5 lb/in. Table 4-3 presents the deflections of the armature under the action of a set of typical design loads. From the table, nominal operational conditions result in armature deflections of less than 0.002 inch, well within the minimum clearance gap of 0.003 inch. Even in a worst-case failure mode the armature deflection is just enough to allow a line-to-line contact with the stator elements of the bearing. It should be noted that for both of these cases, results are conservative because the stops have been ignored.

The series of single-point tests repeatedly yielded stiffness values near 3.8×10^4 lb/in, despite selective armature angular location, tightness of the shaft nut holding the armature to the shaft, and use of Loctite and other adhesives on the shaft nut and armature interfaces.

Table 4-3 also shows typical armature deflections under various load conditions for this stiffness value. As can be seen, the reduced effective armature stiffness results in armature deflections that virtually eliminate magnetic gaps. Even for the passive radial bearing attractive forces, the armature deformation is in excess of the nominal magnetic gap of 0.008 inch. With the stops present, it can easily be seen that this would cause the unit to touchdown, just as it had in actual practice.

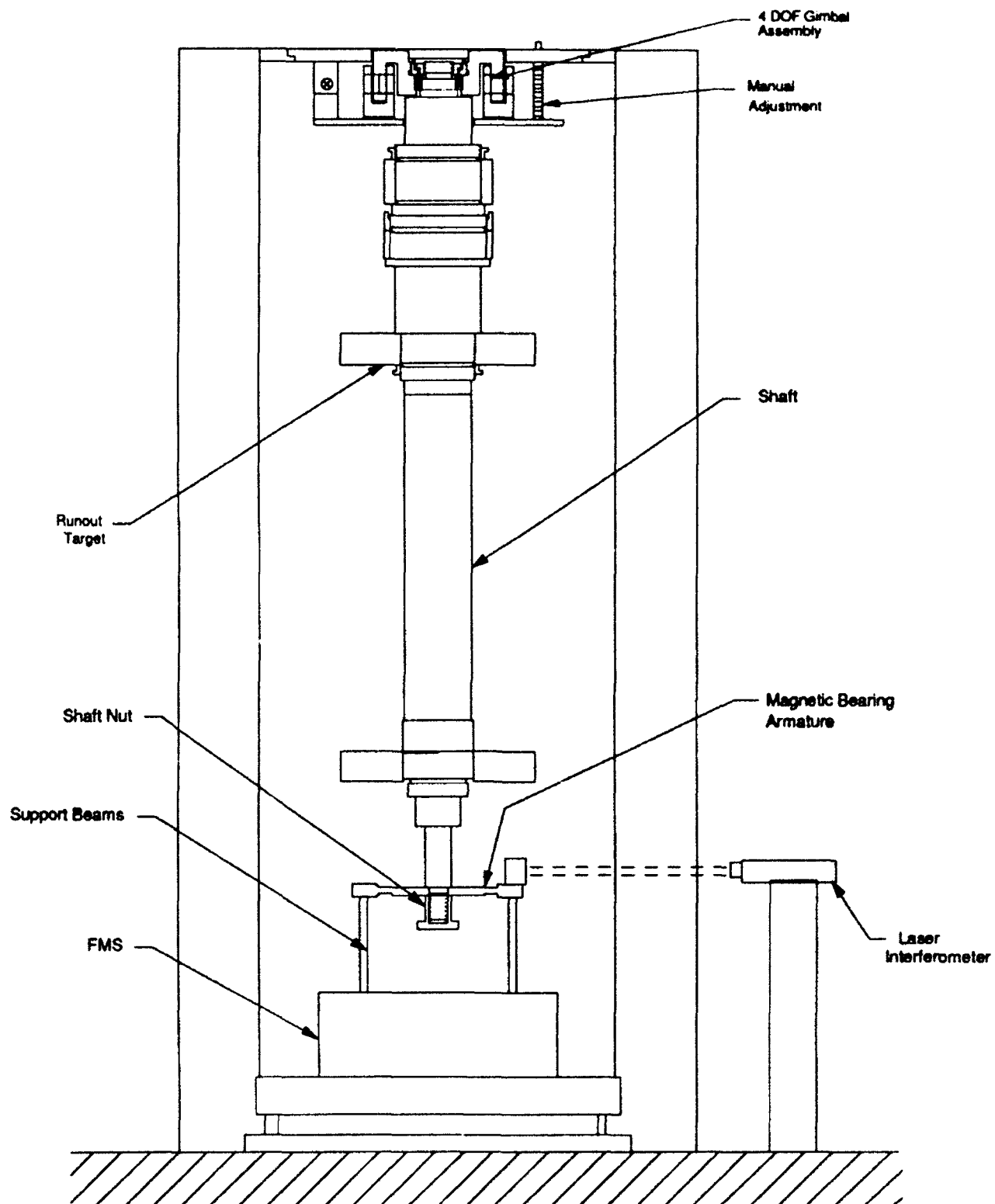


Figure 4-2. Two-point Armature Deflection Test Setup

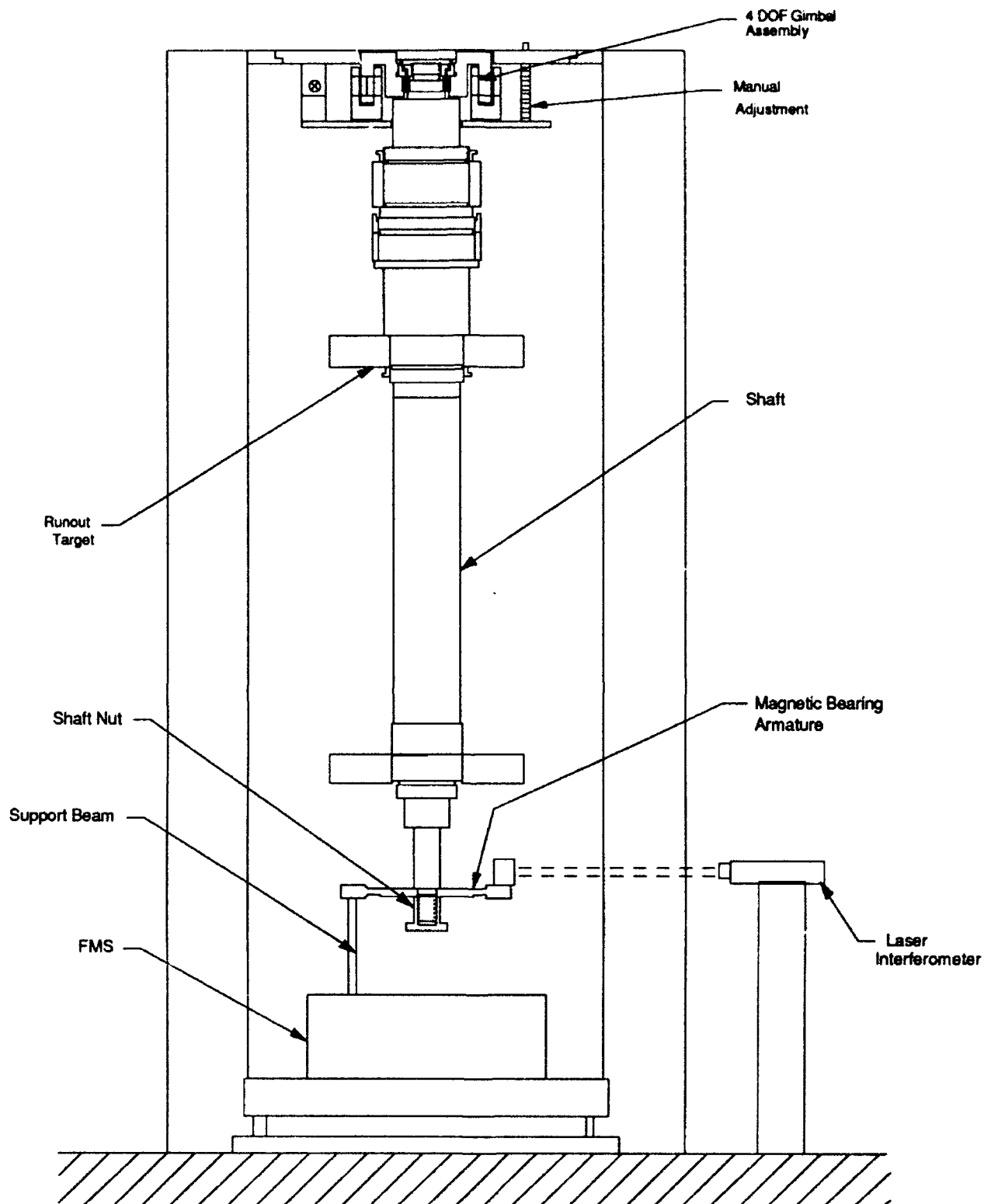


Figure 4-3. Single-point Armature Deflection Test Setup

TABLE 4-3
CRYOBEARING MAGNETIC BEARING ARMATURE STIFFNESS TEST RESULTS

LOAD TEST CONDITION	STIFFNESS (lb/in)	CASE No.	OPERATIONAL LOAD (lb)	DEFLECTION (in)
TWO-POINT	3.0×10^5	1	350	0.0012
		2	550	0.0018
		3	900	0.0030
SINGLE-POINT	3.8×10^4	1	350	0.0093
		2	550	0.0146
		3	900	0.023

CASE No.	CONDITION
1	Passive axial attractive force at 0.005" gap
2	Maximum active axial actuator attractive force
3	Worst case combination of cases 1 and 2

In parallel with the investigative tests, a finite element analysis was performed on COSMOS/M. Figure 4-4 shows the COSMOS/M finite element model of the cryobearing armature and representative deflections. A summary of the results of the analysis is shown in Figures 4-5 and 4-6. A complete definition of the model and results can be found in the Appendix.

Analysis of the as-built configuration resulted in an armature axial stiffness prediction of 2.4×10^4 lb/in. The as-built curve in Figure 4-5 is a plot of the axial deflection along a radius of the armature at the angular location of the point load analyzed in this case. Figure 4-5 reveals that the greatest change in slope of the deflection curve occurs in the region of the undercut in the armature. This recess is meant to accommodate an armature-mounted stop in the full cryogenic magnetic gimbal.

Numerous armature fixes and configurations were analyzed in order to develop a remedy for the low measured assembly stiffness. The plots of Figures 4-5 and 4-6 are samples from this effort.

The curve labelled "Tc=0.270" is the result of the as-built armature without the stop recess. The effective armature stiffness was approximately double that of the as-built configuration but far short of the measured two-point stiffness value.

With the center of the armature and the stop recesses built up to a thickness of 0.500 inch, the effective armature stiffness increased to a magnitude of 7 times that of the as-built design. This is shown as the curve labelled "Tc=0.500". The displacement plot shows the slope of the deflection curve to be relatively smooth without exhibiting any large fluctuations. This case is a conservative analysis of the original armature selected for the cryogenic magnetic gimbal. For that assembly, the stops were mounted to the armature and an initial armature thickness of 0.750 inch was selected.

If the armature center region and stop recesses are built up to an effective thickness of 0.308 inch, the curve "Tc=0.308" results. The stiffness in this case is about 2.5 times that of the as-built design. This case is a conservative analysis of the next to last iteration in the original armature sizing process. The 0.750-inch-thick magnetics were downsized for efficiency to an armature thickness of 0.313 inch. Again, the stops were mounted on the armature.

The magnetic design with the 0.313-inch-thick armature was not built because of material availability problems for the back iron portion of the stator assembly. As a consequence, the design evolved into the final configuration for the cryogenic magnetic gimbal. In that design, the armature became 0.270-inch-thick. The stops remained integrated with the armature as an assembly. For simplicity and ease of assembly, the stops were moved from the armature to the bearing housing for the 4-DOF test fixture application. This corresponds to the as-built configuration.

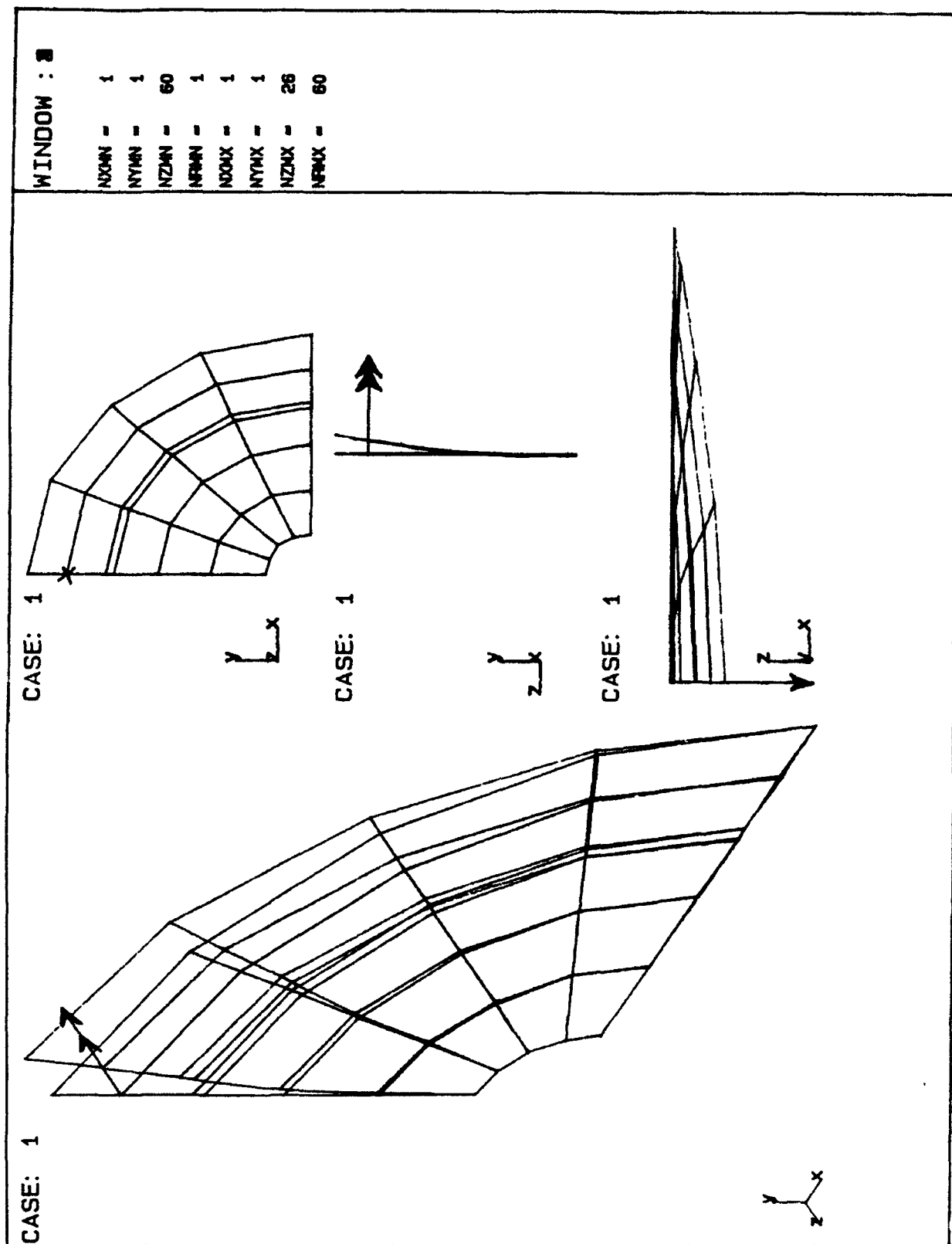


Figure 4-4. FEA Model and Results

CRYOBEARING FINITE ELEMENT RESULTS

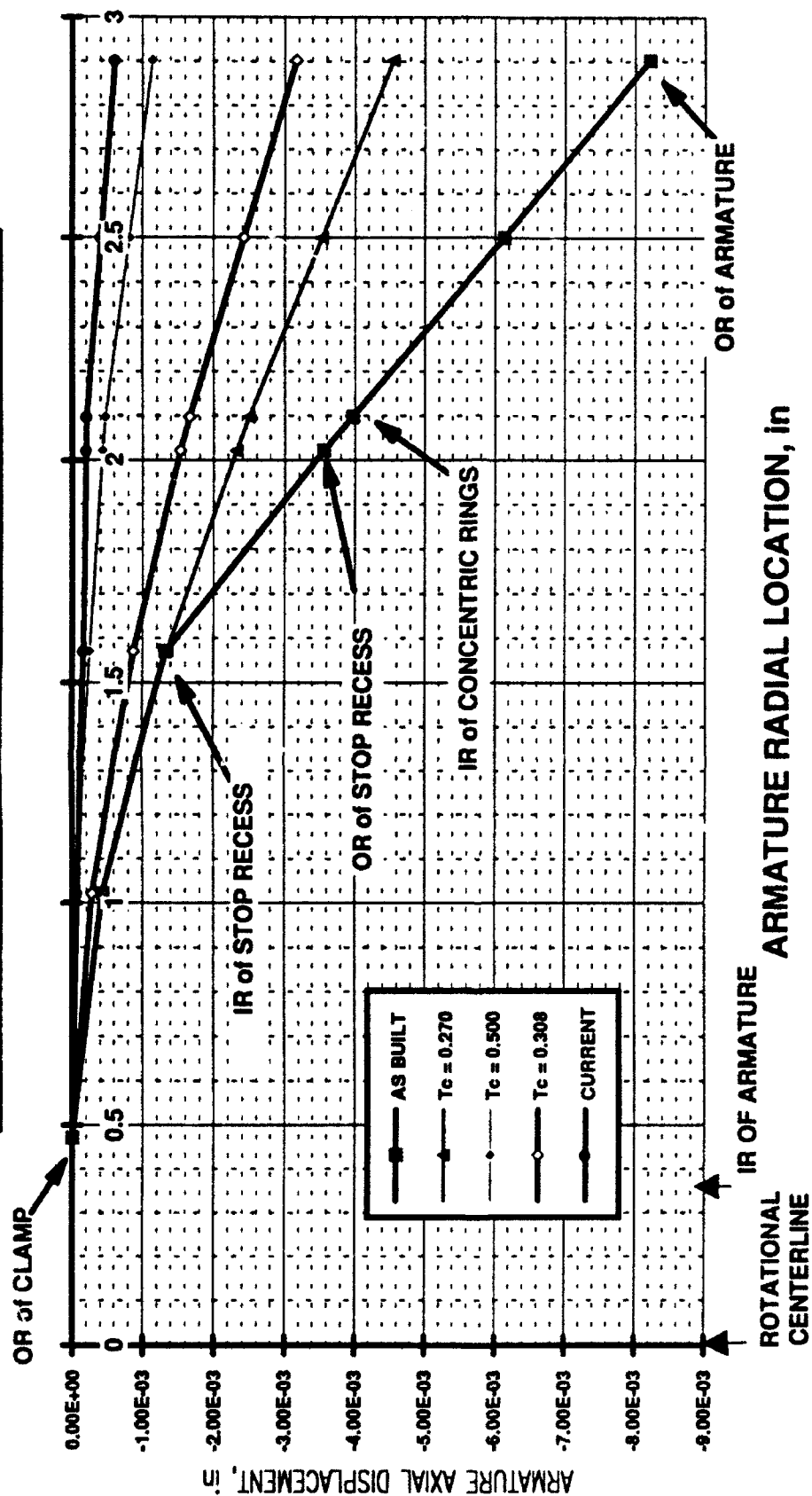


Figure 4-5. FEA Model Displacement Results Plot

CRYOBEARING ARMATURE STIFFNESS

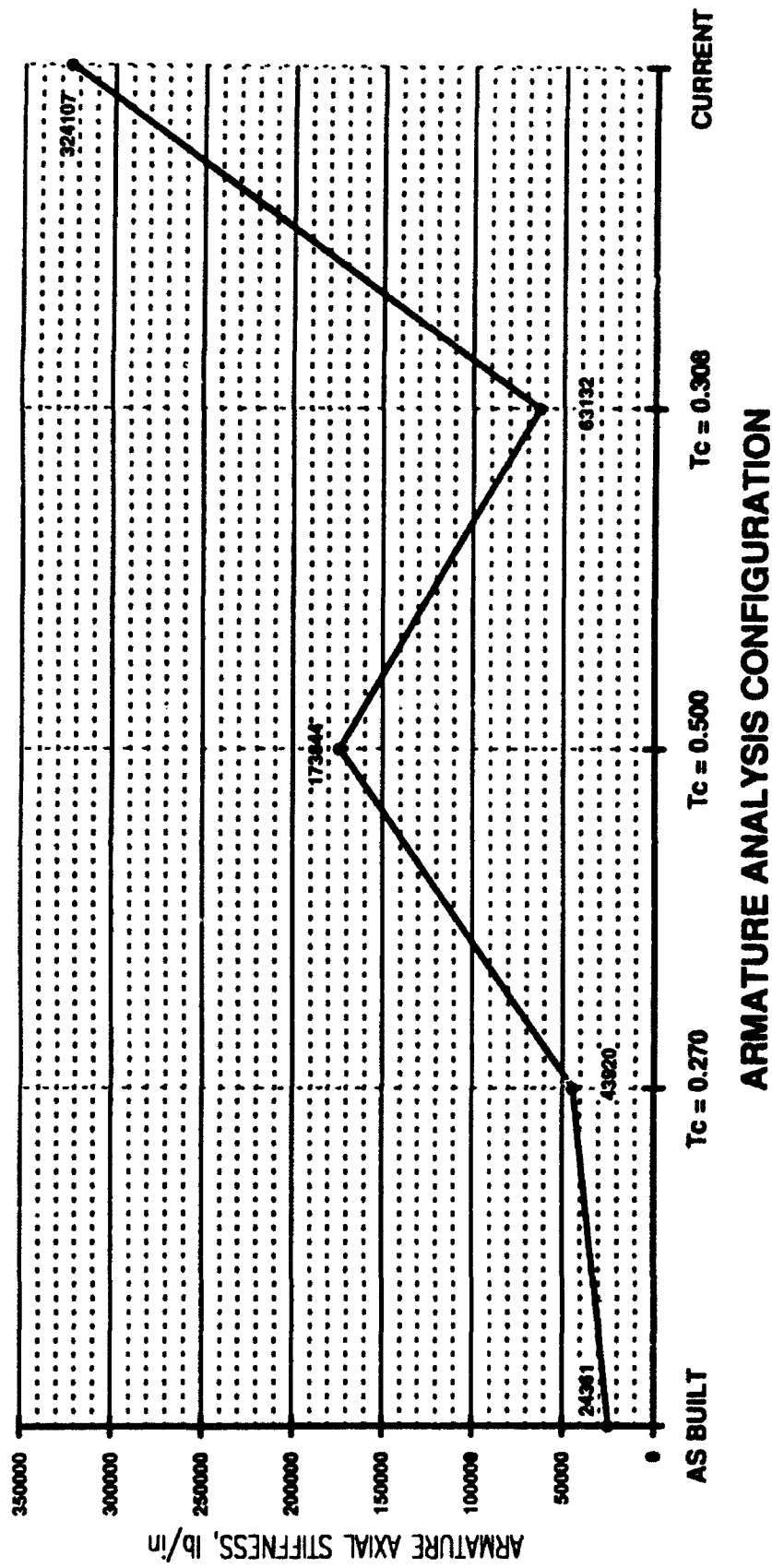


Figure 4-6. FEA Model Stiffness Plot

The set of data labelled "Current" corresponds to a magnetic armature configuration in which the stops have been removed from the stators and attached directly to the as-built armature, resulting in a dramatic improvement in armature stiffness. The predicted armature stiffness is 3.2×10^5 lb/in, which is the same magnitude as was measured in the two-point load tests. The deflection plot shows that this configuration yields far better stiffness properties than thickening the armature central and stop regions.

With the stops attached to the armature, the armature configuration reverts to that shown in the cryogenic magnetic gimbal. This can be considered an analysis of the final armature configuration. The analysis results vividly demonstrate the validity of the design approach finally adopted for the cryogenic magnetic gimbal. Figure 4-6 is a plot of stiffness versus load case, allowing comparison of the relative merits of each approach considered.

The stops were removed from the magnetic bearing housings and attached to the armature using bolts and adhesives. This approach was implemented because of its simplicity and by virtue of the dramatic stiffness improvements projected by the analysis. This is the reason for the data set being labelled "Current" in Figures 4-5 and 4-6. The magnetic bearing armature configuration with the stops attached can be easily seen on the end of the shaft in Figure 3-11.

With the incorporation of the magnetic bearing stops onto the armature, load-deflection tests were repeated. Results of the two-point load tests generated measured stiffness values of 3.0×10^5 lb/in, as expected.

Results of the single-point load tests yielded effective assembly stiffness values on the order of 3.8×10^4 lb/in. This confirmed the suspicions that a major contributor to compliance was the armature interface stiffness.

An effort was made to evaluate possible corrective measures. Principal among this effort was an investigation of increasing the surface size of the attachment interface. An empirical test was performed in which a set of jacking posts were placed between the central region of the armature and a step on the shaft. This test configuration (with jack posts) is shown in Figure 3-11. The single-point load tests were repeated with this setup. Despite the crudeness of the setup, the effective axial stiffness of the assembly increased to 6×10^4 lb/in.

These results substantiated the hypothesis that the shaft interface is the greatest contributor to system compliance. Further, any significant improvements in system rigidity can only be achieved by modifying that interface.

Potential remedies for this lack of rigidity at the armature interface include redesign of the interface to introduce either a substantial thermal fit of the armature to the shaft, or an increase in the mounting surface area at the interface.

4.2.4 Impact on System Performance

The previous sections describe problems encountered with geometrics, interfaces, and mechanical stiffness. This section briefly describes their impact on system performance.

Under ideal conditions, the passive magnetic bearing armature operates parallel to its stator elements, independent of rotation about the gimbal axis. Under these conditions, forces due to passive magnetics are divided into radial restoring forces and axial imbalance forces, and all torques associated with the passive bearing remain negligible relative to the other forces associated with the bearing given the flux pattern shown in Figure 4-7.

Assume that the armature is initially tilted relative to the stator sections. Magnetic flux will tend to follow the path of least reluctance, which is illustrated in Figure 4-8 for this illustrative case. Compliance of the armature-to-shaft interface and of the armature itself will react to this torque to close the magnetic gaps even further, thereby increasing the torque component. This positive-feedback condition persists until the magnetic gap has fully closed, or the mechanical restoring torque of the armature and interface matches the imbalance force of the magnetics. In the 4-DOF test fixture, the interface and armature stiffness was low enough that full rotation of the bearing assembly was not possible without touching down on the hard stops.

The stiffness problems can be corrected by improving the armature and armature interfaces as described in the previous sections; however, there are system-level problems associated with the inherent design features of the PRAA bearing assembly.

There will always be a finite level of misalignment between the armature and stator sections of the magnetic bearing assembly, causing an uneven force distribution across the magnetic interface. This nonuniform distribution causes a torque about an axis in the plane perpendicular to the bearing rotation axis. Assuming the system is stiff enough to prevent the armature from touching down, there will still be a reaction torque place on the stator. As the gimbal rotates, this torque will rotate, causing a reaction disturbance as a function of gimbal rotation. Prior to using or pursuing this bearing concept, the distribution of force across the magnetic interface as a function of external disturbances and rotation needs to be fully understood and the resultant disturbance must be acceptable for the application.

The existing magnetic bearing test fixture provides a good foundation on which to build to test analytical predictions.

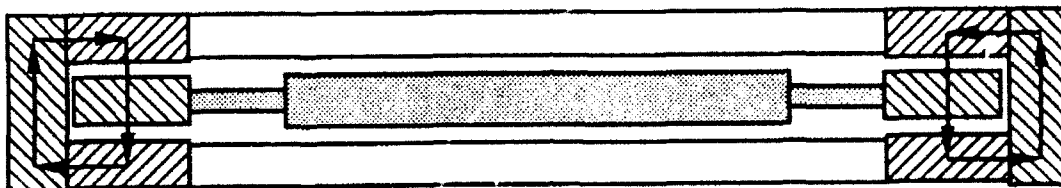


Figure 4-7. Two-dimensional Ideal Passive Actuator Magnetic Flux Paths

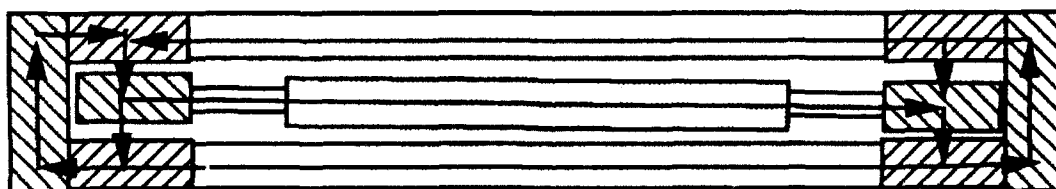


Figure 4-8. Magnetic Flux Path Due Armature Tilt

5. CONCLUSIONS

The cryobearing design, with its small magnetic gaps and large magnetic forces, makes it very sensitive to tolerances and interface design. As a result of the experience derived from designing the cryogenic magnetic gimbal and designing and building the cryogenic magnetic bearing and the 4-DOF cryogenic test fixture, some conclusions can be made.

1. Despite efforts to understand the lower-than-predicted radial restoring stiffness, a proven explanation is yet unavailable. Design predictions, using two separate models, yield the same result. Smoothing the toothed surfaces and reannealing the magnetic iron yielded some performance improvement, but was still far lower than predicted. Additional model and material research is required to understand the reasons for the poor performance.
2. The importance of tolerance and geometric control cannot be underestimated in a device like the cryogenic magnetic bearing, which has very small physical clearances, nor should these be compromised to reduce cost or minimize schedule. Doing so can lead to significant problems.
3. Tolerances and geometrics can be difficult to control at the component level for a device sensitive to tolerance buildups, such as the cryobearing device. To ensure proper assembly function, use should be made of General Machining Assemblies (GMA). By machining at the subassembly and assembly levels, the tolerance buildups are reduced to manageable levels. In the case of the cryobearing magnetics and test fixture, the combination of large internal forces and tolerance buildups resulted in the loss of magnetic gaps. Machining at the assembly level would have eliminated many of the deficiencies uncovered during integration operations.
4. Placement of stops on the armature is the optimum location for the cryobearing. This location not only allows for establishment of assembly-level dimensions, but also serves to reinforce the armature.
5. A major deficiency of the design approach adopted for the cryogenic magnetic bearing was the armature mounting interface. The current ratio of mounting radius to armature radius is in excess of 21:1. A more workable ratio of 5:1 or 10:1 is a more realistic value if the full potential of the magnetic bearing is to be realized. Further tests can establish a workable ratio.
6. Environmental concerns, i.e., operation from room ambient conditions to cryogenic temperatures in hard vacuum, led to a design that was pessimistic in its use of materials. Compounding this was a desire to prohibit the use of any processes that would limit the ability to assemble and disassemble the device. These factors imposed severe limitations on options for fastening, joining, and locking. Greater use of thermal fits and adhesives should have been used. For example,

a good thermal fit on the armature/shaft interface would have yielded a more rigid interface with less susceptibility to compliance. Adhesives to lock the shaft nut to the shaft and to the armature would have further enhanced the unit rigidity. Problems with the flex pivots loosening also would have been avoided.

7. A reference surface that is accessible after assembly is desirable. Without such a surface, all characterization or measurements of assembly geometrics and runouts must be performed indirectly. For devices with stringent dimensional requirements, such as the cryogenic magnetic gimbal or the 4-DOF test fixture, it is important that a reference surface be available to allow for direct measurement.

6. RECOMMENDATIONS

Two follow-on approaches should be carefully considered. One would be to revert to the original, all-active magnetic suspension design, which uses well proven technology and would provide much higher radial/torsional stiffness with lower weight, but would incur the complexity of five axes of active control. The second approach would be to completely re-evaluate the passive bearing design approach, starting with a simplified, larger scale, linear model. The intent would be to isolate the cause of the existing problems to either a design error, a material/fabrication problem, or an over-extended extrapolation of the extremely fine teeth and small gaps employed in this design. The calculation techniques established for the SSO heritage passive bearings were valid, since they were confirmed by hardware test data. Some careful backtracking and modeling effort is an appropriate first step.

The cryogenic magnetic bearing 4-DOF test fixture presents a useful tool to empirically evaluate analytical predictions. Continued analysis and subsequent testing should be performed to correct the deficiencies of this design and prove the concept for flight application.

Given the existing hardware, the armature interface to the shaft should be modified to increase the effective assembly stiffness and allow completion of integration and bearing evaluation operations. Analysis and some lab tests can define the specific changes. One possible option to improve the armature attachment is to increase the contact-surface area by taking advantage of the less-than-predicted passive radial attractive forces. This option would increase the size of the bore through the active axial actuator. As a result, the diameter of the shaft interface could be enlarged. Another option is to mount the armature on a stub shaft that is rigidly attached to the main shaft.

APPENDIX
COSMOS/M ANALYSIS INPUT AND CASE A & K RESULTS

CRYOBEARING ARMATURE FEA MODEL AND INPUT

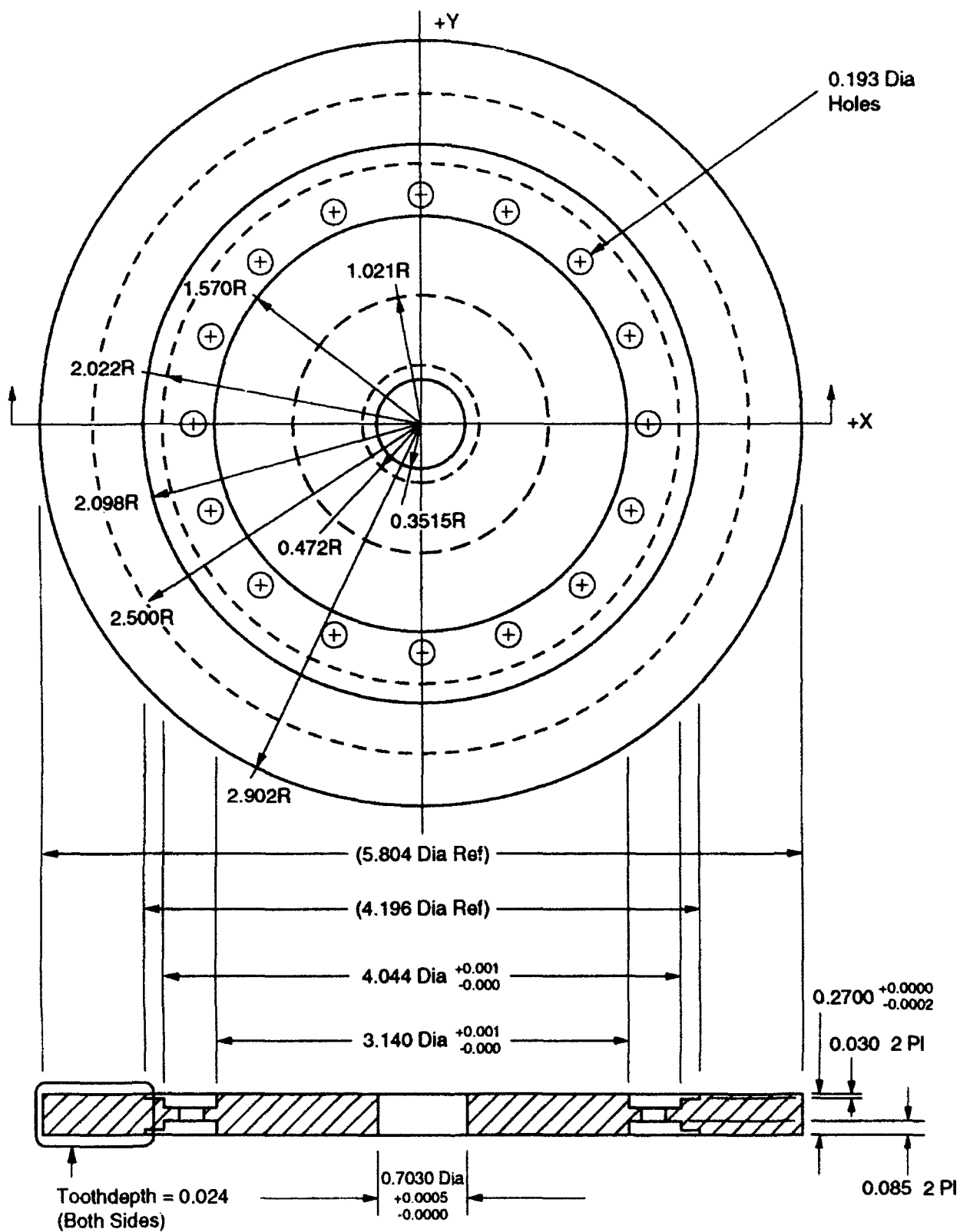


Figure A-1. Cryobearing Armature

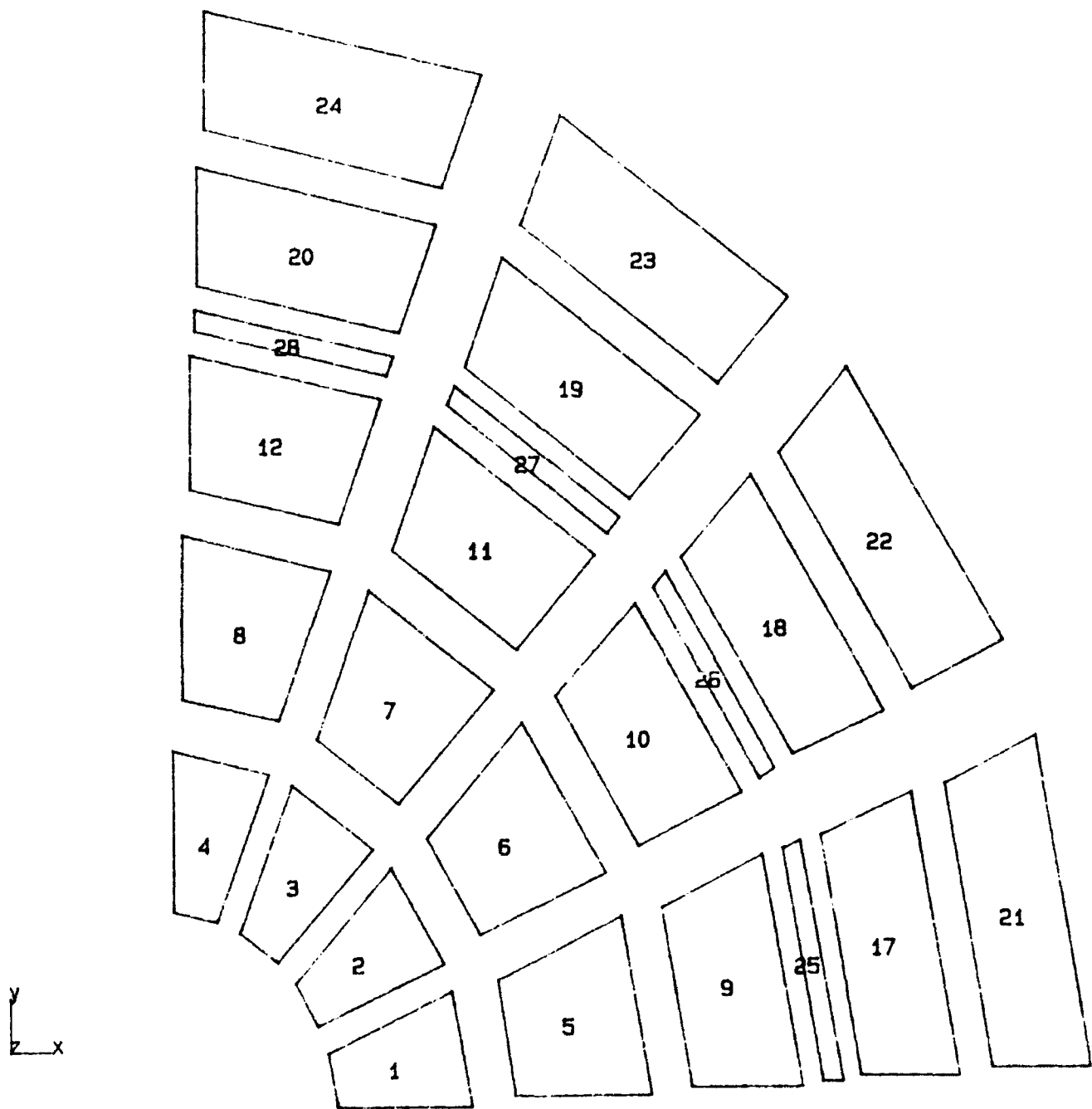


Figure A-2. Cryobearing FEA Model (Exploded) - Plan View

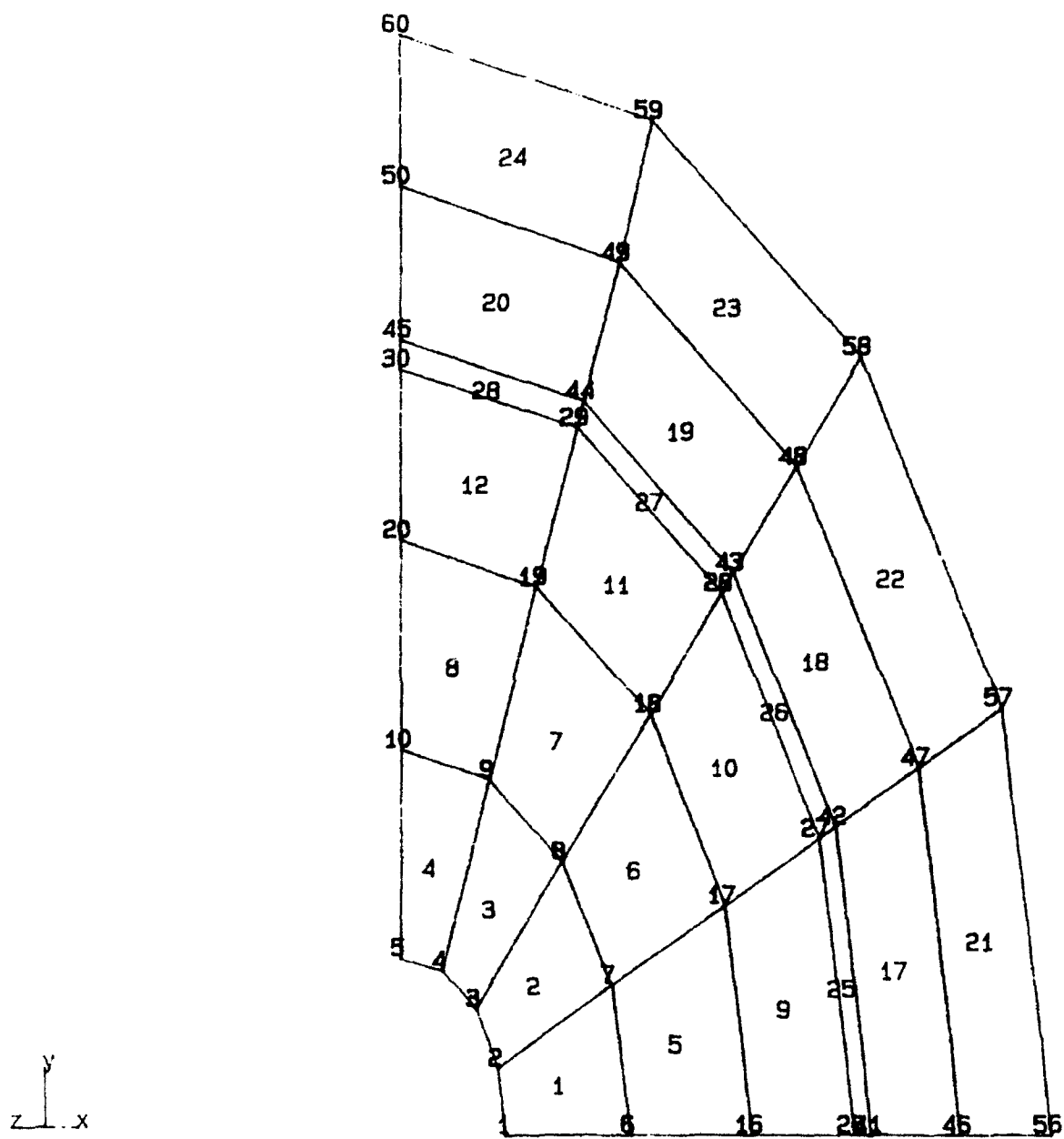


Figure A-3. Cryobearing FEA Model - Isometric View

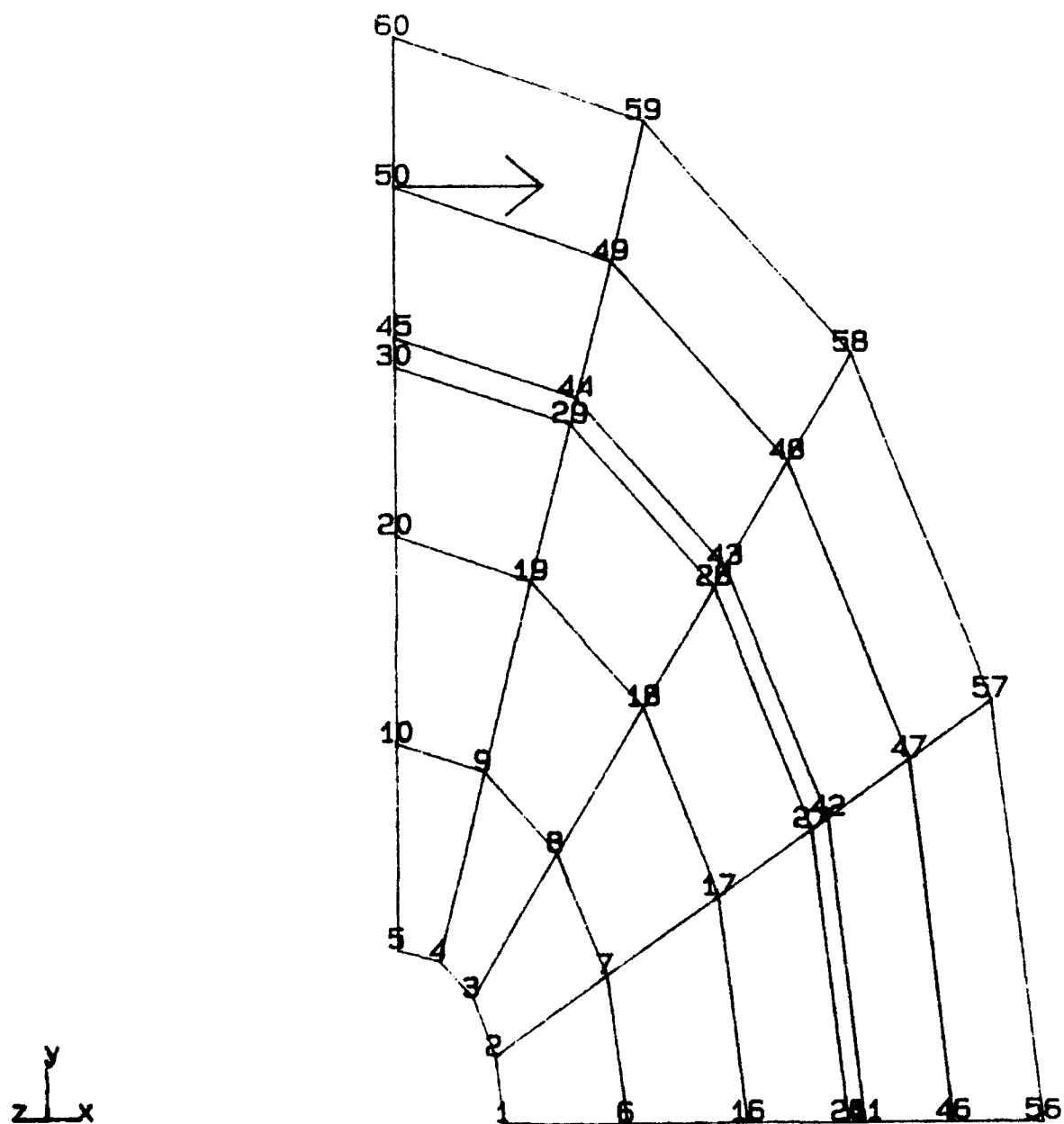


Figure A-4. Cryobearing FEA Model (Applied Load) - Isometric View

Thickness of as-built armature recess = $t_{\text{orig}} = 0.270 - 2(0.085) = 0.100$ in.

Diameter inner = 3.140 in. = D_i = Inner diameter dimension of stop recess

Diameter outer = 4.044 in. = D_o = Outer diameter dimension of stop recess

$$\text{Stop Recess Area} = \frac{\pi(D_o^2 - D_i^2)}{4} = \frac{\pi}{4} [(4.044)^2 - (3.140)^2] = 5.100 \text{ in.}^2 = A$$

Stop Area Thru holes $\Rightarrow \# = 16$

$D_H = 0.193$ = Hole Diameter, in.

$$\text{Hole Area} = A\delta = 16 \left[\frac{\pi}{4} (0.193)^2 \right] = 0.468 \text{ in.}^2$$

$$\text{Effective Area} = A' = A - A\delta = 5.100 - 0.468 = 4.633 \text{ in.}^2$$

$$\text{Volume} = \text{Vol orig} = A t_{\text{orig}} = (5.100) (0.100) = 0.510 \text{ in.}^3$$

$$\text{Effective Volume} = \text{Vol}' = A' t_{\text{orig}} = (4.633) (0.100) = 0.463 \text{ in.}^3$$

$$\text{Let Vol}' = A t' = 0.463 \text{ in.}^3 = (5.100) t'$$

$$\therefore t' = \frac{\text{Vol}'}{A} = \frac{0.463}{5.100} = 0.0908 \text{ in.} = \text{Equivalent Stop Area Thickness}$$

Figure A-5. As-built Armature Stop-area Equivalent Thickness

ALLEGHENY LUDLUM VANADIUM PERMENDUR

Vanadium Permendur is an alloy of equal proportions of iron and cobalt with about 2% vanadium. It is manufactured primarily for use in electrical equipment of special design in which a high magnetic permeability at very high inductions is essential. In these applications, a large weight reduction is realized with subsequent savings in space, copper, insulation, etc.

Vanadium is added to Permendur primarily to make the alloy ductile by slowing the rate of superlattice formation transformation rate so that the ductile disordered structure is retained after quenching from above the critical temperature to room temperature. The rate of cooling is limited by the size of section and must not be too thick if the material is to be cold worked after quenching. When heavy sections are required, they must be formed hot. Light cuts and slow speeds are recommended for machining Vanadium Permendur. All cold work should be performed on the material prior to the final heat treatment.

Table A-1 lists the typical physical, mechanical, and magnetic properties of Vanadium Permendur as hard cold rolled and as annealed after fabrication to develop optimum magnetic properties.

TABLE A-1
VANADIUM PERMENDUR
TYPICAL PHYSICAL, MECHANICAL, AND MAGNETIC PROPERTIES

	After Final Anneal	Hard Cold Rolled Longitudinal
Ultimate Tensile Strength, psi	90,000	195,000
Yield Strength, psi	55,000	185,000
Elongation, Percent in 2 inches	5	1
Modulus of Elasticity, psi	35,000,000	29,000,000
Hardness, Rockwell*	97B	35C
Resistivity, Microhm cm	40	
Specific Gravity	8.15	
Density	0.293 lb/in. ³	
Curie Temperature, °F	1710	
Saturation Induction, B ₀ , Gauss	23,000	
*As quenched from 1650 F, the hardness is 24 Rockwell C. Cold rolled strip in coils is furnished only in the as-cold-rolled condition.		

Table A-2 lists the mean linear coefficient of thermal expansion for Vanadium Permendur.

TABLE A-2
VANADIUM PERMENDUR
MEAN LINEAR COEFFICIENT OF THERMAL EXPANSION

Temperature Range		Coefficient	
°F	°C	per °F	per °C
68-212	20-100	5.1×10^{-6}	9.2×10^{-6}
68-392	20-200	5.3×10^{-6}	9.5×10^{-6}
68-572	20-300	5.4×10^{-6}	9.8×10^{-6}
68-752	20-400	5.6×10^{-6}	10.1×10^{-6}
68-932	20-500	5.8×10^{-6}	10.4×10^{-6}
68-1112	20-600	5.8×10^{-6}	10.5×10^{-6}
68-1292	20-700	6.0×10^{-6}	10.8×10^{-6}
68-1472	20-800	6.3×10^{-6}	11.3×10^{-6}

The hardness of the quenched material is increased by cold rolling but never exceeds a value that cannot be tolerated in punch-press operations. From the quenched state, the tensile strength increases proportionally with the amount of cold reduction. Cold rolled strip in coils is furnished only in the as-cold-rolled condition.

```

C* =====
C*   Input to the problem : ROTOR
C*   Created on                3/27/1991   13:20
C* =====
C* INPUTFILE :      CRYO.MOD
TITLE, CRYOBEARING ARMATURE CHECK  REV A 27MAR91
EG, 1 SHELL4 , 0, 0, 0, 0, 0, 0, 0, 0
EG, 2 SHELL4 , 0, 0, 0, 0, 0, 0, 0, 0
EG, 3 SHELL4 , 0, 0, 0, 0, 0, 0, 0, 0
EG, 4 SHELL4 , 0, 0, 0, 0, 0, 0, 0, 0
EX, 1, 3.500000E+007
NUXY, 1, 3.000000E-001
DENS, 1, 7.583000E-004
RC, 1, 1 2.700000E-001
RC, 2, 2 9.080000E-002
RC, 3, 3 2.100000E-001
RC, 4, 4 2.220000E-001
ACTIVE CS 0
N, 1, 4.720000E-001 0.000000E+000 0.000000E+000
N, 2, 4.349079E-001 1.837237E-001 0.000000E+000
N, 3, 3.337544E-001 3.337544E-001 0.000000E+000
N, 4, 1.837237E-001 4.349079E-001 0.000000E+000
N, 5, 0.000000E-000 4.720000E-001 0.000000E+000
N, 6, 1.021000E+000 0.000000E+000 0.000000E+000
N, 7, 9.407648E-001 3.974193E-001 0.000000E+000
N, 8, 7.219560E-001 7.219560E-001 0.000000E+000
N, 9, 3.974193E-001 9.407648E-001 0.000000E+000
N, 10, 0.000000E-000 1.021000E+000 0.000000E+000
N, 16, 1.570000E+000 0.000000E+000 0.000000E+000
N, 17, 1.446622E+000 6.111149E-001 0.000000E+000
N, 18, 1.110158E+000 1.110158E+000 0.000000E+000
N, 19, 6.111149E-001 1.446622E+000 0.000000E+000
N, 20, 0.000000E-000 1.570000E+000 0.000000E+000
N, 26, 2.022000E+000 0.000000E+000 0.000000E+000
N, 27, 1.863101E+000 7.870537E-001 0.000000E+000
N, 28, 1.429770E+000 1.429770E+000 0.000000E+000
N, 29, 7.870537E-001 1.863101E+000 0.000000E+000
N, 30, 0.000000E-000 2.022000E+000 0.000000E+000
N, 41, 2.098000E+000 0.000000E+000 0.000000E+000
N, 42, 1.933129E+000 8.166363E-001 0.000000E+000
N, 43, 1.483510E+000 1.483510E+000 0.000000E+000
N, 44, 8.166363E-001 1.933129E+000 0.000000E+000
N, 45, 0.000000E-000 2.098000E+000 0.000000E+000
N, 46, 2.500000E+000 0.000000E+000 0.000000E+000
N, 47, 2.303538E+000 9.731128E-001 0.000000E+000
N, 48, 1.767767E+000 1.767767E+000 0.000000E+000
N, 49, 9.731128E-001 2.303538E+000 0.000000E+000
N, 50, 0.000000E-000 2.500000E+000 0.000000E+000
N, 56, 2.902000E+000 0.000000E+000 0.000000E+000
N, 57, 2.673946E+000 1.129589E+000 0.000000E+000
N, 58, 2.052024E+000 2.052024E+000 0.000000E+000
N, 59, 1.129589E+000 2.673946E+000 0.000000E+000
N, 60, 0.000000E-000 2.902000E+000 0.000000E+000
ACTIVE GROUP 1
ACTIVE MAT 1

```

Figure A-6. Cryobearing COSMOS/M Input Log (Sheet 1)

```

ACTIVE REAL 1
E, 1, 1,2,7,6
E, 2, 2,3,8,7
E, 3, 3,4,9,8
E, 4, 4,5,10,9
E, 5, 6,7,17,16
E, 6, 7,8,18,17
E, 7, 8,9,19,18
E, 8, 9,10,20,19
ACTIVE GROUP 2
ACTIVE REAL 2
E, 9, 16,17,27,26
E, 10, 17,18,28,27
E, 11, 18,19,29,28
E, 12, 19,20,30,29
ACTIVE GROUP 4
ACTIVE REAL 4
E, 17, 41,42,47,46
E, 18, 42,43,48,47
E, 19, 43,44,49,48
E, 20, 44,45,50,49
E, 21, 46,47,57,56
E, 22, 47,48,58,57
E, 23, 48,49,59,58
E, 24, 49,50,60,59
ACTIVE GROUP 3
ACTIVE REAL 3
E, 25, 26,27,42,41
E, 26, 27,28,43,42
E, 27, 28,29,44,43
E, 28, 29,30,45,44
D, 1, UX, 0.000000E+000, 1, 1, UY, UZ, ROTX, ROTY, ROTZ
D, 2, UX, 0.000000E+000, 2, 1, UY, UZ, ROTX, ROTY, ROTZ
D, 3, UX, 0.000000E+000, 3, 1, UY, UZ, ROTX, ROTY, ROTZ
D, 4, UX, 0.000000E+000, 4, 1, UY, UZ, ROTX, ROTY, ROTZ
D, 5, UX, 0.000000E+000, 5, 1, UY, UZ, ROTX, ROTY, ROTZ
D, 6, UY, 0.000000E+000, 6, 1, ROTX, ROTZ
D, 7, ROTZ, 0.000000E+000, 7, 1
D, 8, ROTZ, 0.000000E+000, 8, 1
D, 9, ROTZ, 0.000000E+000, 9, 1
D, 10, UX, 0.000000E+000, 10, 1, ROTY, ROTZ
D, 16, UY, 0.000000E+000, 16, 1, ROTX, ROTZ
D, 17, ROTZ, 0.000000E+000, 17, 1
D, 18, ROTZ, 0.000000E+000, 18, 1
D, 19, ROTZ, 0.000000E+000, 19, 1
D, 20, UX, 0.000000E+000, 20, 1, ROTY, ROTZ
D, 26, UY, 0.000000E+000, 26, 1, ROTX, ROTZ
D, 27, ROTZ, 0.000000E+000, 27, 1
D, 28, ROTZ, 0.000000E+000, 28, 1
D, 29, ROTZ, 0.000000E+000, 29, 1
D, 30, UX, 0.000000E+000, 30, 1, ROTY, ROTZ
D, 41, UY, 0.000000E+000, 41, 1, ROTX, ROTZ
D, 42, ROTZ, 0.000000E+000, 42, 1
D, 43, ROTZ, 0.000000E+000, 43, 1
D, 44, ROTZ, 0.000000E+000, 44, 1

```

Figure A-6. Cryobearing COSMOS/M Input Log (Sheet 2)

```

D, 45, UX, 0.000000E+000, 45, 1, ROTY, ROTZ
D, 46, UY, 0.000000E+000, 46, 1, ROTX, ROTZ
D, 47, ROTZ, 0.000000E+000, 47, 1
D, 48, ROTZ, 0.000000E+000, 48, 1
D, 49, ROTZ, 0.000000E+000, 49, 1
D, 50, UX, 0.000000E+000, 50, 1, ROTY, ROTZ
D, 56, UY, 0.000000E+000, 56, 1, ROTX, ROTZ
D, 57, ROTZ, 0.000000E+000, 57, 1
D, 58, ROTZ, 0.000000E+000, 58, 1
D, 59, ROTZ, 0.000000E+000, 59, 1
D, 60, UX, 0.000000E+000, 60, 1, ROTY, ROTZ
ACTIVE LC 1
F, 50, FZ -1.000000E+002
MERGE
      C* Coincident nodes are not found
DATA_CHECK
RENUM,ON
      C*      Attempt to prescribe an undefined node      11
      C*      Attempt to prescribe an undefined node      12
      C*      Attempt to prescribe an undefined node      13
      C*      Attempt to prescribe an undefined node      14
      C*      Attempt to prescribe an undefined node      15
      C*      Attempt to prescribe an undefined node      21
      C*      Attempt to prescribe an undefined node      22
      C*      Attempt to prescribe an undefined node      23
      C*      Attempt to prescribe an undefined node      24
      C*      Attempt to prescribe an undefined node      25
      C*      Attempt to prescribe an undefined node      31
      C*      Attempt to prescribe an undefined node      32
      C*      Attempt to prescribe an undefined node      33
      C*      Attempt to prescribe an undefined node      34
      C*      Attempt to prescribe an undefined node      35
      C*      Attempt to prescribe an undefined node      36
      C*      Attempt to prescribe an undefined node      37
      C*      Attempt to prescribe an undefined node      38
      C*      Attempt to prescribe an undefined node      39
      C*      Attempt to prescribe an undefined node      40
      C*      Attempt to prescribe an undefined node      51
      C*      Attempt to prescribe an undefined node      52
      C*      Attempt to prescribe an undefined node      53
      C*      Attempt to prescribe an undefined node      54
      C*      Attempt to prescribe an undefined node      55
RF, 1, ALL, 60, 1
NODSET, 1, 60
PRINT, 1, 0, 1, 1, 0, 0, 0, 0, 1, 1
      C*      S.R.A.C.      Problem: ROTOR      3/27/1991  13:22:10
      C*      S.R.A.C.      Problem: ROTOR      3/27/1991  13:22:21
      C*      S.R.A.C.      Problem: ROTOR      3/27/1991  13:22:35
      C*      =====
      C*      Begin corrections to the input      3/27/1991  13:23
      C*      =====

```

Figure A-6. Cryobearing COSMOS/M Input Log (Sheet 3)

CRYOBEARING ARMATURE FEA RESULTS -
"AS BUILT" CONFIGURATION
CASE A

```

*****
*****
*
*           C O S M O S / M
*
*           VERSION:    1.52A
*
*           DISTRIBUTED BY:
*
*           STRUCTURAL RESEARCH AND ANALYSIS CORPORATION
*           1661 LINCOLN BLVD. #100
*
*           SANTA MONICA, CALIFORNIA 90404
*
*           TEL. NO.    (213) 452-2158
*
*           COPYRIGHT 1988 S. R. A. C.
*
*****
*****

```

DATE: 3/27/1991 TIME: 13:22:57

TITLE : CRYOBEARING ARMATURE CHECK REV A 27MAR91;

E L E M E N T	G R O U P	D A T A
-----	-----	-----

```

ELEMENT GROUP NUMBER 1
ELEMENT_NAME:
SHELL4      Four node thin shell elements
Type of Shell element= . . . . . 0
  EQ. 0 ; QUAD 2 element
  EQ. 1 ; QUAD 4 element
Material type option = . . . . . 0
  EQ. 0 : Linear elastic material model
  EQ. 1 : Von-Mises elasto-plastic model
Large displacement option = . . . . . 0
  EQ. 0 : Small displacement formulation
  EQ. 1 : Large displacement formulation
Material creep option = . . . . . 0
  EQ. 0 : Do not consider creep effects
  EQ. 1 : Include creep effects
          (Currently not used with plasticity)

```

```

ELEMENT GROUP NUMBER 2
ELEMENT_NAME:
SHELL4      Four node thin shell elements
Type of Shell element= . . . . . 0
  EQ. 0 ; QUAD 2 element
  EQ. 1 ; QUAD 4 element

```

Figure A-7. Cryobearing Armature As-built FEA Results (Sheet 1)

```

Material type option = . . . . . 0
  EQ. 0 : Linear elastic material model
  EQ. 1 : Von-Mises elasto-plastic model
Large displacement option = . . . . . 0
  EQ. 0 : Small displacement formulation
  EQ. 1 : Large displacement formulation
Material creep option = . . . . . 0
  EQ. 0 : Do not consider creep effects
  EQ. 1 : Include creep effects
          (Currently not used with plasticity)

ELEMENT GROUP NUMBER   3
ELEMENT_NAME:
SHELL4      Four node thin shell elements
Type of Shell element= . . . . . 0
  EQ. 0 ; QUAD 2 element
  EQ. 1 ; QUAD 4 element
Material type option = . . . . . 0
  EQ. 0 : Linear elastic material model
  EQ. 1 : Von-Mises elasto-plastic model
Large displacement option = . . . . . 0
  EQ. 0 : Small displacement formulation
  EQ. 1 : Large displacement formulation
Material creep option = . . . . . 0
  EQ. 0 : Do not consider creep effects
  EQ. 1 : Include creep effects
          (Currently not used with plasticity)

ELEMENT GROUP NUMBER   4
ELEMENT_NAME:
SHELL4      Four node thin shell elements
Type of Shell element= . . . . . 0
  EQ. 0 ; QUAD 2 element
  EQ. 1 ; QUAD 4 element
Material type option = . . . . . 0
  EQ. 0 : Linear elastic material model
  EQ. 1 : Von-Mises elasto-plastic model
Large displacement option = . . . . . 0
  EQ. 0 : Small displacement formulation
  EQ. 1 : Large displacement formulation
Material creep option = . . . . . 0
  EQ. 0 : Do not consider creep effects
  EQ. 1 : Include creep effects
          (Currently not used with plasticity)
*****

      R E A L      C O N S T A N T      D A T A
      -----
REAL CONSTANT SET      1
Associated with :
SHELL4      Four node thin shell elements
Thickness of the plate =  0.27000
Temperature Gradient   =  0.00000

```

Figure A-7. Cryobearing Armature As-built FEA Results (Sheet 2)

REAL CONSTANT SET 2
 Associated with :
 SHELL4 Four node thin shell elements
 Thickness of the plate = 0.90800E-01
 Temperature Gradient = 0.00000

REAL CONSTANT SET 3
 Associated with :
 SHELL4 Four node thin shell elements
 Thickness of the plate = 0.21000
 Temperature Gradient = 0.00000

REAL CONSTANT SET 4
 Associated with :
 SHELL4 Four node thin shell elements
 Thickness of the plate = 0.22200
 Temperature Gradient = 0.00000

M A T E R I A L P R O P E R T Y D A T A

MATERIAL PROPERTY SET 1

EX : X Elastic Modulus = 0.35000E+08
 NUXY : Poisson Ratio = 0.30000
 DENS : Mass Density = 0.75830E-03

N O D A L I N P U T D A T A

NODE BOUNDARY CONDITION CODES

(0 = FREE ; 1 = FIXED)

NODAL POINT COORDINTES

	X	Y	Z	XX	YY	ZZ	X	Y	Z
1	0	0	0	0	0	0	0.47200	0.00000	0.00000
2	0	0	0	0	0	0	0.43491	0.18372	0.00000
3	0	0	0	0	0	0	0.33375	0.33375	0.00000
4	0	0	0	0	0	0	0.18372	0.43491	0.00000
5	0	0	0	0	0	0	0.00000	0.47200	0.00000
6	0	0	0	0	0	0	1.0210	0.00000	0.00000
7	0	0	0	0	0	0	0.94076	0.39742	0.00000
8	0	0	0	0	0	0	0.72196	0.72195	0.00000
9	0	0	0	0	0	0	0.39742	0.94076	0.00000
10	0	0	0	0	0	0	0.00000	1.0210	0.00000
16	0	0	0	0	0	0	1.5700	0.00000	0.00000
17	0	0	0	0	0	0	1.4466	0.61111	0.00000
18	0	0	0	0	0	0	1.1102	1.1102	0.00000
19	0	0	0	0	0	0	0.61111	1.4466	0.00000
20	0	0	0	0	0	0	0.00000	1.5700	0.00000
26	0	0	0	0	0	0	2.0220	0.00000	0.00000
27	0	0	0	0	0	0	1.8631	0.78705	0.00000
28	0	0	0	0	0	0	1.4298	1.4298	0.00000
29	0	0	0	0	0	0	0.78705	1.8631	0.00000
30	0	0	0	0	0	0	0.00000	2.0220	0.00000
41	0	0	0	0	0	0	2.0980	0.00000	0.00000

Figure A-7. Cryobearing Armature As-built FEA Results (Sheet 3)

42	0	0	0	0	0	0	1.9331	0.81664	0.00000
43	0	0	0	0	0	0	1.4835	1.4835	0.00000
44	0	0	0	0	0	0	0.81664	1.9331	0.00000
45	0	0	0	0	0	0	0.00000	2.0980	0.00000
46	0	0	0	0	0	0	2.5000	0.00000	0.00000
47	0	0	0	0	0	0	2.3035	0.97311	0.00000
48	0	0	0	0	0	0	1.7678	1.7678	0.00000
49	0	0	0	0	0	0	0.97311	2.3035	0.00000
50	0	0	0	0	0	0	0.00000	2.5000	0.00000
56	0	0	0	0	0	0	2.9020	0.00000	0.00000
57	0	0	0	0	0	0	2.6739	1.1296	0.00000
58	0	0	0	0	0	0	2.0520	2.0520	0.00000
59	0	0	0	0	0	0	1.1296	2.6739	0.00000
60	0	0	0	0	0	0	0.00000	2.9020	0.00000

E L E M E N T D A T A

ELEM	GROUP	MAT	REAL	NOD1	NOD2	NOD3	NOD4
1	1	1	1	1	2	7	6
2	1	1	1	2	3	8	7
3	1	1	1	3	4	9	8
4	1	1	1	4	5	10	9
5	1	1	1	6	7	17	16
6	1	1	1	7	8	18	17
7	1	1	1	8	9	19	18
8	1	1	1	9	10	20	19
9	2	1	2	16	17	27	26
10	2	1	2	17	18	28	27
11	2	1	2	18	19	29	28
12	2	1	2	19	20	30	29
17	4	1	4	41	42	47	46
18	4	1	4	42	43	48	47
19	4	1	4	43	44	49	48
20	4	1	4	44	45	50	49
21	4	1	4	46	47	57	56
22	4	1	4	47	48	58	57
23	4	1	4	48	49	59	58
24	4	1	4	49	50	60	59
25	3	1	3	26	27	42	41
26	3	1	3	27	28	43	42
27	3	1	3	28	29	44	43
28	3	1	3	29	30	45	44

N O D A L L O A D S

NODF	FX	FY	FZ	MX	MY	MZ
50	0.0000	0.0000	-100.0	0.0000	0.0000	0.0000

Figure A-7. Cryobearing Armature As-built FEA Results (Sheet 4)

C O N T R O L I N F O R M A T I O N

NUMBER OF LOAD CASES	(NLCASE) =	1
SOLUTION MODE	(MODEX) =	0
EQ. 0, STATIC ANALYSIS		
EQ. 1, BUCKLING ANALYSIS		
EQ. 2, DYNAMIC ANALYSIS		
THERMAL LOADING FLAG	(ITHERM) =	0
EQ. 0, NO THERMAL EFFECTS CONSIDERED		
EQ. 1, ADD TEMPERATURE EFFECT		
GRAVITY LOADING FLAG	(IGRAV) =	0
EQ. 0, NO GRAVITY LOADING CONSIDERED		
EQ. 1, ADD GRAVITY LOADING EFFECT		
CENTRIFUGAL LOADING FLAG	(ICNTRF) =	0
EQ. 0, NO CENTRIFUGAL LOADING CONSIDERED		
EQ. 1, ADD CENTRIFUGAL LOADING EFFECT		
IN-PLANE STIFFENING FLAG	(INPLN) =	0
EQ. 0, NO IN-PLANE EFFECTS CONSIDERED		
EQ. 1, IN-PLANE EFFECTS CONSIDERED		
SOFT SPRING ADDITION FLAG	(ISOFT) =	0
EQ. 0, NO SOFT SPRING OPTION		
EQ. 1, SOFT SPRING ADDED		
SAVE DECOMPOSED STIFFNESS MATRIX FLAG . . .	(ISAVK) =	0
EQ. 0, DO NOT SAVE DECOMPOSED K		
EQ. 1, SAVE DECOMPOSED K		
FORM STIFFNESS MATRIX FLAG	(IFORMK) =	0
EQ. 0, FORM STIFFNESS MATRIX		
EQ. 1, USE EXIST DECOMPOSED STIFFNESS MATRIX		

T O T A L S Y S T E M D A T A

NUMBER OF EQUATIONS	(NEQ) =	210
NUMBER OF MATRIX ELEMENTS	(NWK) =	7143
MAXIMUM HALF BANDWIDTH	(MK) =	60
MEAN HALF BANDWIDTH	(MM) =	34
NUMBER OF ELEMENTS.	(NUME) =	24
NUMBER OF NODAL POINTS.	(NUMNP) =	35
NUMBER OF BLOCKS.	(NBLK) =	1

MAXIMUM DIAGONAL STIFFNESS MATRIX VALUE = 0.331870E+09
 MINIMUM DIAGONAL STIFFNESS MATRIX VALUE = 0.215308E+05

Figure A-7. Cryobearing Armature As-built FEA Results (Sheet 5)

R E A C T I O N F O R C E					
NODE	DIRECTION	REACTION FORCE	NODE	DIRECTION	REACTION FORCE
1	1	0.00000	17	6	0.00000
1	2	0.00000	18	6	0.00000
1	3	-59.643	19	6	0.00000
1	4	-1.3348	20	1	0.00000
1	5	2.3564	20	5	-0.33604
1	6	0.00000	20	6	0.00000
2	1	0.00000	26	2	0.00000
2	2	0.00000	26	4	2.3391
2	3	-45.079	26	6	0.00000
2	4	6.4736	27	6	0.00000
2	5	-0.31941	28	6	0.00000
2	6	0.00000	29	6	0.00000
3	1	0.00000	30	1	0.00000
3	2	0.00000	30	5	-0.81846
3	3	32.194	30	6	0.00000
3	4	23.873	41	2	0.00000
3	5	-10.834	41	4	10.039
3	6	0.00000	41	6	0.00000
4	1	0.00000	42	6	0.00000
4	2	0.00000	43	6	0.00000
4	3	112.07	44	6	0.00000
4	4	47.260	45	1	0.00000
4	5	-11.022	45	5	5.6530
4	6	0.00000	45	6	0.00000
5	1	0.00000	46	2	0.00000
5	2	0.00000	46	4	18.529
5	3	60.462	46	6	0.00000
5	4	20.648	47	6	0.00000
5	5	-13.486	48	6	0.00000
5	6	0.00000	49	6	0.00000
6	2	0.00000	50	1	0.00000
6	4	19.126	50	5	23.599
6	6	0.00000	50	6	0.00000
7	6	0.00000	56	2	0.00000
8	6	0.00000	56	4	8.6396
9	6	0.00000	56	6	0.00000
10	1	0.00000	57	6	0.00000
10	5	-26.545	58	6	0.00000
10	6	0.00000	59	6	0.00000
16	2	0.00000	60	1	0.00000
16	4	14.669	60	5	15.331
16	6	0.00000	60	6	0.00000

TOTAL STRAIN ENERGY = 0.306547E+00

Figure A-7. Cryobearing Armature As-built FEA Results (Sheet 6)

DISPLACEMENTS

NODE	X-DISPL.	Y-DISPL.	Z-DISPL.	XX-ROT.	YY-ROT.	ZZ-ROT.
1	0.00000	0.00000	1.79718E-11	4.02195E-13	-7.10033E-13	0.00000
2	0.00000	0.00000	1.35834E-11	-1.95064E-12	9.62450E-14	0.00000
3	0.00000	0.00000	-9.70088E-12	-7.19342E-12	3.26446E-12	0.00000
4	0.00000	0.00000	-3.37679E-11	-1.42404E-11	3.32131E-12	0.00000
5	0.00000	0.00000	-1.82187E-11	-6.22184E-12	4.06366E-12	0.00000
6	0.00000	0.00000	6.97889E-05	-5.76301E-12	-1.85396E-04	0.00000
7	0.00000	0.00000	-3.12997E-06	-3.16957E-04	-1.12971E-04	0.00000
8	0.00000	0.00000	-1.73669E-04	-7.21164E-04	1.33235E-05	0.00000
9	0.00000	0.00000	-3.51872E-04	-1.12391E-03	6.71272E-05	0.00000
10	0.00000	0.00000	-4.29881E-04	-1.33397E-03	7.99871E-12	0.00000
16	0.00000	0.00000	2.17230E-04	-4.41999E-12	-3.58766E-04	0.00000
17	0.00000	0.00000	1.97734E-06	-5.76661E-04	-2.98068E-04	0.00000
18	0.00000	0.00000	-5.12493E-04	-1.16720E-03	-2.09394E-04	0.00000
19	0.00000	0.00000	-1.07395E-03	-1.70151E-03	-1.13719E-04	0.00000
20	0.00000	0.00000	-1.32176E-03	-1.87077E-03	1.01255E-13	0.00000
26	0.00000	0.00000	3.32542E-04	-7.04822E-13	2.05175E-04	0.00000
27	0.00000	0.00000	-1.25620E-04	-1.29845E-03	2.98364E-04	0.00000
28	0.00000	0.00000	-1.30884E-03	-2.92286E-03	3.27286E-04	0.00000
29	0.00000	0.00000	-2.77950E-03	-4.55301E-03	3.18451E-05	0.00000
30	0.00000	0.00000	-3.56045E-03	-5.45986E-03	2.46621E-13	0.00000
41	0.00000	0.00000	3.17862E-04	-3.02503E-12	1.80668E-04	0.00000
42	0.00000	0.00000	-1.83982E-04	-1.33831E-03	2.54057E-04	0.00000
43	0.00000	0.00000	-1.48248E-03	-2.96841E-03	2.43088E-04	0.00000
44	0.00000	0.00000	-3.09846E-03	-4.57221E-03	-7.35619E-05	0.00000
45	0.00000	0.00000	-3.97477E-03	-5.44522E-03	-1.70009E-12	0.00000
46	0.00000	0.00000	2.78616E-04	-5.58318E-12	1.21097E-05	0.00000
47	0.00000	0.00000	-4.53865E-04	-1.53761E-03	-9.96445E-06	0.00000
48	0.00000	0.00000	-2.36149E-03	-3.18672E-03	-2.01457E-04	0.00000
49	0.00000	0.00000	-4.75927E-03	-4.66974E-03	-5.47942E-04	0.00000
50	0.00000	0.00000	-6.13094E-03	-5.27949E-03	-7.11080E-12	0.00000
56	0.00000	0.00000	3.09304E-04	-2.60330E-12	-1.63392E-04	0.00000
57	0.00000	0.00000	-6.53900E-04	-1.64966E-03	-2.52229E-04	0.00000
58	0.00000	0.00000	-3.17781E-03	-3.21007E-03	-5.40675E-04	0.00000
59	0.00000	0.00000	-6.39179E-03	-4.78448E-03	-8.70793E-04	0.00000
60	0.00000	0.00000	-8.20969E-03	-5.18435E-03	-4.61951E-12	0.00000

SOLUTION TIME LOG IN SEC

FOR PROBLEM

TIME FOR INPUT PHASE	=	5
TIME FOR CALCULATION OF STRUCTURE STIFFNESS MATRIX=		10
TRIANGULARIZATION OF STIFFNESS MATRIX	=	2
TIME FOR LOAD CASE SOLUTIONS	=	1
TIME FOR UPDATING DATA BASE	=	5
TOTAL SOLUTION TIME	=	23

Figure A-7. Cryobearing Armature As-built FEA Results (Sheet 7)

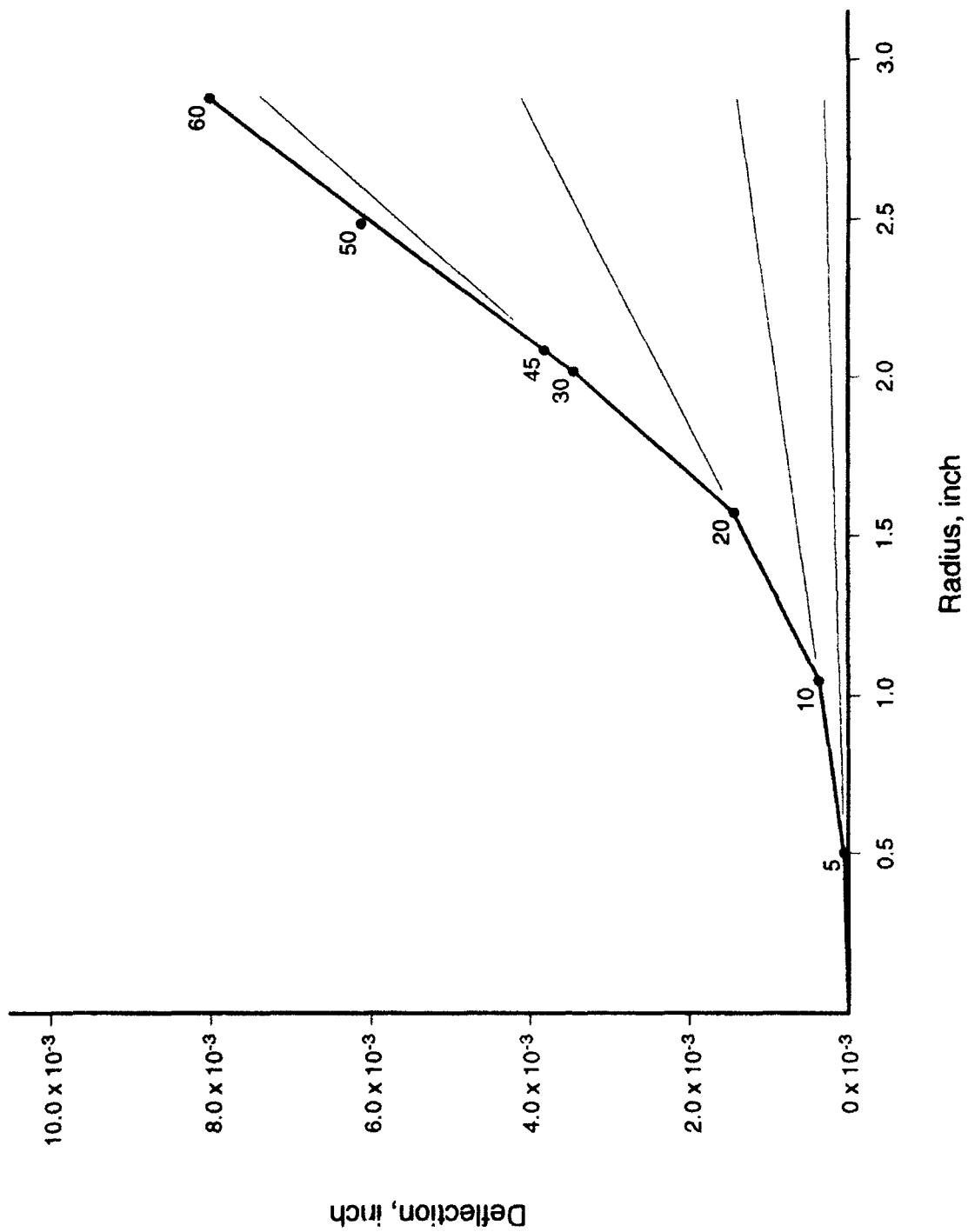


Figure A-9. Representative As-built Armature Deflection Versus Radial Location

CRYOBEARING ARMATURE FEA RESULTS -
"CURRENT" CONFIGURATION
CASE K


```

*****
*****
*
*
*           C O S M O S / M
*
*           VERSION: 1.52A
*
*           DISTRIBUTED BY:
*
*           STRUCTURAL RESEARCH AND ANALYSIS CORPORATION
*
*           1661 LINCOLN BLVD. #100
*
*           SANTA MONICA, CALIFORNIA 90404
*
*           TEL. NO. (213) 452-2158
*
*           COPYRIGHT 1988 S. R. A. C.
*
*****
*****

DATE: 4/ 2/1991 TIME: 10:39: 7

TITLE : CRYOBORG ORIG STOP ON ARM WO FILLER REV K 2APR91
*****

REAL CONSTANT DATA
-----

REAL CONSTANT SET 1
SHELL4 Four node thin shell elements
Thickness of the plate = 0.27000

REAL CONSTANT SET 2
SHELL4 Four node thin shell elements
Thickness of the plate = 1.4040

REAL CONSTANT SET 3
SHELL4 Four node thin shell elements
Thickness of the plate = 0.21000

REAL CONSTANT SET 4
SHELL4 Four node thin shell elements
Thickness of the plate = 0.22200
*****

MATERIAL PROPERTY DATA
-----

MATERIAL PROPERTY SET 1
EX : X Elastic Modulus = 0.35000E+08
NUXY : Poisson Ratio = 0.30000
DENS : Mass Density = 0.75830E-03

```

Figure A-10. Cryobearing Stop on Armature (Sheet 1)

MODAL LOADS

MODE	FX	FY	FZ	MX	MY	NZ
50	0.0000	0.0000	-100.0	0.0000	0.0000	0.0000

DISPLACEMENTS

MODE	X-DISPL.	Y-DISPL.	Z-DISPL.	XX-ROT.	YY-ROT.	ZZ-ROT.
1	0.00000	0.00000	-1.02448E-12	-1.58218E-13	7.82113E-13	0.00000
2	0.00000	0.00000	-2.14323E-12	-3.08814E-13	9.38578E-13	0.00000
3	0.00000	0.00000	-2.53553E-12	-9.11875E-13	7.36154E-13	0.00000
4	0.00000	0.00000	-2.96037E-12	-1.23215E-12	3.76099E-13	0.00000
5	0.00000	0.00000	-1.39918E-12	-3.84032E-13	1.49943E-13	0.00000
6	0.00000	0.00000	-4.82877E-05	-5.81798E-13	1.18946E-04	0.00000
7	0.00000	0.00000	-5.13666E-05	-6.77491E-05	1.15133E-04	0.00000
8	0.00000	0.00000	-5.94535E-05	-1.28327E-04	9.17373E-05	0.00000
9	0.00000	0.00000	-6.78764E-05	-1.72805E-04	5.22152E-05	0.00000
10	0.00000	0.00000	-7.09964E-05	-1.94702E-04	5.52879E-13	0.00000
16	0.00000	0.00000	-9.22781E-05	-1.01091E-11	1.03392E-05	0.00000
17	0.00000	0.00000	-1.01070E-04	-3.32745E-05	7.92421E-06	0.00000
18	0.00000	0.00000	-1.22757E-04	-6.01398E-05	1.28210E-06	0.00000
19	0.00000	0.00000	-1.46399E-04	-7.73459E-05	-2.64973E-06	0.00000
20	0.00000	0.00000	-1.57080E-04	-8.57880E-05	-5.50015E-13	0.00000
26	0.00000	0.00000	-9.55063E-05	-7.98179E-12	4.40500E-06	0.00000
27	0.00000	0.00000	-1.08647E-04	-3.51416E-05	2.05369E-07	0.00000
28	0.00000	0.00000	-1.41260E-04	-6.22226E-05	-7.10312E-06	0.00000
29	0.00000	0.00000	-1.78009E-04	-8.05001E-05	-1.00272E-05	0.00000
30	0.00000	0.00000	-1.95963E-04	-8.82317E-05	-4.48675E-12	0.00000
41	0.00000	0.00000	-9.57835E-05	-3.57415E-14	3.01018E-06	0.00000
42	0.00000	0.00000	-1.09634E-04	-3.51505E-05	-1.63737E-06	0.00000
43	0.00000	0.00000	-1.44177E-04	-5.66962E-05	-2.18041E-06	0.00000
44	0.00000	0.00000	-1.85211E-04	-1.38667E-04	-2.98657E-05	0.00000
45	0.00000	0.00000	-2.09716E-04	-2.58503E-04	-5.04108E-14	0.00000
46	0.00000	0.00000	-9.60282E-05	-4.93911E-14	-1.70695E-06	0.00000
47	0.00000	0.00000	-1.12700E-04	-3.07119E-05	-7.98518E-06	0.00000
48	0.00000	0.00000	-1.58281E-04	-6.29358E-05	-1.67634E-05	0.00000
49	0.00000	0.00000	-2.60969E-04	-2.65261E-04	-8.28617E-05	0.00000
50	0.00000	0.00000	-4.18154E-04	-5.50172E-04	-7.84369E-13	0.00000
56	0.00000	0.00000	-9.45531E-05	-1.61783E-14	-4.73680E-06	0.00000
57	0.00000	0.00000	-1.12944E-04	-2.82710E-05	-1.43295E-05	0.00000
58	0.00000	0.00000	-1.89874E-04	-6.91890E-05	-4.27527E-05	0.00000
59	0.00000	0.00000	-3.52839E-04	-3.11558E-04	-1.33030E-04	0.00000
60	0.00000	0.00000	-6.17080E-04	-4.92903E-04	-4.70015E-13	0.00000

Figure A-10. Cryobearing Stop on Armature (Sheet 2)